Dissertation

Design Criteria for GCHP-Systems with Seasonal Storage (Anergienetze)

ausgeführt zum Zwecke der Erlangung des akademischen Grades eines

Doktors der technischen Wissenschaften (Dr. techn.) unter der Leitung von

Ao.Univ.Prof. Dipl.-Ing. Dr.techn. Karl Ponweiser

Institut für Energietechnik und Thermodynamik / E302

eingereicht an der Technischen Universität Wien

Fakultät für Maschinenwesen und Betriebswissenschaften

von

Johannes Nagler

0716436

Liechtensteinstraße 130/18, 1090 Wien

Gutachter:

Univ.Prof. Dipl.-Ing. Dr.techn. Thomas Bednar
Institut für Hochbau und Technologie, TU Wien

Ao.Univ.Prof. Dipl.-Ing. Dr.techn. Andreas Werner
Institut für Energietechnik und Thermodynamik, TU Wien

Wien, October 1, 2018 **eigenhändige Unterschrift**

Abstract

The widespread challenges related to the reduction of carbon dioxide emissions affects also building services like heating and cooling. This work presents a heat pump based system for heating and cooling purposes of residential areas comprising several buildings. The heat pump's anergy supply takes place with a low temperature ring network which allows the exploitation of low temperature industrial/commercial waste heat. A seasonal storage system represented as borehole thermal energy storage (BTES) decouples the thermal energy's supply and demand and allows due to the low temperature levels throughout the whole year efficient long term thermal energy storage. The system's sustainability is assured by means of balanced BTES control strategy throughout every operational year. Due to the low temperature levels of 5 °C (winter) to 20 °C (summer) the proposed system allows for low-energy consuming cooling of buildings in free cooling mode. Given this fact the work covers another increasingly important emphasis in energy supply: district cooling. Therefore connected buildings to the ring network are represented as prosumers (thermal energy PROducers and conSUMERs). They act as heat sources during the summer months and as heat sinks during winter time. The impact of network size, population density, building quality and network structure on the system design and performance is investigated and an estimation about the economic feasibility is given. The results show that the system setup, especially large and dense networks are competitive to other heat generation and distribution technologies, also if elevated future electricity price increases are taken into consideration. Beside the network size the population density was identified to have a great impact on the system's economic feasibility.

Kurzfassung

Die Herausforderungen die sich mit der Notwendigkeit der Umsetzung von CO2-Emissionsreduktionsmaßnahmen ergeben betreffen unter anderem auch den Bereich der Gebäudeversorgung mit thermischer Energie (Wärme- und Kälteenergie). In dieser Arbeit wird die Möglichkeit der wärmepumpenbasierten Wärme- und Kälteversorgung eines Areales, das aus mehreren Gebäuden besteht untersucht. Die Versorgung der Wärmepumpen mit Anergie erfolgt durch ein Niedrigtemperaturringnetzwerk, welches es ermöglicht industrielle und gewerbliche Abwärme auf niedrigem Temperaturniveau nutzbar zu machen und energetisch für Heizzwecke zu verwenden. In Zusammenhang mit einem saisonalen Speicher der hier als Erdsondenspeicher modelliert wird kann die Bereitstellung der thermischen Energie von dessen Bedarf entkoppelt werden. Durch die niedrigen Temperaturen im geothermisch versorgten Anergienetz kann die Speicherung von thermischer Energie verlustarm auch für längere Zeitintervalle realisiert werden. Im Sinne der Nachhaltigkeit derartiger Systeme wird in den Modellannahmen vorausgesetzt, dass der Erdsondenspeicher über den Zeitraum von einem Betriebsjahr stets ausgeglichen bilanziert wird. Das Netztemperaturniveau bewegt sich im Jahresverlauf zwischen fünf und 20 °C. Diese Tatsache ermöglicht bei Bedarf die Kühlung der angeschlossenen Gebäude im energieeffizienten Free-Cooling-Betrieb. Damit wird der immer wichtiger werdende Aspekt der energieeffizienten Kühlung (Fernkälte) abgedeckt. Die an das Niedertemperatur-Ringnetz angeschlossenen Gebäude werden daher als Prosumer (PROducer und comSUMER thermischer Energie) abgebildet, die Wärmesenke bildet in diesem Fall der Heizbetrieb im Winter, der Kühlbetrieb im Sommer hingegen stellt die Wärmequelle für das System Ringnetzwerk und Erdsondenspeicher dar. Der Einfluss von Netzgröße, Bevölkerungsdichte, Gebäudequalität und Netzstruktur auf die Systemauslegung und Betriebskennzahlen wird untersucht und eine Wirtschaftlichkeitsanalyse durchgeführt. Die Ergebnisse zeigen, dass das vorgestellte Konzept, vor allem große Netwerke in der Lage sind mit konventionellen Wärmeerzeugungs- und -verteilungstechnologien zu konkurrieren. Auch wenn höhere zukünftige Preissteigerungsraten für Elektrizität angenommen werden. Neben der Netzgröße wurde auch die Bevölkerungsdichte als wichtiger Einflussfaktor auf die Wirtschaftlichkeit des Konzeptes identifiziert.

Acknowledgements

Diese Danksagung ergeht an alle, die mich bei der Fertigstellung dieser Arbeit motiviert und unterstützt haben.

Besonders herzlicher Dank gebührt natürlich Ao.Univ.Prof. Dipl.-Ing. Dr.techn. Karl Ponweiser für seine vorbildhaft wissenschaftliche und konstruktive Betreuung und Zusammenarbeit, für die zahlreichen Besprechungen und unzähligen aussagekräftigen Skizzen.

Bedanken möchte ich mich auch bei Univ.Prof. Dipl.-Ing. Dr.techn. Markus Haider und Ao.Univ.Prof. Dipl.-Ing. Dr.techn. Andreas Werner, die es mir ermöglicht haben am Institut für Energietechnik und Thermodynamik tätig zu werden und damit einen Grundstein für diese Arbeit gelegt haben. Auch den anderen Institutsangehörigen, insbesondere Dominik, Felix, Gregor, Stefan, Stylianos, Thomas und Wolfgang, die mich während unserer Zusammenarbeit unterstützt, abgelenkt und motiviert haben sei an dieser Stelle gedankt.

Außerdem bedanke mich mich bei Univ.Prov. Dipl.-Ing. Dr.techn. Thomas Bednar für die Begutachtung und die fachbereichsübergreifende Ermöglichung eines Praxiseinsatzes der Netzwerksimulation.

Ein weiterer Dank geht an die Projektmitarbeiter und Diskussionspartner Gregor Götzl und Martin Fuchsluger, für ihren Exkurs in die Welt der Geologie.

Meinen Eltern und meiner Schwerster danke ich für die bedingungslose Unterstützung und den mentalen Rückhalt während meiner Studienzeit.

Zum Schluss danke ich meiner Freundin Lea, die mich stets verständnisvoll unterstützt und liebevoll aufgemuntert hat.

Contents

Nomenclature

Acronyms

4GDH	4th generation district heating
ASHP	air-source heat pump
BHE	borehole heat exchanger
BTES	borehole thermal energy storage
CD	yearly cooling demand
CDD	cooling degree-days
COP	HP's coefficient of performance
CRC	capital-related cost
DH	district heating
DHSE	domestic hot water preparation with storage tank
DHW	domestic hot water
DRC	demand-related cost
DST	duct storage system
EQS	equation system
GCHP	ground coupled heat pumps
GSHP	ground-source heat pump
HD	yearly heating energy demand
HP	heat pump
ITHE	domestic hot water preparation, instantaneous preparation
LCOE	levelized cost of energy
LTDH	low-temperature district heating
LTDHC	low-temperature district heating and cooling
ORC	operation-related cost
PHE	plate heat exchanger
PVT	photovoltaic thermal hybrid solar collector
TRT	Thermal response test

Greek symbols

α	equation system factor	-
ϵ_{hp}	HP's thermodynamic perfectibility	-
η	efficiency	-
κ	DHW circulation loss percentage	-
λ	thermal conductivity	$\frac{\mathrm{W}}{\mathrm{m\,K}}$
μ	dynamic viscosity	$\frac{\mathrm{kg}}{\mathrm{m\,s}}$
ϕ	part load factor	-
ρ	density	$\frac{\mathrm{kg}}{\mathrm{m}^3}$
ϑ	temperature	°C
ζ	pressure loss coefficient	-

Roman symbols

ΔT	temperature difference	K
Δt	time step	s
$\dot{m}$	mass flow	$\frac{\mathrm{kg}}{\mathrm{s}}$
$\dot{Q}$	heat flow	W
$\dot{q}$	specific heat flow	$\frac{\mathrm{W}}{\mathrm{m}^2}$
$\dot{V}$	volume flow	$\frac{\mathrm{m}^3}{\mathrm{s}}$
A	(heat transfer) area	m^2
a	thermal diffusivity	$\frac{\mathrm{m}^2}{\mathrm{s}}$
C	volumetric heat capacity	$\frac{\mathrm{J}}{\mathrm{m}^3\,\mathrm{K}}$
c_p	specific isobaric heat capacity	$\frac{\mathrm{J}}{\mathrm{kg\,K}}$
D	diameter	m
E	energy/work	J
f_D	Darcy friction factor	-
Fo	Fourier number	-
H	hydraulic head	m
h	enthalpy	$\frac{\mathrm{J}}{\mathrm{kg}}$
k	heat transfer coefficient	$\frac{\mathrm{W}}{\mathrm{m}^2\,\mathrm{K}}$
L	length	m
m	heater superscript	-
n	number of probes within a borehole field	-
Nu	Nusselt number	-
P	power	W
p	pressure	$\frac{\mathrm{N}}{\mathrm{m}^2}$
R	thermal resistance	$\frac{\mathrm{m\,K}}{\mathrm{W}}$

r	radius	m
R_a	absolute roughness	m
Re	Reynolds number	-
s	borehole spacing	m
t	time	s
u	flow velocity	$\frac{\mathrm{m}}{\mathrm{s}}$
V	volume	m^3
v	flow velocity	$\frac{\mathrm{m}}{\mathrm{s}}$
x	length in x direction	m

Subscripts

a	year
amb	ambient
B	balanced
b	borehole
bc	boundary condition
C	cooling
c	condenser
ca	Carnot
cir	circulation
cp	cold pipe
cum	cumulative
D	demand, total
d	day/daily
dhw	domestic hot water
e	evaporator
el	electricity
ext	external
f	fluid
fg	fluid - grouting material (thermal resistance)
fw	fresh water
g	grouting material
gb	grouting material - borehole wall (thermal resistance)
gg	grouting material - grouting material (thermal resistance)
H	heating
hex	heat exchanger
hp	heat pump
HT	heat transfer

I	indoor
m	mean
N	design point
p	pump
R	return
S	supply
s	soil
$s0$	borehole wall - soil material (thermal resistance)
sm	service and maintenance
ss	storage supply
st	storage
w	water
we	water equivalent
wp	warm pipe
x	x direction

Chapter 1

Introduction

The overall energy demand for heating and cooling accounts for more than one third of the final worldwide energy consumption. In European countries the fraction of the sector private and public homes and services amounts to 35% in Austria (*Statistik Austria*) and approx. 42% in Switzerland (*Bundesamt für Energie*) and Germany (*Umweltbundesamt*). The share of energy for heating purposes within this sector is above 80%. Therefore, more than a quarter of the final energy consumption is needed to heat homes and water. A large slice of this cake is still covered by the usage of fossil fuels. Due to this fact the building sector produces a large amount of greenhouse gas emissions that could be avoided with state of the art technologies. Much effort has been given to increase the share of renewables in the electricity system, but still a huge potential in the heating and cooling sector is not exploited yet. This matter of fact opens up a large amount of research fields. The district heating sector has a high potential to achieve reductions in carbon dioxide emissions, but as *Werner* states in the international review of district heating and cooling, [90], the utilization of district heating in buildings is still low and the population shows only moderate commitment in the fundamental idea of district heating. Nevertheless the evolution in district heating progresses. The well known progression towards 4th generation district heating (4GDH, [53]), enables for a wide range of possibilities. The Smart Grid concept ([29], [43] [50]) is only one of many attempts to improve the grid related energy distribution systems efficiency. Another approach is found in the energy hub concept, [65]. The combination of electricity and heat networks enables for more possibilities in enhancing the overall thermal energy and exergy efficiency of energy networks ([51] [39])

An overview of recent trends in European research and development in district heating technologies is provided by *Sayegh* in [77]. It shows that the subject areas go beyond the technical and economical point of view and consider also the impact on the environment and the human health. *Molyneaux* presents in [59] an environomic optimization for a district heating network and concludes that heat pumps offer great potentials for greenhouse gas reductions. *Lake et al.* finds in his review of district heating and cooling systems for a sustainable future [47], that

the optimization of district energy systems should not only consider thermal efficiency but also economic an environmental issues. The trend of ongoing urbanization increases the necessity of having efficient and clean energy systems. *Henchoz* provides in [38] some heat pump based concepts to provide heating and cooling services in urban areas. High population densities in cities increase the probability in finding suitable and accessible waste heat sources. *Fang et. al* state in [27] and [26] that industrial and commercial waste heat is being recognized as an important energy source for DH systems. The lower the waste heat temperature level, the more technical effort has to take place to exploit it for heating purposes. For close to ambient temperatures the heat pump technology is well suited for the recycling of waste heat. Therefore, a heat pump based approach is chosen here to become one more tool towards a more efficient and cleaner future heat supply. The condition for the usage of low grade waste heat are low network temperatures. Hence, the state of the art in low temperature district heating networks is analyzed in the following.

1.1 Low Temperature District Heating Networks

Reducing the temperature in district heating networks was and is still a main ongoing research goal. Many research groups around the world seek to optimize energetic (and exergetic) efficiencies and lower costs by decreasing the supply temperatures of existing and future heat energy delivering networks. Also the trend towards 4^{th} generation district heating (4GDH), which was shaped by *Lund* et al. in [53] is driven by this development. Lower network temperatures not only decrease thermal network losses, but they also allow for the integration of new heat sources to the network. The future district heating networks have supply temperatures according to *Lund* et al. of around 30-70 °C. Ground coupled heat pump (GCHP) systems or ground-source heat pump (GSHP) systems use remarkably lower network temperatures to connect the heat pump evaporators with a heat source. However, some literature references are fuzzy about the distinction between district heating network and ground coupled heat pump systems. The terminology related to this topic also changes between different countries. While in Germany low temperature district heating (and cooling) networks are called *cold networks*, Swiss researchers use the term *anergy networks*. Within the IEA research groups and the English speaking community the notion *Low-Ex networks*, which means low exergy, is quite common.

The concept presented within this work is rather a GCHP system then a district heating network. However, it combines aspects of both systems. On one hand it uses heat pumps to generate heating or cooling energy and on the other hand it consists of a network which connects the energy customers and the storage system. *Allegrini* et al. use in [2] a more general term, namely *district-scale energy systems* which is more appropriate. The authors give a current overview of realized modeling approaches of such systems and provide a matrix of twenty cross-disciplinary simulation tools. The presented work aims for combining GSHP systems with district heating aspects. It is ab attempt to link the network theory, in mathematical therms the graph

theory, with a simple model of a seasonal heat storage and a number of heat pumps. In that way a cold district heating system is obtained which comprises the GSHP concept. Considering GSHP systems a large variety of possible concepts is available in the literature. De Carli et al., for instance, present in [15] a closed loop GSHP concept for a city in Italy. The authors criticize the lack of papers considering GSHP for district heating applications. So far, GSHP is mostly used for single buildings. In addition to the heat pumps as heat generators the concept contains additional boilers for the peak loads during winter time. One innovative aspect of this paper is that the authors consider the population density to give a quantitative assessment of the seasonal storage's space requirement. They try to combine the housing density with the storage system, which constitutes a low density ground energy resource. A proper designed underground storage system makes the usage of anti-freezing fluids no longer necessary.

The Swiss *Anergienetz* (Anergy network) concept comprises a GCHP concept with a connected central borehole field. Some applications for instance in Zürich and Rotkreuz have been in operation since a few years. *Sulzer* provides in [55] a basic document with a description of the Swiss anergy networks. Key feature is a water heating and/or cooling network that delivers water with a temperature level close to the ambient temperature from suppliers do consumers. The conversion from anergy to useful energy is done by heat pumps and refrigerating machines for heating or cooling needs. The energy conversion plants are assumed to be driven by electrical compressors. Another key characteristic is the seasonal energy storage which is assumed to be a ground storage. The energy balance within one operating year has to be balanced, hence, the same amount of thermal energy which has been provided to the storage within one year has to be withdrawn within the same time period of consideration. This condition has to be fulfilled to assure a consistent operation over many years and to avoid long term shifts in network temperatures. *Sulzer* et al. expand the anergy network concept in [56] to a *Multi Energy Grid* concept which allows for the efficient use of decentralized (renewable) energy sources. To assure a future sustainable energy supply it is necessary to transform and transfer locally available energy streams (electrical, thermal, gas) in an appropriate way. In this context the authors propose the usage of ring networks instead of the popular tree networks for the distribution of thermal energy. Based on the ring network structure and suitable control strategies it will be possible in the future to couple thermal networks and to share network infrastructure like e.g. the seasonal heat storage and heat suppliers. The concept proposed by Sulzer has been simulated in IDA-ICE by *Kräuchi* et al., [45], [71]. Key features are a non-insulated Ring network consisting of a pair of pipes, bidirectional heat consumers and a simplified model of a BTES. Simulation results are COPs of the heat pumps, mass flows for the network pipes and pressure differences of the pumps at the heat consumers.

A recently published paper by *Ruesch & Haller* , [76] uses the swiss anergy network concept to perform more detailed investigations considering direct or "free" cooling by low-temperature district heating and cooling (LTDHC) networks. For the simulation of the networks the authors used the software Polysun®. As the network temperature is relatively low throughout the whole

year, it is possible to cool residential buildings by simply using a heat exchanger. The borehole field is regenerated by the thermal energy yield obtained by free cooling of the buildings. The authors come to the finding that the potential of borehole field regeneration by free cooling of residential buildings is very limited. Other sources of thermal energy are needed to assure the seasonal storage's energy balance.

Main requirement for GCHP or LTDH systems to assure long term operation is the even energy balance of the connected ground storage. *Vetterli & Sulzer* show in [89] what happens if that is not the case. The low temperature district heating and cooling network "Suurstoffi" has been monitored since 2012. The actual heating demand in operation was twice as high than expected. The heat sources for the system, free cooling did not meet the expectations and was significantly lower than expected. Due to different completion times of a number of construction stages some of the heat sources were not available yet at the begin of the operation. As a consequence the network temperatures were declining over the years. The network operators reacted with the installation of additional heat generators to assist the heat pump's operation. Main outcome of the study was that appropriate monitoring is crucial in being able to react to offsets between planning and operation. Monitored data was also used for model calibration of similar projects in the planning stage.

Another study from 2017 by Prasanna et al., [73] is about the energy performance of district energy systems within the background of the Swiss anergy network concept. A case study in Rotkreuz, Switzerland, constitutes the database for a MILP optimization model. Scenarios with electric and thermal storage as well as PV electricity production are considered. Aim of the study was to find optimal storage shares with subject to the minimization of the annual carbon emissions. Since the considered system is entirely electricity based, the objective function corresponds to a minimization of the electricity purchased from the grid. The results show that the installed PV panels are able to cover 100% of the necessary annual heat pump and hydraulic pump energy, but only 35% can be used within the system without electrical short therm thermal storage systems. If short term storage capacities are present, the share of usable PV production can be increased up to 77%.

In Germany the *LowEx* approach is subject to a number of ongoing research projects. This concept corresponds to the Swiss approach but focuses more on the exergy efficiency. However, the supply temperatures in the LowEx approach are slightly higher compared to the Swiss concepts. A study by *Schmidt* et al., [79] investigates low temperature district heating (LTDH) networks and emphasizes the exergy efficiency of the total energy chains for community supply systems. The paper addresses the IEA DHC Annex TS1 which aims for diffusing the idea of future concepts for heat delivery systems at a international scale. A comprehensive view from heat generation over heat distribution to thermal energy consumption within the buildings is given. The authors show a roadmap for the development of the district energy sector for the future.

The usage of waste heat within a district heating network is subject of a paper by *Torio*

et al. In [87] the authors perform a exergy analysis for a case study in Kassel, Germany. The high-quality energy sources (natural gas) are substituted by low energy sources (waste heat). By lowering the supply and return temperatures of an existing district heating network, the final exergy efficiency of the system can be increased significantly. The paper provides a tool for exergy analysis within the context of district energy systems.

A German research group investigated in [36] the potential of low temperature networks for increasing the share of renewables at district scale. Aim of the project was to determine the necessary amount of waste heat and solar thermal energy to cover the energy needs for a district in Munich, Germany. The thermal and electrical energy source are photovoltaic thermal hybrid solar collectors (PVT). The seasonal shift between solar supply and user's demand is bridged by a seasonal storage, the authors consider a borehole thermal energy storage as well as a large tank storage. Supply temperatures for the case study range between 10 and 40 °C. The outcomes show that it is possible to run low temperature networks by PVT collectors only. Additional short-term storage tanks have to be installed to buffer the solar yield's peaks during summer months. In comparison to conventional district heating networks the authors claim to reduce the thermal losses by 85%. Based on the results the authors provide planning guidelines for similar systems.

Another German approach to low temperature district heating networks are GCHP systems which use shallow geothermal energy. *Pietruschka* et al. give in [72] an overview of the so called agricultural collectors. A specifically developed installation type based on excavators allows for an affordable shallow heat source. Special attention may be given to the network temperatures to prevent freezing on the heat pump's evaporators.

Farzin et al. present in [30] a viability study for a hybrid GSHP system that also uses solar thermal collectors for the supply of heating dominated buildings in Canada. Hybrid GSHP systems are GSHP systems that have an additional heat exchanger above the ground as a further heat sink/source in addition to the ground source/sink. The authors use a borehole ground heat exchanger to store solar thermal energy with the aim to reduce the borehole depth and hence to reduce installation costs. As a result the study shows that for one house with a aperture area of 6.81m^2 for the solar panel the borehole depth reduces by 15%.

Li & Svendsen perform in [49] an exergy and energy analysis of a low temperature district heating network consisting of 30 low energy residential houses. In this context low temperature means 55 °C supply and 25 °C return temperature, which corresponds to the danish concept of 4GDH (or LTDH). The authors present two different in-house substations for domestic hot water preparation: ITHE (instantaneous preparation) and DHSE (with storage tank). The results of an exergy analysis show that the latter one produces lower network losses, however the exergy efficiency is only slightly higher than the one for the DHSE concept. Another outcome of the study shows that a network which has been designed with an improved method and which leads to smaller pipeline diameters helps in reducing heat losses.

1.2 Scope and Limitations

Scope of this work is to get a deeper insight in the behavior of GCHP-systems. The ongoing research activity show that it could be of interest to highlight some aspects of the systems described here. Operators of comparable systems in operation can further benefit from the methodology and the results shown below. After reading this work, the reader can answer the following questions:

- Which amount of energy at which temperature level need the supplier to provide?
- How large does the borehole field get?
- How much is the initial investment?
- Which specific cost of heating energy can a customer expect?
- Does the network's topology have a significant impact on the system's performance?
- How do the systems perform if the expected customer's heat demand is not as it was expected in the design stage?

These main investigation issues are found by using a multidimensional approach to GCHP-systems. How the answers of the questions above change in respect to certain boundary conditions is another scope of this work. Answers are found for the following system boundary conditions:

- Network structure
- Population density
- Network size (energy and space demand)
- Building quality

The next chapter starts with the definition of the GCHP-Systems boundary conditions network size (space demand) and population density. The network size in terms of energy demand and it's structure is found in chapter 2. The methodology in creating a mathematical representation of a GCHP-System with the assumptions and limitations made in this section is declared in the chapters 3 and 4. Chapter 5 is about an economic feasibility of systems like the presented one. A dynamic investment calculation helps to find an educated guess in heat production costs and initial investment values. The answers to the questions above are finally given in chapter 6 and discussed in the following one.

Scope here is not to compete with other simulation programs like professional vertical heat exchanger software. It is rather to create a relatively simple but accurate model to determine the key performance indicators of such systems. Due to the complete statement of the methodology it should be possible to adapt the presented model for other purpose or altered boundary conditions. The cost data used for the economic feasibility study are strongly conditional on the source of the information, the country and may also vary over time. Therefore it is attempted to provide as much as possible simulation data for the reader for the purpose to estimate the investment costs based on his own data.

1.3 System Description

Focus are ring networks with a varying number and size of connected energy customers (producer and consumers). Together with a central borehole thermal energy storage (BTES) and the ring network piping the system setup is defined and shown in fig. 1.1.

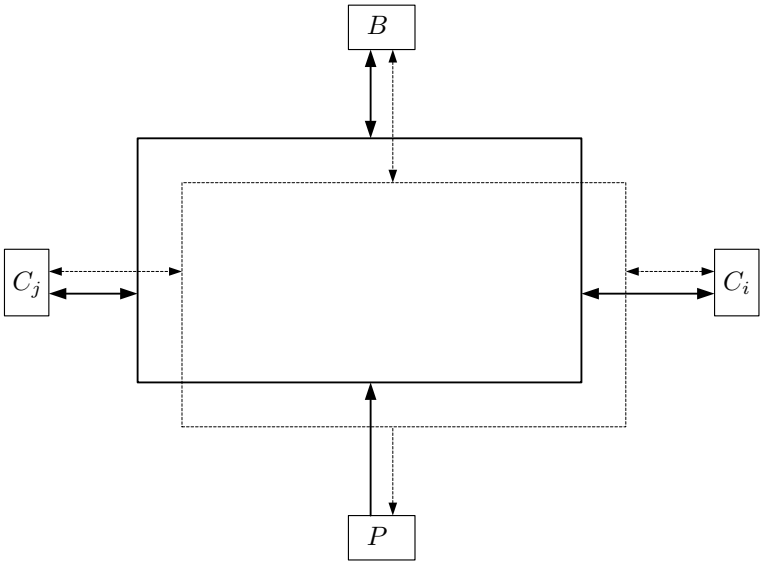

FIGURE 1.1: System setup, warm grid (solid line) and cold grid (dashed line), unidirectional producer P, bidirectional consumers C_i and BTES B

Based on different scenarios a varying number of dwellings need to be supplied with heating and cooling energy. Water as the heat carrier fluid is distributed in a ring network, in a warm and a cold pipe ring, which interconnect the energy customers and the BTES. The consumers are intended to represent buildings with a given heating and cooling demand. Depending on the season a consumer either demands thermal energy from the system (winter) or supplies thermal energy to the system (summer). Therefore the consumers are modelled like a bidirectional customer (prosumer). Additionally, every network has one heat producer, which provides warm water to the network. This producer does not consume any thermal energy and is therefore modelled in a unidirectional way. The producer is essential because the yearly amount of heating energy demand dominates over the cooling energy demand within the considered climate zone. On the other hand this enables for the integration of low temperature waste heat. A common feature of all the considered scenarios is a central borehole thermal energy storage (BTES), with the duty to store thermal energy over longer time periods. The difference in consumed and provided thermal energy for every time step is provided by the BTES. It constitutes a passive network component whose flow direction changes in respect to the customer's aggregated heat load profiles.

The network concept is similar to the Swiss anergy network concept, anyway, the focus here is

on the network theory. Based on the graph theory, which is the mathematical representation of a water delivery network, it is investigated if the key performance indicators change when locations or connection nodes of certain components are changed. The pipes that make up the network are uninsulated PE pipes. Water temperatures within the network are close to ambient temperatures throughout the whole year. This makes heat losses in the piping network manageable if the piping geometries are designed properly. Therefore, pipe insulation is not necessary. As shown in fig. 1.1 the network consists of two circuits, the warm and the cold piping network. Based on the actual value of the energy demand, the consumers can tap water either from the warm or the cold pipe.

In the following the influence factors defined in section 1.2 network structure, population density, network size and building quality are defined.

Network structure

One influence factor for the GCHP-Systems covered in this work is the network structure or degree of decentralization. The effect of systems with the same energy demand but different number of connected buildings is carried out by changing the network topology from a rather central network configuration with a small number of buildings to a more decentralized system with a more but smaller buildings. The following figure sketches the idea of centralized and decentralized network configurations.

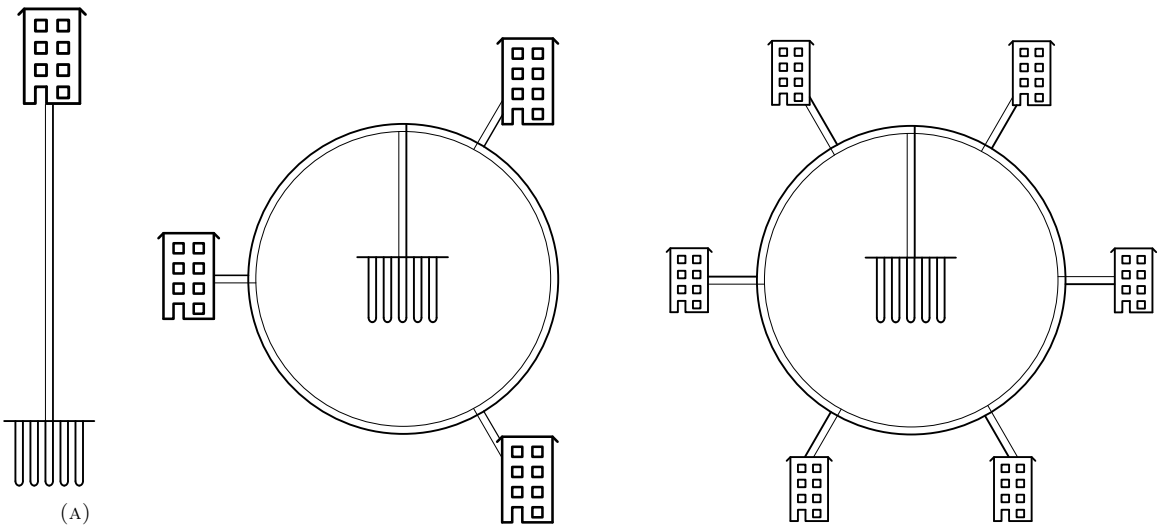

(A) centralized without ring network

(B) centralized

(C) decentralized

FIGURE 1.2: Network structures

Here, three possible network structures are considered. One rather centralized and homogeneous network configuration with 3-5 house connections and two decentralized configurations with 10-12 house connections. One of the latter one is homogeneous and the other one heterogeneous, hence, the connected buildings have different energy demands. The two homogeneous configurations are theoretical extreme cases, whereas the inhomogeneous one goes more towards real world implementation. The following abbreviations are used for the later considerations:

TABLE 1.1: network structure classification

	network structure	building structure
CH	central	homogeneous
DH	decentral	homogeneous
I	decentral	inhomogeneous

Population density

European cities like Vienna have a population density range of 50-500 inhabitants per hectare building land. The city center where the older buildings are located has the highest population densities. At the city development areas which are located in the suburbs of Vienna the population densities are lower, about 50-300 inhabitants per hectare. Those areas are appropriate for the heat supply concept presented within this work. Due to the fact the population density affects the network size, two different population densities are considered. A high population density scenario with 300 and a low population density scenario with 100 inhabitants per hectare. All the scenarios presented in table 1.2 are modeled for both of the population density scenarios. The sizing of the ring networks is executed with respect to the average number of inhabitant per dwelling which is, according to [57] 2.06. An energy central connected to the ring network with an associated number of supplied flats, as shown in table 1.2 is represented as a circle with a corresponding space requirement. The tightest packing of a circular arrangement of all the circles within one scenario determines the network's supply area. This approach is shown in fig 1.3 for one of the simulation scenarios.

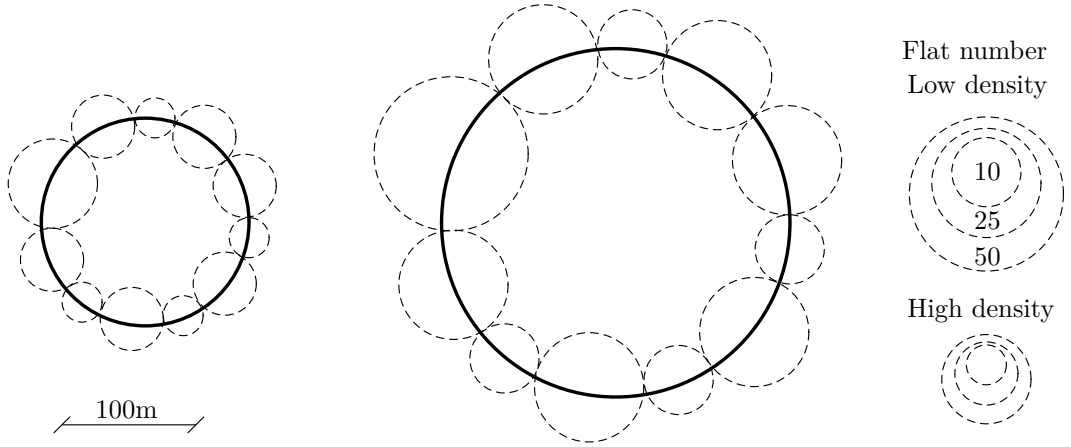

FIGURE 1.3: Ring network size according to population densities, left: high, right: low.

Network size

The network sizes in terms of energy demand and supplied dwellings are a further influence factor especially for the economic feasibility study. It is investigated here how the number of connected customers and the associated energy demand for heating, domestic hot water and cooling affects the network's performance and cost structure. The determination of hourly data for energy demands is carried out in chapter 2. The possible network sizes for the simulations are set here by means of the number of served dwellings equal to 250, 500, 1000 and 2000.

Building quality

The ability of buildings to store energy is the main idea of this influence factor. The building's thermal inertia has a great impact on the (hourly) heat loads. The aim is to find out how this fact influences the design and performance of a GCHP-System. Although the issue heat storage/thermal inertia in buildings is a branch of science for itself (see [24, 74, 75]), here it is treated only qualitatively. The simulation models get as an input different customer heat loads for heating, domestic hot water and cooling. Two possible scenarios are considered. One, depicted as V is the heat load for buildings with poor thermal inertia capacities. The heat loads have larger gradients than the other group, named S. The latter case has smoother heat loads with smaller gradients. Note that the yearly energy demand does not change between the two different heat load shapes. Only the hourly energy loads in terms of power are subject to changes. The methodology in finding the heat loads for the energy customers is shown in chapter 2.

1.4 Scenarios

By combining the four influence factors, namely network structure, population density, network size and building quality a number of 48 simulation scenarios has been developed, see tab. 1.2. The notation is

[POPULATION DENSITY] | [NETWORK SIZE] | [NETWORK STRUCTURE] | [BUILDING QUALITY]

TABLE 1.2: simulation scenarios based on the building quality (BQ), network size (SIZE), population density and network structures CH, DH and I

BQ	SIZE	HIGH POPULATION DENSITY			LOW POPULATION DENSITY		
		CH	DH	I	CH	DH	I
S	250	H|250|CH|S	H|250|DH|S	H|250|I|S	L|250|CH|S	L|250|DH|S	L|250|I|S
	500	H|500|CH|S	H|500|DH|S	H|500|I|S	L|500|CH|S	L|500|DH|S	L|500|I|S
	1000	H|1000|CH|S	H|1000|DH|S	H|1000|I|S	L|1000|CH|S	L|1000|DH|S	L|1000|I|S
	2000	H|2000|CH|S	H|2000|DH|S	H|2000|I|S	L|2000|CH|S	L|2000|DH|S	L|2000|I|S
V	250	H|250|CH|V	H|250|DH|V	H|250|I|V	L|250|CH|V	L|250|DH|V	L|250|I|V
	500	H|500|CH|V	H|500|DH|V	H|500|I|V	L|500|CH|V	L|500|DH|V	L|500|I|V
	1000	H|1000|CH|V	H|1000|DH|V	H|1000|I|V	L|1000|CH|V	L|1000|DH|V	L|1000|I|V
	2000	H|2000|CH|V	H|2000|DH|V	H|2000|I|V	L|2000|CH|V	L|2000|DH|V	L|2000|I|V

To achieve comparable results the methodology for the network design follows the same rules for each simulation scenario. Firstly a heat distribution network is designed. That includes pipe geometries, heat exchangers, hydraulic pumps and the seasonal heat storage's size. The networks are then fed with different heat flow specifications in order to provide answers to the questions from section 1.2.

1.5 Mathematical Equations and Methods

The mathematical representation of GSHP-systems is defined in the chapters 3 and 4. Both, the hydraulic network computation and the temperature calculation of the network and the BTES base essentially on the heat transport equation. This is the reason why it's derivation is shown in the following. In addition, a brief outline of handling and solving the linear equation systems, which are obtained in the course of the mathematical network representation, is given.

1.5.1 Transport Equation

The general form of the Transport Equation which is used later for heat and mass transfer problems is shown in this chapter. In reference to [11] and [41] the derivation is based on the balance of the extensive quantity m on the volume element with the dimensions dx, dy and dz.

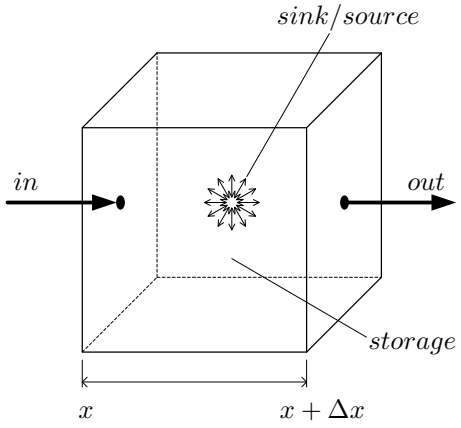

FIGURE 1.4: Control volume for the heat transport equation derivation

$$(in - out)\, A\, \Delta t + Source/Sink\, V\, \Delta t = Storage \tag{1.1}$$

$$(J(x) - J(x + \Delta x))\, A\, \Delta t + S\, V\, \Delta t = m(t + \Delta t) - m(t) \tag{1.2}$$

dividing by $A = \Delta y\, \Delta z$, Δx and Δt and introducing the volume/mass-based intensive quantities $\widehat{\phi}$ and ϕ yields

$$-\frac{(J(x) - J(x + \Delta x))}{\Delta x} + S = \frac{\widehat{\phi}(t + \Delta t) - \widehat{\phi}(t)}{\Delta t} \tag{1.3}$$

and for $\Delta t, \Delta x \to 0$ finally

$$\frac{\partial J}{\partial x} + \frac{\partial \widehat{\phi}}{\partial t} = S \tag{1.4}$$

The generalization for each spatial direction results in the differential form of the general balance equation for mass based intensive quantities ϕ

$$\boldsymbol{\nabla}\, \boldsymbol{J} + \frac{\partial}{\partial t}\,(\rho\, \phi) = S \tag{1.5}$$

The flow vector $\boldsymbol{J}$ consists in general of convection and diffusion fluxes:

$$\boldsymbol{J} = \underbrace{(\rho\,\boldsymbol{u}\,\phi)}_{convection} \quad \underbrace{-\Gamma\,\boldsymbol{\nabla}\,\phi}_{diffusion} \tag{1.6}$$

Inserting the flow vector (1.6) in the balance equation (1.5) yields the convection-diffusion equation in a differential form:

$$\boldsymbol{\nabla}\,(\rho\,\boldsymbol{u}\,\phi) + \frac{\partial}{\partial t}\,(\rho\,\phi) = \boldsymbol{\nabla}\,(\Gamma\,\boldsymbol{\nabla}\,\phi) + S \tag{1.7}$$

and in tensor notation with Einstein summation convention:

$$\frac{\partial}{\partial x_i}\,(\rho\,u_i\,\phi) + \frac{\partial}{\partial t}\,(\rho\,\phi) = \frac{\partial}{\partial x_i}\,(\Gamma\,\frac{\partial \phi}{\partial x_i}) + S \tag{1.8}$$

1.5.2 Simulation Environment

The modeling of water distribution networks in this work is based on linear equation systems. The determination of network pressures, mass flows and temperatures corresponds to the solving of the linear equation systems defined in chapter 3 and 4. The mathematical standard literature provides a large variety of solution approaches based on the appearance of the involved matrices. The compilation of the equation systems and their following calculation is done in MATLAB®. The solution is found by using the *mldivide* (backslash) operator. The factor matrix's structure is sparse, that means that only a few elements of the matrix entries are different from zero. Based on the sparse matrices the backslash function analyzes the linear equation system's structure and selects the appropriate solution algorithm. Due to the unsymmetric and sparse matrix structure the *UMFPACK* routine is used to solve the equation system. This package uses the Unsymmetric MultiFrontal method and sparse LU factorization, for further details see [22].

Chapter 2

Heat Loads

2.1 Energy Demand

The technical and economic efficiency of the of the presented concept is strongly dependent on the heating system's temperature level. The lower the HP's secondary side (house side) supply temperature the better the HP's COP and the less electrical energy is needed to fulfill the consumers heating energy demands. Hence, the presented concept is suited for new and/or refurbished buildings with high building standards. The assumptions considering heating loads in energy values are presented in the following section.

2.1.1 Heating

In Austria the yearly energy consumption of buildings for heating is classified by different building categories. The authors of the report [23] distinguish between *Passivhaus* ($HD \leq 10\,\frac{\mathrm{kW\,h}}{\mathrm{m^2}}$), *Niedrigstenergiehaus* ($HD \leq 25\,\frac{\mathrm{kW\,h}}{\mathrm{m^2}}$) and *Niedrigenergiehaus* ($HD \leq 50\,\frac{\mathrm{kW\,h}}{\mathrm{m^2}}$). The directive in [66] proposes a maximal yearly energy consumption for heating with $54.4\,\frac{\mathrm{kW\,h}}{\mathrm{m^2}}$. In typical Austrian multi-storey and multi-family buildings architects and building service equipment planners calculate with $35\,\frac{\mathrm{kW\,h}}{\mathrm{m^2}}$.

For simulation needs the building's heat demands are determined in an hourly resolution, hence, for every hour within a year a heating power is supplied to the simulation model. The methodology to obtain the heat load's hourly resolution is based on [3], which is a methodology that is also employed for natural gas consumption determination. The authors evaluated statistical data of non load metered natural gas consumers. Due to the fact the database is composed of a large amount of small customers, arbitrary daily fluctuations are averaged out and the results are condensed in the resulting load profiles. The heat generators (HP) in this work supply a big amount of small heat consumers, hence the methodology in obtaining hourly heat load profiles by the presented methodology should be adequate.

The authors in [3] provide qualitative heat load profiles in respect to the ambient temperature

in the range $-20\,°\mathrm{C} < \vartheta_{amb} < 30\,°\mathrm{C}$. There is no information about the energy demand within a day. In determining the daily energy demand for heating the standard $HGT_{20/12}$ in ÖNORM EN 12831 (former ÖNORM B8135), [7] is used. The necessary daily mean value of the ambient temperature is gathered from the online-tool *BizzEE*, [13] for the city of Vienna.

The daily heating power curve's shape is dependend on the building envelope's materials (thermal conductivities and storage capacity). The lower the thermal conductivities of the building's envelope and the higher the storage capacity of the building, the lower is the heating power curve's dynamics. To obtain a qualitative assessment on this circumstances the heating power curve is modified by convolution ($*$) with a function g:

$$\tilde{\dot{Q}}_H = \dot{Q}_H * g \tag{2.1}$$

Furthermore in calculating the heating degree days of a building with enhanced storage capacity the ambient temperature is averaged over three previous days, [3, 9]:

$$\tilde{\vartheta}^d_{amb} = \frac{\vartheta^d_{amb} + 0.5\,\vartheta^{d-1}_{amb} + 0.25\,\vartheta^{d-2}_{amb} + 0.125\,\vartheta^{d-3}_{amb}}{1 + 0.5 + 0.25 + 0.125} \tag{2.2}$$

The normalized heat demand curves of a single day (00:00-24:00) are shown in fig. 2.1.

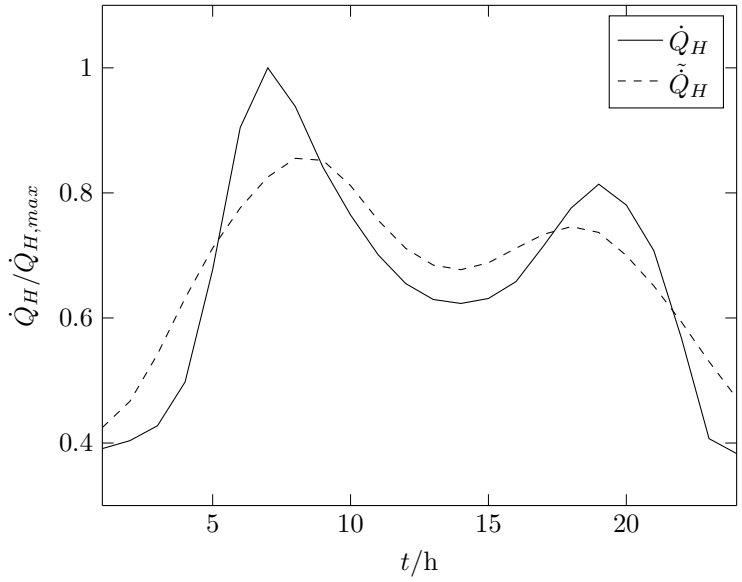

FIGURE 2.1: Standardized heat load profile for 24 hours; solid line: [3], building quality V; dashed line: building quality S

The mean value of the ambient temperature therefore has an impact on the heat load profile's shape (relative daily peak load) and influences the daily energy demand through the heating degree days. The yearly heat load profile is scaled in the way the integral of all the hours within a year equals the total yearly energy demand for heating to be $35\,\frac{\mathrm{kW\,h}}{\mathrm{m^2}}$. The specific heat load

profile is scaled up with the gross floor area to obtain the aggregated heat load for the HP's supply area. The methodology in translating the supply area's heat load profile into the HP's timetable as well as the assumptions considering temperatures and mass flows are shown in chapter 2.

2.1.2 Domestic hot water

Due to the different supply temperatures energy demands related with domestic hot water are considered separately. To obtain higher efficiencies in heating energy deployment the preparation of hot water for heating and domestic hot water are carried out with different heat producers. The hot water demand is highly dependent on subjective comfort of the building's inhabitants, [28]. Furthermore, also national standards have to be taken into account, considering the legionella bacteria issue which is regulated in the ÖNORM B 5019, [6].

The energy efficiency in the production and delivery of domestic hot water is quite poor, see also the building equipment planners guide in [28]. It can be found that the actually used heat energy at the consumer's taps is about 40% lower than the supplied energy. This fact is taken into account when calculating the necessary heat energy supply for DHW preparation. The following table 2.1 shows DHW-demands for different housings:

Table 2.1: DHW consumption for different housing standards and comfort categories

	normal comfort	enhanced comfort	high comfort	
subsidized housing	20	40	40	$\mathrm{l\,Person^{-1}}$
	19.9	37.9	37.9	$\mathrm{kWh\,m^{-2}\,a^{-1}}$
general housing	30	50	50	$\mathrm{l\,Person^{-1}}$
	25.1	41.8	41.8	$\mathrm{kWh\,m^{-2}\,a^{-1}}$
sophisticated housing	40	60	70	$\mathrm{l\,Person^{-1}}$
	29.9	44.9	52.4	$\mathrm{kWh\,m^{-2}\,a^{-1}}$

The previous table is based on the following assumptions: $\vartheta_{dhw,S} = 60\,°\mathrm{C}$; $\vartheta_{dhw,fw} = 12\,°\mathrm{C}$; average number of inhabitants per flat: 2.08; mean apartment size: $75\mathrm{m}^2$ (subsidized housing), $85\mathrm{m}^2$ (general housing), $95\mathrm{m}^2$ (sophisticated housing); 40% distribution heat losses.

An expert interview revealed that a common value for the yearly DHW energy demand is $28\,\frac{kWh}{m^2a}$. Following Austrian building equipment planner's practical experience this value is taken for the following calculations.

Unlike the hourly values of the heat load curve for heating, the heat load curve for DHW is not dependent on the ambient temperature. As shown in [3] there is a dependency on the day of the week. Furthermore the number of supplied customers has to be taken into account, as this has a great impact on the demand side peak load. Here the simultaneity factor presented in [83]

is used. With the number of supplied units n it has the following appearance:

$$SF(n) = 0.4497 + \frac{0.5512}{1 + \left(\frac{n}{53.8438}\right)^{1.7627}} \tag{2.3}$$

2.1.3 Cooling

The determination of the cooling load curve is carried out in analogy to the computation of the heat load profile. Some authors like Schlaisich in [78] or Christenson et al. in [18] used 18.3 °C as the threshold temperature ϑ_C for the calculation of the cooling degree-days (CDD). The calculation was done using the ASHRAE [4] definition:

$$CDD(\vartheta_C) = \delta \sum_{i=1}^{n} (\vartheta_{amb} - \vartheta_C) \qquad \delta = \begin{cases} 1 & \text{if } \vartheta_{amb} \geq \vartheta_C \\ 0 & \text{if } \vartheta_{amb} < \vartheta_C \end{cases} \tag{2.4}$$

The yearly cooling energy demand is assumed like the autors in [18] propose to be proportional to the number of CDD. For Vienna, Austria the absolute value for the yearly cooling energy demand for apartment block buildings was found in the EU funded project Entranze, [94] with 7.4 kWh/m^2. For all the days where $\vartheta_{amb} \geq \vartheta_C$ is true, it is assumed that cooling takes place between 08:00 AM and 07:00 PM including two hours of starting and stopping ramps. This is the methodology how the time-series of cooling loads for the building quality V (see section 1.3) are obtained. To get a qualitative evidence if the hourly resolved heating and cooling heat loads have an impact on the system's performance the second version (building quality S) of the cooling load is assumed to be constant for 24 hours, the yearly energy demand, however, does not change.

2.1.4 Summary

The assumptions considering energy demands for heating, domestic hot water and cooling depend strongly on influence factors like building standards, consumer's comfort, climate, the building's orientation, and sea level. Here typical values for Vienna were chosen. Due to the large range of considered networks, (see 1.4) the generalization for other locations with differing specific heat loads is still possible by considering the aggregated energy demand shown in table 2.2:

TABLE 2.2: Yearly energy demand in respect to the network size

supply area		yearly energy demand in MWh		
number of dwellings	living space in m^2	heating	hot water	cooling
2000	150000	5250	4200	1125
1000	75000	2652	2100	562.5
500	37500	1312.5	1050	281.3
250	18750	656.3	525	140.6

2.2 Supply and Return Temperatures

The methodology in calculating the necessary supply and corresponding return temperatures on the heating HP's secondary side (house side) is demonstrated in this chapter. The resulting temperatures are used for the HP heat load determination in chapter 2.3.1.

The following well known equations determine the heat flow for room heating purposes:

$$\dot{Q}_H = \dot{m}_w \, c_p \, (\vartheta_S - \vartheta_R) = \dot{m}_w \, c_p \, \Delta T_w \tag{2.5}$$

$$\dot{Q}_H = k \, A \, (\vartheta_H - \vartheta_I) = k \, A \, \Delta T_{HT} \tag{2.6}$$

$$\dot{Q}_H \propto (\vartheta_I - \vartheta_{amb}) \tag{2.7}$$

The first equation (2.5) is the heat flux coming from the heating fluid to heat a room, the second one (2.6) characterizes the heat transfer from the fluid to the room and the third one describes a proportionality of the heat flux which leaves the considered space through it's envelope.

The relation of equation (2.5) to the conditions in the design point N [1] and the heating temperature ϑ_H, which is assumed to be $\frac{\vartheta_S+\vartheta_R}{2}$ yields to

$$\frac{\dot{Q}_H}{\dot{Q}_{H,N}} = \frac{\dot{m}_w}{\dot{m}_{w,N}} \, \frac{2(\vartheta_S - \vartheta_H)}{\Delta T_{w,N}} \tag{2.8}$$

The relation of the heat transfer coefficients k is proportional to the relation of the heat-transfer temperature differences with the exponent n:

$$\frac{k}{k_N} = \left(\frac{\Delta T_{HT}}{\Delta T_{HT,N}} \right)^n \tag{2.9}$$

This gives together with equation (2.6)

$$\frac{\dot{Q}_H}{\dot{Q}_{H,N}} = \left(\frac{\Delta T_{HT}}{\Delta T_{HT,N}} \right)^m = \left(\frac{\vartheta_H - \vartheta_I}{\Delta T_{HT,N}} \right)^m \tag{2.10}$$

The elimination of ϑ_H in equation (2.8) with equation (2.10) results in the equation for the supply temperature:

$$\frac{\dot{Q}_H}{\dot{Q}_{H,N}} = \frac{\dot{m}_w}{\dot{m}_{w,N}} \, \frac{2 \left(\vartheta_S - \vartheta_I - \left(\frac{\dot{Q}_H}{\dot{Q}_{H,N}} \right)^{\frac{1}{m}} \, \Delta T_{HT,N} \right)}{\Delta T_{w,N}} \tag{2.11}$$

The dependency on the ambient temperature ϑ_{amb} is hidden in the fraction $\frac{\dot{Q}_H}{\dot{Q}_{H,N}}$:

[1] N indicates the heating system's design point which is defined as the maximum heat load at ambient temperature $\vartheta_{amb} = -15\,^{\circ}\mathrm{C}$.

$$\frac{\dot{Q}_H}{\dot{Q}_{H,N}} = \frac{\vartheta_I - \vartheta_{amb}}{\vartheta_I - \vartheta_{amb,N}} \tag{2.12}$$

It is assumed that the heat load regulation is realized with the change of the supply temperature ϑ_S, hence $\frac{\dot{m}_w}{\dot{m}_{w,N}} = 1$. The final equation for the supply temperature results then in

$$\vartheta_S = \frac{\vartheta_I - \vartheta_{amb}}{\vartheta_I - \vartheta_{amb,N}} \frac{\Delta T_{w,N}}{2} + \vartheta_I + \left(\frac{\vartheta_I - \vartheta_{amb}}{\vartheta_I - \vartheta_{amb,N}} \right)^{\frac{1}{m}} \Delta T_{HT,N} \tag{2.13}$$

For different heating surfaces the heater superscript $m = n + 1$ value is listed in table 2.3.

TABLE 2.3: heating superscripts for different heaters

heating surface	**m**
radiator	1.33
tube (plain)	1.25
convector	1.25-1.45
floor heating	1.1

Eq. (2.13) allows for the determination of the supply temperature if the values in the design point N, the ambient temperature and the heat load are known. Supply and return temperatures in respect to the ambient temperature for floor heating are shown in fig. 2.2. The design temperatures $\vartheta_{S,N}$ and $\vartheta_{R,N}$ are shown in the figure at $\vartheta_{amb} = -15\,°\text{C}$. The desired indoor temperature was set to 25 °C.

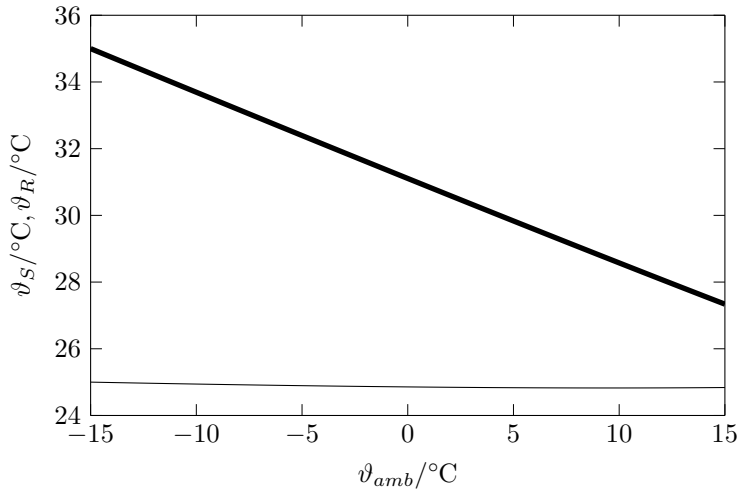

FIGURE 2.2: Supply and return temperatures in respect to the ambient temperature for floor heating

As shown in the equations above, the supply temperature is adjusted in respect to the ambient temperature to fulfill the consumer's heating demand. Due to the heating superscript m close

to 1 the return temperature shows only a weak dependency on the ambient temperature.

2.3 Hydraulic implementations

Hot water preparation is assumed here to take place by heat pumps. To decouple the heat production from the consumer's demand each HP is connected to a hot water storage tank. The methodology in determining the HP's load curve in an hourly resolution by adapting the building's heat load curve is shown in the following.

2.3.1 Heating

The building's heating systems consist of a heat pump - buffer storage combination. The heat load control in respect to the ambient temperature takes place by changing the heating fluid's supply temperature T_S. For that purpose return water is mixed through a valve with hot water deriving from the HP and/or the hot water storage tank. Fig. 2.3 shows a simplified configuration of the necessary hydraulic components for room heating. The visualization of control components is omitted here.

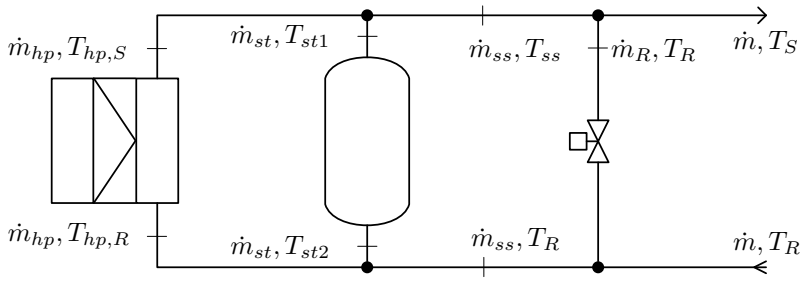

FIGURE 2.3: Heating HP's hydraulic implementation on the building side

As the heat pump is the connection point to the ring network, the main objective of this chapter is to translate the building's heat demand into a time dependent HP load curve. Therefore a simple equation system for the heating system is shown in the following. By applying mass balance and energy conservation equations on the pipes and nodes of fig. 2.3 an equation system (2.14) is obtained. It is used for the determination of the HP's heat load curve in respect to the required supply and return temperatures, the heat load and the ambient temperature. Note that the equation system changes slightly as the water storage's operating mode is changed from charging to discharging.

The mathematical representation of the water storage tank in the equation system (2.14) is a model based on the work of *Falkner*, [25]. It is a transient model based on a finite volume method of a thermally stratified storage tank with consideration of heat losses through the storage's envelope. The model was tested with standardized test function and is able to provide the storage tank's vertical temperature distribution as well as storage efficiencies.

$$EQS^H : \begin{cases} i: & \dot{m}_{ss} + \dot{m}_R = \dot{m} \\ ii: & \dot{m}_{ss}\, T_{ss} + \dot{m}_R\, T_R = \dot{m}\, T_S \\ iii: & \dot{Q}_H = \dot{m}\, c_p\, (T_S - T_R) \\ iv: & \dot{Q}_{hp} = \dot{m}_{hp}\, c_p\, (T_{hp,S} - T_{hp,R}) \\ v: & \begin{cases} \dot{m}_{st} + \dot{m}_{ss} = \dot{m}_{hp} & \text{charge} \\ \dot{m}_{st} + \dot{m}_{hp} = \dot{m}_{ss} & \text{discharge} \end{cases} \\ vi: & \begin{cases} \dot{m}_{hp}\, T_{hp,R} = \dot{m}_{st}\, T_{st2} + \dot{m}_{ss}\, T_R & \text{charge} \\ \dot{m}_{ss}\, T_{ss} = \dot{m}_{st}\, T_{st1} + \dot{m}_{hp}\, T_{hp,S} & \text{discharge} \end{cases} \\ vii: & \begin{cases} T_{st1} = T_{hp,S} & \text{charge} \\ T_{st2} = T_R & \text{discharge} \end{cases} \\ viii: & \begin{cases} T_{ss} = T_{hp,S} & \text{charge} \\ T_{hp,R} = T_R & \text{discharge} \end{cases} \\ ix: & \begin{cases} T_{st2} = T_{st2}(T_{st1}, \dot{m}_{st}) & \text{charge} \\ T_{st1} = T_{st1}(T_{st2}, \dot{m}_{st}) & \text{discharge} \end{cases} \end{cases} \tag{2.14}$$

The system's behavior is described with this equation system. The variables T_S and T_R in respect to the ambient temperature were found by the method shown in section 2.2. With a given storage tank size and the heat demand $\dot{Q}_H$ the HP's heat load curve is determined. To avoid hourly oscillations in the HP's operation the HP's heat load curve is allowed to change every 8 hours. This results in three heat load states of the heat pump during one day. The quantitative values of these three heat load states are found by a numerical optimization. The permitted interval of the heat load states is defined as $0.7\,\bar{\dot{Q}}^i < \bar{\dot{Q}}^i < 1.3\,\bar{\dot{Q}}^i$ with $\bar{\dot{Q}}^i$ being the average heat load during the day i:

$$\bar{\dot{Q}}^i = \frac{1}{24} \sum_{t=1}^{24} \dot{Q}_t^i$$

To account for the minimum possible part load operation of the HP another constraint is applied to the optimization:

$$\max\left(0.7\,\bar{\dot{Q}}^i;\, 0.25\,\dot{Q}_{hp,max}\right) < \bar{\dot{Q}}^i < \min\left(1.3\,\bar{\dot{Q}}^i; \dot{Q}_{hp,max}\right)$$

Note that the part load factor here is set to 25%. It is assumed that every HP module consists of two independent HPs of whose each one has a minimum possible part load factor of 50%.

The variable to be minimized by the optimization algorithm is the standard deviation of the vertical temperature distribution inside the storage tank. This optimization procedure assures a stable temperature distribution in the storage tank and avoids mixing due to poor storage volume utilization.

2.3.2 Domestic Hot Water

The DHW-preparation HP's hydraulic implementation and the required components are shown in the following fig. 2.4:

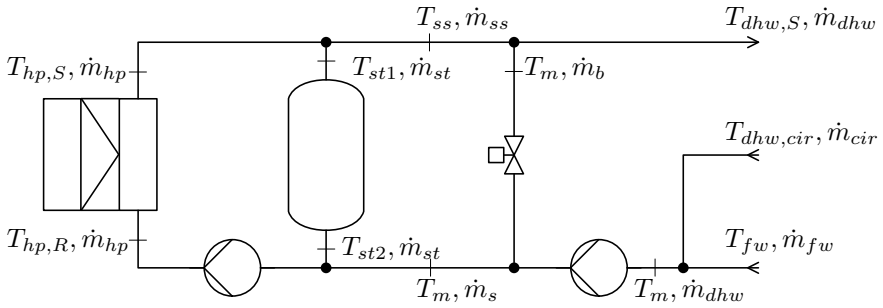

FIGURE 2.4: Domestic hot water HP's hydraulic implementation on the building side

To obtain temperatures, mass flows and storage capacities mass balance and energy conservation equations are applied to the hydraulic scheme, which yield the equation system EQS^{DHW}.

$$
EQS^{DHW} = \begin{cases}
i: & \dot{Q}_{hp} = \dot{m}_{hp}\, c_p\, (T_{hp,S} - T_{hp,R}) \\
ii: & \dot{Q}_{cir} = \kappa\, \dot{Q}_{dhw} \\
iii: & \dot{Q}_{cir} = \dot{m}_{cir}\, c_p\, (T_{dhw,S} - T_{dhw,R}) \\
iv: & \Delta T_{cir} = T_{dhw,S} - T_{dhw,cir} \\
v: & \dot{m}_{cir}\, T_{dhw,cir} + \dot{m}_{fw}\, T_{fw} = \dot{m}_{dhw}\, T_m \\
vi: & \dot{Q}_{dhw} = \dot{m}_{dhw}\, c_p\, (T_{dhw,S} - T_m) \\
vii: & \dot{m}_{dhw} = \dot{m}_{cir} + \dot{m}_{fw} \\
viii: & \dot{m}_{dhw}\, T_{dhw,S} = \dot{m}_b\, T_m + \dot{m}_{ss}\, T_{ss} \\
ix: & \dot{m}_{dhw} = \dot{m}_{ss} + \dot{m}_b \\
x: & \begin{cases} \dot{m}_{ss}\, T_m + \dot{m}_{st}\, T_{st2} = \dot{m}_{hp}\, T_{hp,R} & \text{charge} \\ T_{hp,R} = T_m & \text{discharge} \end{cases} \\
xi: & \begin{cases} T_{st2} \approx T_{st2}\,(\dot{m}_{st}) & \text{charge} \\ T_{st1} \approx T_{st1}\,(\dot{m}_{st}) & \text{discharge} \end{cases} \\
xii: & \begin{cases} T_{st1} = T_{hp,S} & \text{charge} \\ T_{st2} = T_m & \text{discharge} \end{cases} \\
xiii: & \begin{cases} \dot{m}_{hp} = \dot{m}_{ss} + \dot{m}_{st} & \text{charge} \\ \dot{m}_{ss} = \dot{m}_{hp} + \dot{m}_{st} & \text{discharge} \end{cases} \\
xiv: & \begin{cases} T_{ss} = T_{hp,S} & \text{charge} \\ \dot{m}_{st}\, T_{st1} + \dot{m}_{hp}\, T_{hp,S} = \dot{m}_{ss}\, T_{ss} & \text{discharge} \end{cases}
\end{cases}
\tag{2.15}
$$

The storage tank in fig. 2.4 acts as a hydraulic separator which connects the hot water production with it's distribution. Here the HP is connected directly to the system, due to the HP's working fluid it could be necessary to add a secondary circuit between HP and DHW storage tank. In determining the optimal storage tank size and HP's heating power for every time step the proposed equation system is solved with the following boundary conditions:

Circulation losses: $\kappa = 30\,\%$

Circulation temperature drop: $\Delta T_{cir} = 3\,K$

Supply temperature: $T_{dhw,S} = 55\,°\mathrm{C}$

Fresh water inlet temperature: $T_{fw} = 10\,°\mathrm{C}$

HP delivery temperature: $T_{hp,S} = 60\,°\mathrm{C}$

Storage tank geometry ratio: $\frac{h_{st}}{d_{st}} = 2$

Due to the legionella regulations the HP's supply temperature is set to 60 °C, therefore, if necessary, the whole DHW-system can be flooded periodically with hot water.

Here, a two-staged design process for the determination of the hot water tank capacity and necessary HP heat load is used. The overall aim is to get a smooth heat pump load during the whole operational period. First, the necessary storage tank volume is calculated with the mean value of the DHW-heat demand by solving the equation system on a hourly basis. As the DHW-demand is not dependent on seasons but only on weekdays, the observation period $0 < t < \tau$ of two weeks with $n = 336$ hours is satisfactory for the DHW-system design.

The storage tank's volume is minimized with the following objective function:

$$\begin{aligned} \min_{\chi} \quad & V_{st}^{dhw}(\dot{Q}_{hp}(\chi), \dot{Q}_{dhw}(t), \vartheta_{dhw,S}, \vartheta_{dhw,cir}, \ldots) \\ \text{subject to} \quad & \vartheta_{st}^{top}(t) \geq \vartheta_{dhw,s},\ t = 1, \ldots, \tau. \end{aligned} \tag{2.16}$$

with

$$\dot{Q}_{hp} = \frac{\chi}{\tau} \sum_{t=0}^{\tau} \dot{Q}_{dhw}(t) = const. \tag{2.17}$$

The factor $\chi > 1$ here is an additional charge to the mean value of the DHW heat load that is necessary because of mixing effects at the storage's inlet, as well as heat losses through the storage wall.

The result of the simple optimization problem presented in (2.16) is the smallest possible storage volume for a given DHW load curve considering a constant HP load and the storage tank's periphery. Since the equation system contains also the mass flux $\dot{m}_{hp}$ for the heat pump, a design value for the hydraulic pump's feed rate $\dot{m}_{hp}^{N}$ is obtained. This is the input for the second optimization step. A constant HP's load was assumed in equation (2.17). If the storage

tank is completely filled with hot water the storage tank's bottom temperature and subsequently the HP's return temperature $\vartheta_{hp,R}$ rises. Since the HP's load as well as it's supply temperature remain constant, $\dot{m}_{hp}$ will increase consequently. Due to the limited flow rate capacity of the hydraulic pump that supplies the HP with cold water there is needed some kind of control strategy to address this issue. For this a part load factor, $\phi < 1$, is introduced here. The formerly constant $\dot{Q}_{hp}$ evolves to the vector $\dot{\boldsymbol{Q}}_{\boldsymbol{hp}}$, which contains the $\dot{Q}_{hp}$ values for every time step $0 < t < \tau$. The second step in finding the minimal storage tank capacity and the related DHW HP's heat load curve is defined with the following optimization problem:

$$\begin{aligned} \min_{\chi,\phi} \quad & V_{st}^{DHW}(\dot{\boldsymbol{Q}}_{\boldsymbol{hp}}(\chi,\phi,t), \dot{Q}_{DHW}(t), \vartheta_{dhw,s}, \vartheta_{dhw,c}, \ldots) \\ \text{subject to} \quad & \vartheta_{st}^{top}(t) \geq \vartheta_{dhw,s},\ t = 1,\ldots,\tau. \\ & \dot{m}_{hp}(t) \leq 1.1\,\dot{m}_{hp}^{N},\ t = 1,\ldots,\tau. \end{aligned} \tag{2.18}$$

with

$$\dot{\boldsymbol{Q}}_{\boldsymbol{hp}}(t+1) = \begin{cases} \dot{Q}_{hp} & \text{if } t = 1 \\ \dot{\boldsymbol{Q}}_{\boldsymbol{hp}}(t)\,\phi & \text{if } \vartheta_{st,2}(t) > \vartheta_{limit} \\ \dot{\boldsymbol{Q}}_{\boldsymbol{hp}}(t) & \text{otherwise} \end{cases} \tag{2.19}$$

The presented control strategy in (2.19) is a two-point control with hysteresis. If the trigger temperature ϑ_{limit} at the bottom of the storage is reached, which means the storage tank is filled with hot water and would lead to an increase of $\dot{m}_{hp}$, the HP throttles to part load. The HP's hydraulic pump's maximal mass flow is allowed to reach 110% of the design massflow $\dot{m}_{hp}^{N}$ obtained from (2.16).

2.4 Thermal Energy Central

The energy demand for heating, domestic hot water and cooling needs to be satisfied by hot/cold thermal energy generators. For the heating and DHW loads two distinct heat pumps are employed, the cooling loads are covered by the seasonal energy storage (BTES). This chapter presents a flow chart that connects the necessary components to fulfill the consumer's energy demands. The combination of two heat pumps for heating and one plate heat exchanger for cooling purposes which make up the building's thermal energy central is presented in fig. 2.5.

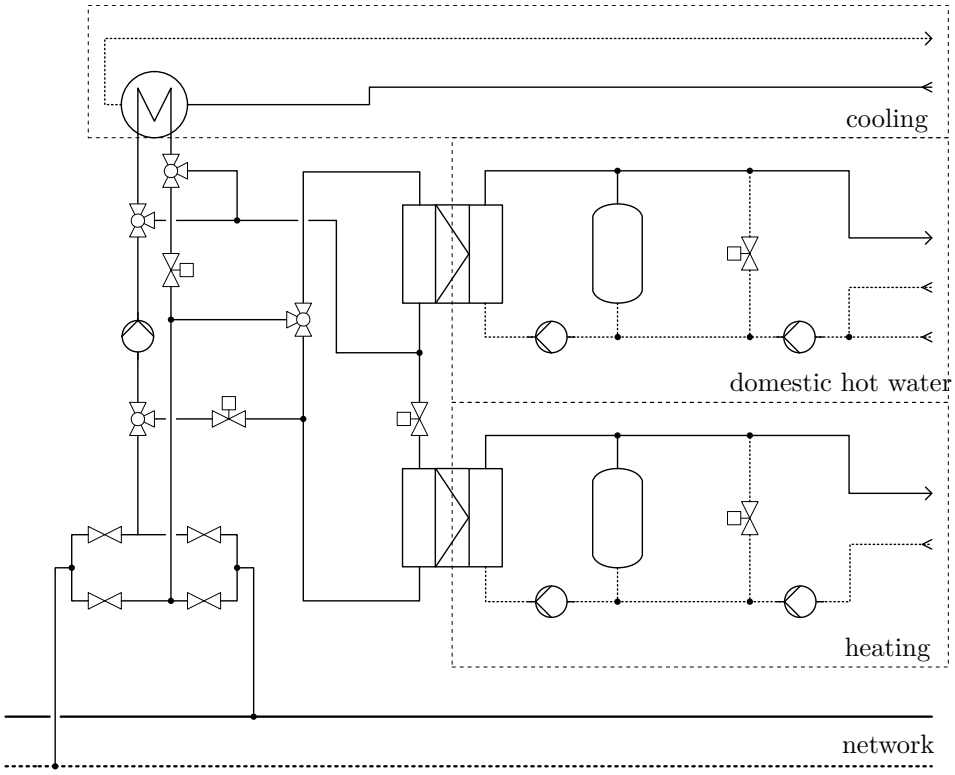

FIGURE 2.5: Simplified energy central hydraulic diagram

The four valves that connect the building to the network enable for the seasonal switch between heating and cooling mode. In winter the heating central's main pump extracts warm water from the network and charges chilled water back to the grid. In summer times the cooling heat exchanger heats up the extracted cold water and delivers warm water to the network and further on to the storage system. The proposed configuration enables for three operating modes:

- winter: *heating* and *domestic hot water* production is active ($\dot{Q}_H \neq 0$; $\dot{Q}_{dhw} \neq 0$; $\dot{Q}_C = 0$)
- transition period: *domestic hot water* production only ($\dot{Q}_H = 0$; $\dot{Q}_{dhw} \neq 0$; $\dot{Q}_C = 0$)
- summer: *domestic hot water* production and *cooling* active ($\dot{Q}_H = 0$; $\dot{Q}_{dhw} \neq 0$; $\dot{Q}_C \neq 0$)

During the summer months when cooling is active the building provides a heat source and requires on the other hand a heat source for the production of DHW. In that case it is assumed, that the thermal energy central provides/receives the resulting heat flow of the building's heat balance to/from the network. Warm water coming from the cooling heat exchanger is distributed directly to the DHW-HP before flowing back to the network. The limitation for the summer mode is $\dot{Q}_{dhw}(t) < \dot{Q}_C(t)$, which is, as seen in the previous chapters given.

Thermal power control within the heat sinks (HP) and heat sources (PHE) inside the buildings is realized with a fixed cooling/heating rate of the network water. The temperature difference between inlet and outlet of these components is assumed to be always $\Delta T = \Delta T_C = \Delta T_{hp}^{dhw} = 4K$. All build in pumps and valves used to control the thermal power are assumed to provide/handle the necessary mass flow to assure the achievement of the given heat demand. The seasonal temperature fluctuation within the network pipes is owed to the seasonal heat storage system, whose model description can be found in chapter 4.

2.4.1 Summer Operation

The energy centrals switch to summer operation mode if there is a cooling demand, i.e. if $\dot{Q}_C > 0$. In that case cold water is needed, hence water is tapped from the network's cold pipe. Depending on the characteristics of the domestic hot water and cooling demand two different operation modes can be identified. They are shown in fig. 2.6:

- Summer Mode I: $\dot{Q}_C > \dot{Q}_{dhw}^e$ if $\Delta T_C = \Delta T_{hp}^{dhw} \Rightarrow \dot{m}_C > \dot{m}_{hp}^{dhw}$
- Summer Mode II: $\dot{Q}_C < \dot{Q}_{dhw}^e$ if $\Delta T_C = \Delta T_{hp}^{dhw} \Rightarrow \dot{m}_C < \dot{m}_{hp}^{dhw}$

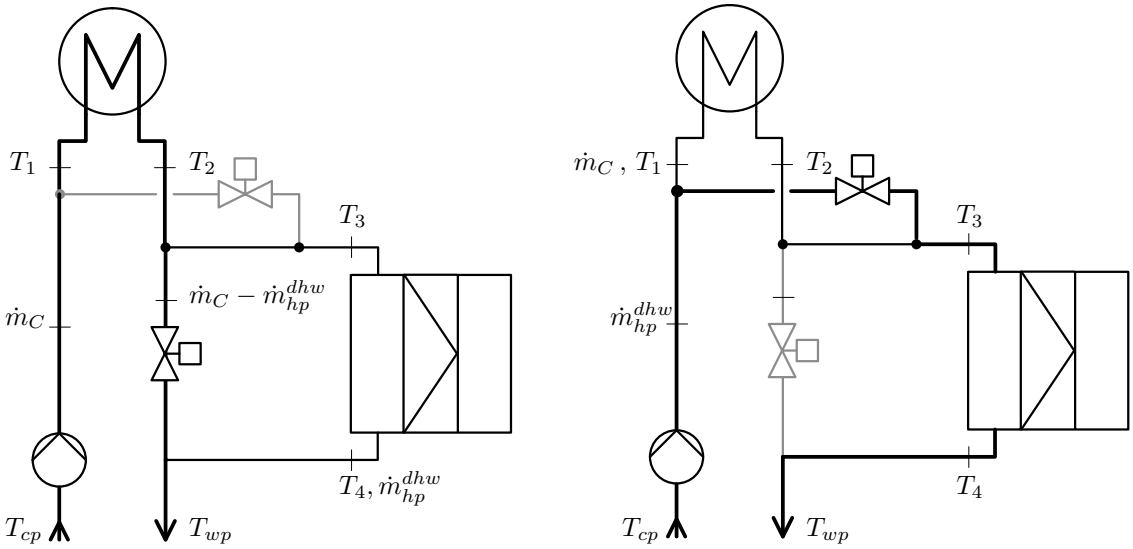

(A) Summer Mode I: $\dot{m}_C > \dot{m}_{hp}^{dhw}$ (B) Summer Mode II: $\dot{m}_C < \dot{m}_{hp}^{dhw}$

FIGURE 2.6: Summer operation modes, DHW HP (right) and cooling heat exchanger (top)

The inlet temperature for the network T_{wp} is obtained using the following relationship:

$$T_{wp} = \begin{cases} T_{cp} - \frac{\dot{m}_{hp}^{dhw}}{\dot{m}_C} \Delta T_{hp}^{dhw} + \Delta T_C & \text{for Summer Mode I} \\ T_{cp} + \frac{\dot{m}_c}{\dot{m}_{hp}^{dhw}} \Delta T_C + \Delta T_{hp}^{dhw} & \text{for Summer Mode II} \end{cases} \tag{2.20}$$

with

$$\dot{m}_C = \frac{\dot{Q}_C}{c_p \, \Delta T_C}$$

$$\dot{m}_{hp}^{dhw} = \frac{f \, \dot{Q}_{dhw}}{c_p \, \Delta T_{hp}^{dhw}} = \frac{\dot{Q}_{dhw}^{e}}{c_p \, \Delta T_{hp}^{dhw}}$$

$$f = 1 - \frac{1}{\epsilon_{hp} \, COP_{ca}}$$

$$COP_{ca} = \begin{cases} \frac{T_S^{dhw} + \Delta T_{hp}}{T_S^{dhw} + 2\,\Delta T_{hp} - T_4} & \text{for Summer Mode I} \\ \frac{T_S^{dhw} + \Delta T_{hp}}{T_S^{dhw} + 2\,\Delta T_{hp} - T_H} & \text{for Summer Mode II} \end{cases}$$

For the latter case an equation system for T_{wp} and $\dot{m}_{hp}^{dhw}$ has to be solved. Due to the low supply temperature for the heat pump's evaporator in Summer Mode II the COPs is low. It would be more efficient in that case to tap water from the warm network pipe (winter operating mode). To avoid permanent switching from winter to summer mode and since $\dot{Q}_C > \dot{Q}_{dhw}^{e}$ is true for the majority of one summer day's this efficiency loss for a small number of hours is accepted.

2.5 Heat pump model

In this work the hot water production for heating and domestic hot water is assumed to be executed by compression heat pumps. Existing systems in Switzerland use primarily ammonia (R717) as refrigerant. Due to the relatively low normal boiling point of 33.2 °C, the elevated critical temperature 132.3 °C and it's high volumetric refrigerating capacity, [84], R717 suits well for the requirements within the proposed system.

Every heating central consists of two distinct heat pumps. One for the production of water for room heating with lower temperatures as the other one for the DHW production. Due to the ability of being able to throttle the HP's output heat flow the heating HP is assumed to consist of two distinct heat pumps. Standardized heat pumps available on the market have part load capacities of min. $40-50\%$. Therefore, the minimum possible part load for the proposed system is assumed to be 25% which fits well to the ambient temperature dependent heating limit, (see

chapter 2.1.1).

Within the simulation environment the HP's performance, in terms of Coefficient of Performance (COP) is calculated depending on the evaporator's inlet temperature $T_{e,in}$, it's cooling rate ΔT_e and the condenser's inlet and outlet temperatures $T_{c,in}$ and $T_{c,out}$. The efficiency factor ϵ_{hp} which in literature is sometimes also referred to as *thermodynamic perfectibility*, [81], is a depreciation factor for the inverse of the ideal Carnot cycle efficiency to obtain the actual (real) COP. The efficiency factor is defined as follows:

$$\epsilon_{hp} = \frac{COP_{real}}{COP_{ca}} \tag{2.21}$$

with the carnot cycle efficiency

$$\eta_c = 1 - \frac{T_{f,min}}{T_{f,max}} = \frac{1}{\epsilon_{hp}} \tag{2.22}$$

it follows for the actual COP

$$COP_{real} = \frac{\epsilon_{hp}}{1 - \frac{T_{e,in} - \Delta T_e - \Delta T_{hex}}{\frac{T_{c,in} + T_{c,out}}{2}}} \tag{2.23}$$

Oluleye provides in [63] value ranges from $0.3 - 0.8$ for the efficiency factor ϵ_{hp}. Some national research projects in Germany and Austria found the efficiency factor for ammonia heat pumps to be between 0.4 and 0.57, [60]. Ochs et al. provide a diagram in [61] where the efficiency factor for ammonia heat pumps at low condenser temperatures is above 60%. Due to the small yearly temperature variations on the heat source (evaporator) and heat sink (condenser) the efficiency factor for the simulations executed within this work is assumed to be 55%.

The required mass flow the network has to supply for a given HP heat load $\dot{Q}_{hp}$ is calculated with:

$$\dot{m}_e = \frac{\dot{Q}_{hp}\ (COP_{real} - 1)}{COP_{real}\, c_{p,w}\, \Delta T_e} \tag{2.24}$$

The HP model requires the network temperature, heat load and the condenser temperatures and provides the necessary mass flow, the return temperature to the network and the electrical power demand in terms of COP. Fig. 2.7 provides the black-box model used here for the HP performance calculation.

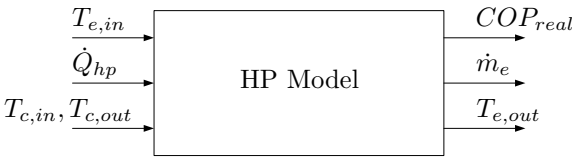

FIGURE 2.7: Black-box HP model

2.6 External Thermal Energy Source

The thermal energy demand for heating purposes (heating and domestic hot water) for residential buildings located in Austria is in general higher than the necessary cooling amount of energy during summer time. Therefore there is a need for an external thermal energy source which provides thermal energy to the network. The preconditions for such a heat source is the ability to supply water in the temperature range of approx. 8 to 25 °C. Of course also higher water temperatures are possible, in this configuration it is assumed, that the temperature difference between the cold and the warm pipe of the network is 4K. Hence, the external thermal energy supplier receives cold water from the network and feeds it back with a temperature difference of 4K. The time sequence of thermal energy delivery by the external thermal energy source is determined in this section.

Starting point is the aggregated thermal power demand $\dot{Q}_D(t)$ of all the connected thermal energy customers. The sign of $\dot{Q}_D(t)$ is > 0 for heating and < 0 for cooling. The subsequent integration of the thermal load time series yields the system's aggregated energy demand curve:

$$E_D(t) = \int_0^t \dot{Q}_D(t)\, dt \quad t = 1...t_n \tag{2.25}$$

The last point of E_D, $E_D(t = t_n)$ is, due to the surplus of heating demand in respect to cooling thermal energy demand, greater than zero. If the external thermal energy supplier is assumed to deliver at a constant heat rate during $t = 1...t_n$ the necessary amount of external heat supply is determined as follows:

$$\dot{Q}_{ext} = -\frac{E_D(t_n)}{t_n} = const. \tag{2.26}$$

and

$$E_{ext}(t) = \int_0^t \dot{Q}_{ext}\, dt \quad t = 1...t_n \tag{2.27}$$

The new balanced aggregated energy curve of the system is calculated with respect to the external thermal energy source, Fig. 2.8:

$$E^B(t) = \int_0^t (\dot{Q}_D(t) + \dot{Q}_{ext})\, dt \quad t = 1...t_n \tag{2.28}$$

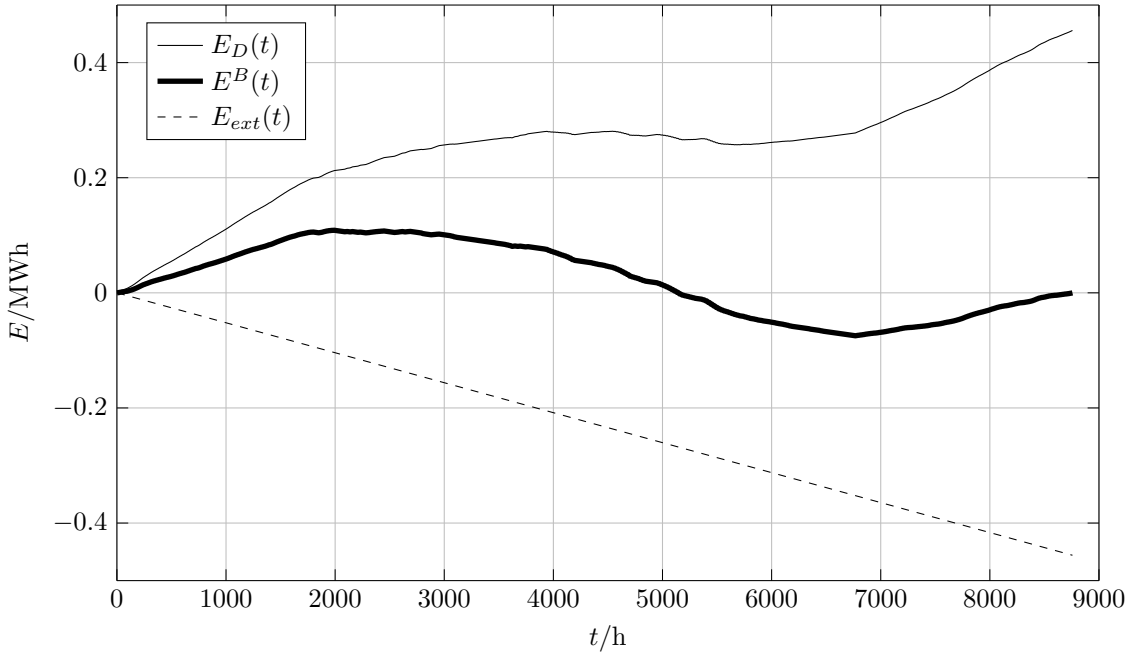

FIGURE 2.8: Determination of the balanced cumulative energy curve

The balanced aggregated energy curve shows the system's energy demand for one year and is related to the seasonal storage's aggregated energy curve. If there was no seasonal thermal energy storage the supplier would have to supply at every time exactly the same amount of energy that is used by the customers. Due to the fact that in reality the capacity of the external energy supplier in therms of heating rate is limited and in general smaller than the network's peak load, the seasonal heat storage helps in smoothing the supplier's heat load. The time intervals when the TES gets charged or discharged are equal to the sign of the balanced aggregated energy curve's slope. Hence, in winter times the TES gets discharged and starts charging in the transition period between winter and summer. During summer time the system continues in charging until discharging starts again in autumn. The effective TES aggregated energy curve depends on the boreholes number as well as their geometry and the thermophysical properties of the soil. The difference between TES aggregated energy curve and the network's balanced aggregated energy curve is an indicator for the temperature glide during the operational time. Here a borehole thermal energy storage (BTES) is used as a seasonal heat storage. In order to obtain a smooth aggregated BTES energy curve the external thermal energy source's heating rate is provided to the simulation. After the determination of $E^B(t)$ with equations (2.25) - (2.28) a sinus regression of the form

$$f(t) = \sum_{i=1}^{3} a_i \, \sin(b_i \, t + c_i)$$

is applied to $E^B(t)$ and transforms it to $\widehat{E}^B(t)$. Since $E_D(t) + E_{ext}(t) \approx \widehat{E}^B(t)$ the external thermal energy source's heat rate can be calculated with:

$$\dot{\widehat{Q}}_{ext}(t) = \frac{d(\widehat{E}^B(t) - E_D(t))}{d\,t} \tag{2.29}$$

Fig. 2.9 shows the appearance of $\dot{\widehat{Q}}_{ext}(t)$ if a sinus regression on the system's aggregated energy curve is applied.

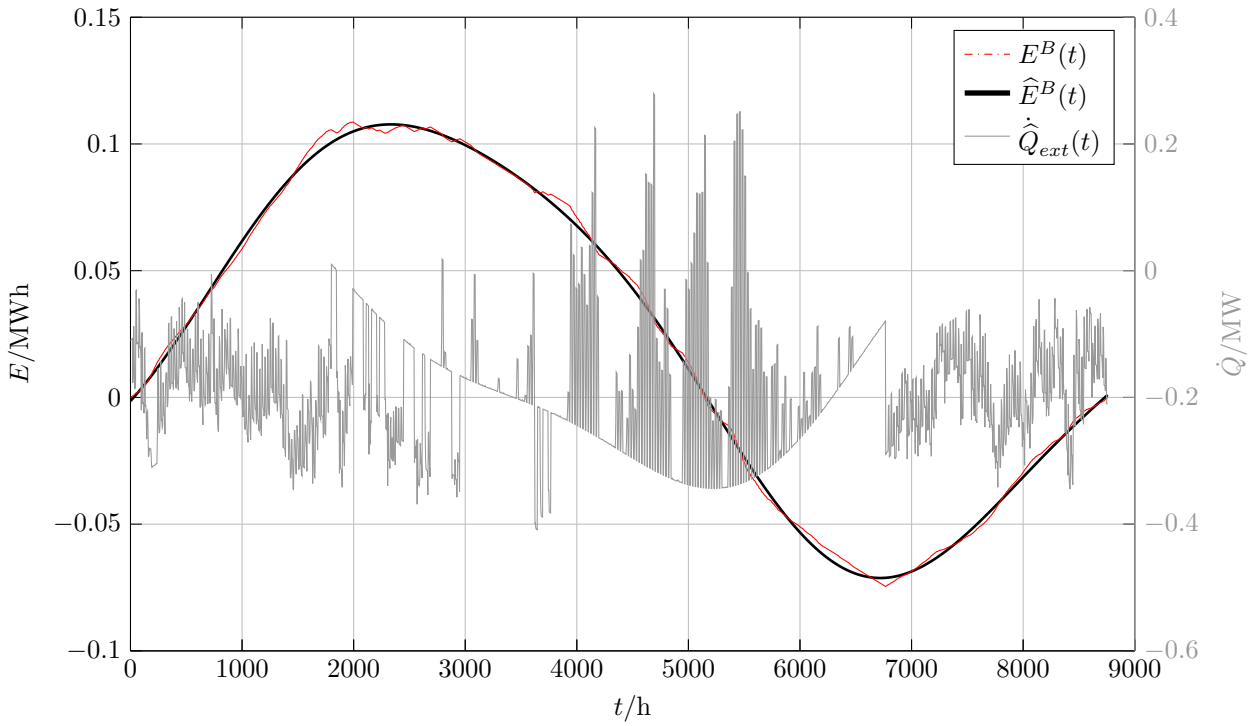

FIGURE 2.9: Methodology in obtaining the time series for the external heat rate $\dot{\widehat{Q}}_{ext}(t)$ (right side ordinate) and yearly cumulative energy curves (left side ordinate)

Note that in summer $\dot{\widehat{Q}}_{ext}(t)$ becomes > 0. That means that the external thermal energy source has to cool the network's water. In the following positive values of $\dot{\widehat{Q}}_{ext}(t)$ are not allowed and hence, small deviations from the ideal sinus regression are permitted.

Chapter 3

Water Network

This chapter gives an overview over the terms which are used in this work associated to the water network. After a general overview over district heating network theory the equations and numerical methods for the hydraulic and thermal network calculation are shown.

3.1 Overview

The *network* consists of a pair of thermally uninsulated pipes, one carries warm water and the other one cold water. In the following this two sets of pipes are referred as *warm pipe* and *cold pipe*. The temperature difference between the warm pipe and the cold pipe is approx. 4 K. This is due to the heat exchangers that provide and extract thermal energy to/from the network. This heat exchanging units are temperature difference controlled with a set point of 4 K.

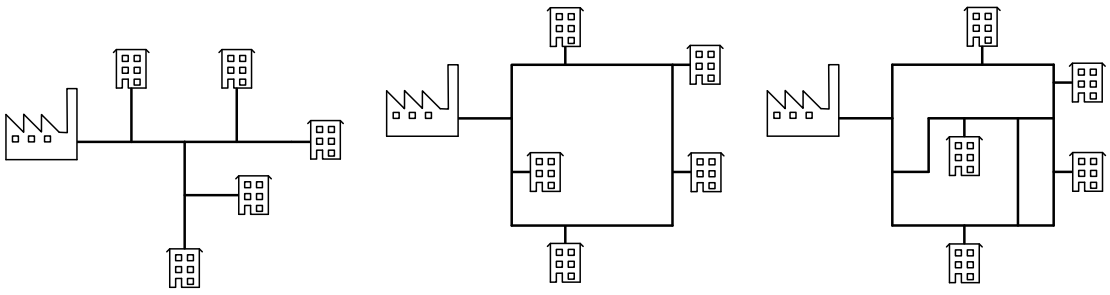

(A) Tree network (B) Ring network (C) Mesh network

FIGURE 3.1: District heating network topologies

The network interconnects different heat customers and a seasonal thermal energy storage, here a borehole thermal energy storage, see chapter 4. In the context of district heating networks

different network topologies are possible. The three network topologies depicted in Fig. 3.1 are the possible ones for district heating networks. For Ground Coupled Heat Pump systems (GCHP) the ring or meshed network topology (3.1b, 3.1c) is the most common one. Due to the relatively small number of heat consumers within this work the ring network topology is used here.

In conventional district heating networks the water pressure is controlled with the main pump which is placed usually near the heat generator. Setpoint for the pump is the differential pressure at one or more distinct network points. This setpoint is usually a customer which is located far away from the heat supplying facility and/or generally is difficult to steadily supply with warm water. The main pump pressurizes the whole network so that the single customers can tap water from the network by simly opening a valve. The pressure in the supply line, which corresponds to the warm pipe lies in every network point above the return line pressure, see Fig 3.2.

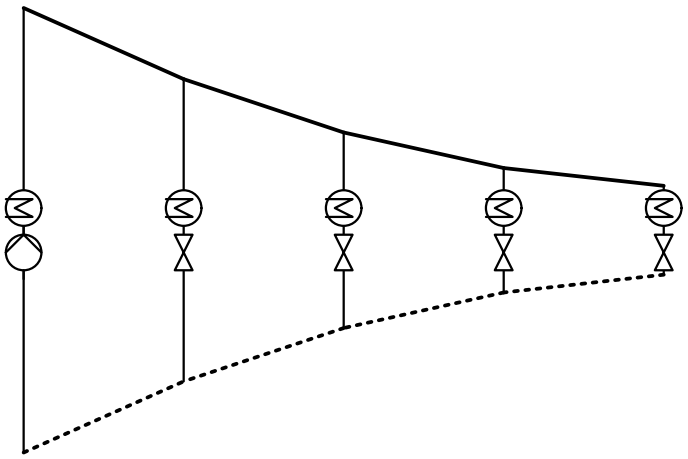

FIGURE 3.2: Pressure control in conventional district heating networks, left: main hydraulic pump and heat generator, center: heat customers, right: differential pressure setpoint

The presented Ground Coupled Heat Pump (GCHP) system does not have only one main hydraulic pump, instead every network end point (customers and suppliers) has a hydraulic pump. This network end points are called in the following *prosumers*, which is an artificial word built by producers and consumers. Heat customers can either extract warm water from the network during winter months to feed the heat pump's evaporators or feed warm water into the network during summer months when the buildings have a cooling load greater than zero. Hence heat flows in both directions are possible. Note that in every network configuration there is one prosumer that acts only as a heat supplier to the network. That special prosumer in the following is referred to as the *supplier*. The physical shape of the prosumer is the *energy central* which is described in section 2.4. Within the energy central water is tapped from the network through a hydraulic pump. The main pump in conventional district heating networks from fig. 3.2 is replaced with a number of smaller hydraulic pumps which are located inside the energy centrals inside the connected buildings. The appearance of the differential pressure between warm pipe

and cold pipe strongly depends on the heat loads of each and every connection point as well as on the pipe dimensions. Fig. 3.3 shows one possible pressure field of a ring network.

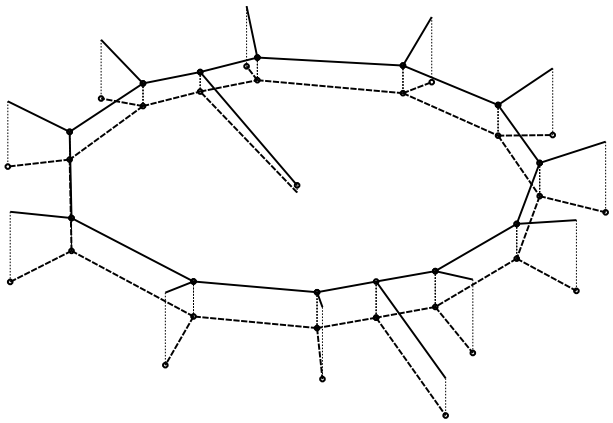

FIGURE 3.3: Qualitative network pressure conditions for the summer cooling mode. The bullets denote the pipe's outlet nodes

Some possible pressure distributions along the network are shown in fig. 3.4. The figure shows different configurations whether the prosumers tap the water in the pumping mode or valve mode during heating seasons. The underlying network configuration is the ring network, hence the most right point of the figures 3.4a-3.4d corresponds to the most left point, respectively, and represents the BTES. The BTES itself in hydraulic point of view is a passive element, that means that the flow through the BTES can not be set with any pump or valve. It acts as a mass-flow balancing element which provides or consumes the difference of consumed and provided warm pipe mass flow. Therefore, the BTES mass flow can be calculated with the following simple equation:

$$\dot{m}_{BTES} = \sum \dot{m}_{supply} - \sum \dot{m}_{demand}$$

The BTES can act either as a heat sink ($\dot{m}_{BTES} > 0$) or heat source ($\dot{m}_{BTES} < 0$), depending whether it is fed with the warm or the cold water pipe. A qualitative assessment of the pressures in the cold and hot pipe for the previously mentioned cases is given in fig.3.4a and fig.3.4b. Note that water is always flowing from higher to lower absolute pressure values, hence the slope of the solid and dashed lines give information about the pressure drops along the pipe network. Depending on the supplier's distance to the network it can also be possible that the pressure drop along the pipe that connects the ring network with the supplier becomes large. Since the pressure at the supplier's connection point in the cold pipe is smaller than the warm pipe's pressure the supplier needs a hydraulic pump to deliver warm water to the network. This situation again with the two possible BTES operation modes are shown in fig.3.4c and fig.3.4d. Note that as the BTES acts like a consumer due to the increased mass flow the pressure drop in the warm pipe

in the tube between the supplier (center) to the first consumer is larger in fig.3.4d in respect to fig.3.4c. As high water flow velocities induce high pressure losses which affect due to the ring network topology the whole network, the pipe diameters have to be designed properly. For this purpose the network is designed by diameter related specific pressure losses. The literature provides a range of different values. Schmitt et al. assume in [80] 80-150 $\frac{\text{Pa}}{\text{m}}$, Thalmann et al. 150-200 $\frac{\text{Pa}}{\text{m}}$, [86] and the pipe manufacturer Isoplus 60-80 $\frac{\text{Pa}}{\text{m}}$ specific pressure losses. *Dalla Rosa* proposes in [21] a methodology for the pipe design in relation with low energy district heating. The insulation thickness for $4GDH$ systems can be chosen by a procedure shown in [54]. The pipes used here are simple, uninsulated PE pipes. Due to the small temperature difference between warm and cold pipe and the related higher volume flows the lowest value is taken for the design of the pipe network.

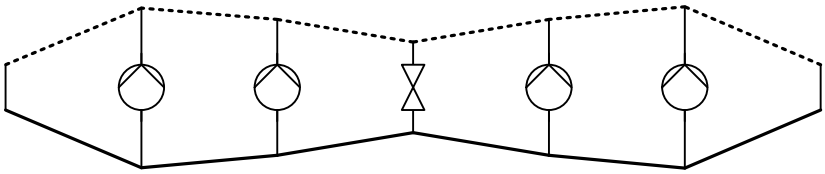

(A) BTES: discharging ($\dot{m}_{BTES} < 0$), Supplier: valve mode

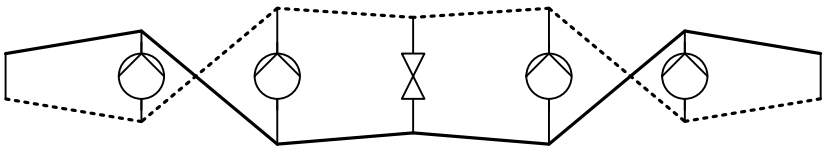

(B) BTES: charging ($\dot{m}_{BTES} > 0$), Supplier: valve mode

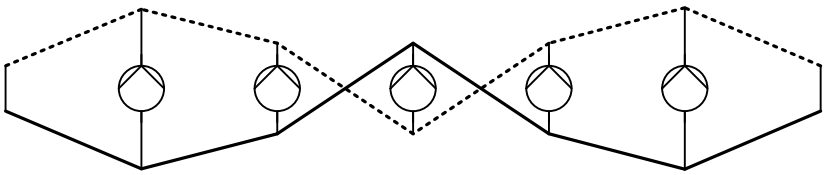

(C) BTES: discharging($\dot{m}_{BTES} < 0$), Supplier: pump mode

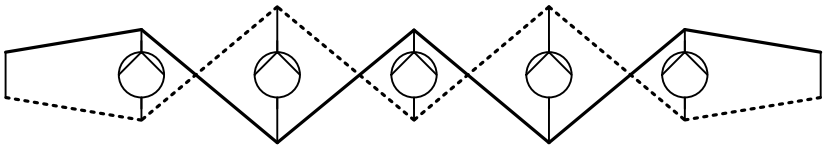

(D) BTES: charging ($\dot{m}_{BTES} > 0$), Supplier: pump mode

FIGURE 3.4: Possible appearances of the pressure difference between warm pipe (solid line) and cold pipe (dashed line), winter mode. Network connections from left to right: BTES, prosumer, prosumer, Supplier, prosumer, prosumer, BTES

3.2 Network calculation tools

There is a number of tools available on the market to perform (district heating) network calculations. Most of them support the hydraulic computation to determine pressure losses and flow velocities. These software tools are widely used for network planning as well as for off-design calculations, hence for the determination of load flows in given district heating systems with changed boundary conditions (heat loads, new connections). Tab. 3.1 provides an overview of the common software packages and their abilities.

TABLE 3.1: Software packages for fluid network calculation, from [14].

Software	fluid			computing ability	
	seawage	district heating	gas	hydraulic	thermal
PSS® SINCAL	✓	✓	✓	✓	(✓)
STANET®	✓	✓	✓	✓	(✓)
Simplex	-	✓	-	✓	✓
Bentley® sisHYD	✓	✓	✓	✓	✓
EPANET	✓	-	-	✓	-
TERMIS	-	✓	-	✓	✓
SIR-3S	✓	✓	✓	✓	(✓)

3.3 Methodology

The network calculation aims to determine the network state for each simulation time step. The variables for the network calculation is the pressure and massflow for the hydraulic calculation and temperature and heat losses for the thermal network calculation. The network calculation results can be distinguished into arc and node specific variables. Node related variables are the node pressures and the node temperatures and arc related are the mass/volume flows through the pipes as well as the temperature distribution along a tube. The determination of the variables takes place by solving a system of equations. This section aims to describe the compilation of the equation system in general, the system characterizing equations for both the hydraulic and the thermal problem are shown in the following subsections. The network calculation consists of a quasi-stationary hydraulic and a transient thermal calculation. Both of them are calculated for each simulation time step consecutively. Once the hydraulic network state is known, that means the pressure and mass flow field are found, the calculation proceeds with the temperature field calculation. The results of the hydraulic computation are the boundary conditions for the following thermal calculation and the other way around for the next time step. The compilation of the hydraulic problem's equation system is based on the graph theory, [33]. A network is represented here by n nodes and m arcs which are aggregated within the incidence matrix. Figure 3.5 shows the evolution from a network map to the incidence matrix which is the network's mathematical representation.

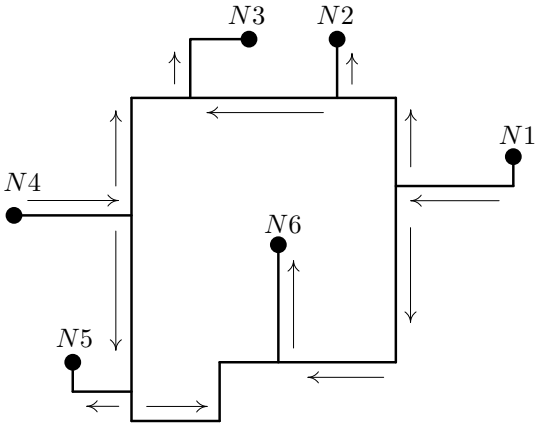

(A) Network map and flow directions of a small ring network connecting 6 Prosumers

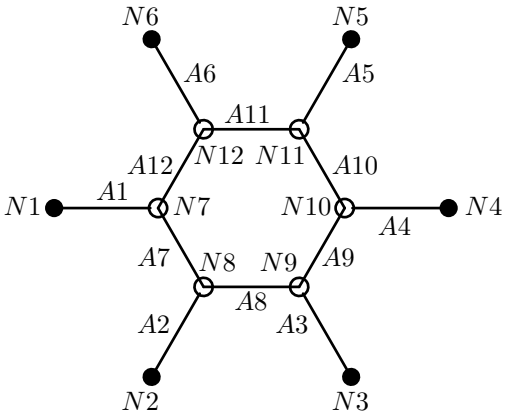

(B) Simplified network model with arc and node labels

$$\mathbf{I} = \begin{array}{c} \\ N1 \\ N2 \\ N3 \\ N4 \\ N5 \\ N6 \\ N7 \\ N8 \\ N9 \\ N10 \\ N11 \\ N12 \end{array} \begin{array}{c} \begin{array}{cccccccccccc} A1 & A2 & A3 & A4 & A5 & A6 & A7 & A8 & A9 & A10 & A11 & A12 \end{array} \\ \left[\begin{array}{cccccccccccc} 1 & 0 & 0 & 0 & 0 & 0 & 0 & 0 & 0 & 0 & 0 & 0 \\ 0 & -1 & 0 & 0 & 0 & 0 & 0 & 0 & 0 & 0 & 0 & 0 \\ 0 & 0 & -1 & 0 & 0 & 0 & 0 & 0 & 0 & 0 & 0 & 0 \\ 0 & 0 & 0 & 1 & 0 & 0 & 0 & 0 & 0 & 0 & 0 & 0 \\ 0 & 0 & 0 & 0 & -1 & 0 & 0 & 0 & 0 & 0 & 0 & 0 \\ 0 & 0 & 0 & 0 & 0 & -1 & 0 & 0 & 0 & 0 & 0 & 0 \\ -1 & 0 & 0 & 0 & 0 & 0 & 1 & 0 & 0 & 0 & 0 & 1 \\ 0 & 1 & 0 & 0 & 0 & 0 & -1 & 1 & 0 & 0 & 0 & 0 \\ 0 & 0 & 1 & 0 & 0 & 0 & 0 & -1 & -1 & 0 & 0 & 0 \\ 0 & 0 & 0 & -1 & 0 & 0 & 0 & 0 & 1 & 1 & 0 & 0 \\ 0 & 0 & 0 & 0 & 1 & 0 & 0 & 0 & 0 & -1 & 1 & 0 \\ 0 & 0 & 0 & 0 & 0 & 1 & 0 & 0 & 0 & 0 & -1 & -1 \end{array}\right] \end{array}$$

(C) Incidence matrix for $m = 12$ nodes and $n = 12$ arcs

FIGURE 3.5: Evolution from network map to incidence matrix

The incidence matrix $\mathbf{I} = (\mathbf{I})_{ij} = (i_{ij})$ for a directed graph has the following entries:

$$i_{ij} = \begin{cases} 0 & \text{no relation between node i and arc j} \\ 1 & \text{node i related to arc j, i is the input node} \\ -1 & \text{node i related to arc j, i is the output node} \end{cases} \tag{3.1}$$

The methodology for the network calculation is an enhancement of the one used in [14].

The key features of the hydraulic and the thermal computation are highlighted in the following subsections. One difference between GCHP systems as the one presented in this work and conventional district heating networks for whom the sound calculation models were developed is the fact that heat customers are not only demanders of thermal energy but they can also be suppliers. Paired with the fact that every customer connected to the network is temperature differential controlled, makes is necessary to couple supply and return water distribution networks. The return temperature of the water leaving the customers building and flowing back to the ring network is not independent from the supply temperature anymore. The assumption of constant return temperatures is not feasible anymore for systems like the one presented here. This is particularly related to the thermal computation (see 3.3.2). The physical background for the calculation of pressure losses and the flow velocity distribution as well as the methodology in compiling and solving the equation system for the hydraulic problem is shown in 3.3.1.

3.3.1 Hydraulic computation

Pipe friction is the main influence factor within a water distribution network. The pressure along a pipe sinks in flow direction. Inside a ring network with a number of connected water customers the amount of water flowing through each pipe is strongly dependent from pipe friction. The pump has to assure a certain pressure differential that water can flow into the desired direction. In the context of pumps the pressure difference is often translated into a hydraulic head:

$$\Delta H = \frac{\Delta p}{\rho\, g} \tag{3.2}$$

The generalization for the calculation of ΔH resulting from the flow through a pipe is as follows:

$$\Delta H = k\, \dot{V}^n \tag{3.3}$$

And for pressure losses:

$$\Delta p = \hat{k}\, \dot{V}^n \tag{3.4}$$

Depending on the kind of equation for hydraulic head losses, different factors k and n can be used. The most commonly used one in network calculations is the Darcy-Weisbach equation. For a cylindrical pipe with uniform diameter, flowing full, it is

$$\Delta p = \frac{8\, f_D\, L\, \rho}{D^5\, \pi^2}\, \dot{V}^2 \tag{3.5}$$

hence

$$k = \frac{8\, f_D\, L}{g\, D^5\, \pi^2}, \qquad \hat{k} = \frac{8\, f_D\, L\, \rho}{D^5\, \pi^2} \quad \text{and} \quad n = 2 \tag{3.6}$$

With given pipe geometry, volume flow and temperature the loss in hydraulic head for a single pipe can be calculated straight forwardly. To determine the whole system's pressure losses, Eq.

(3.3) and (3.4) have to be applied to every pipe in the system. For pipe A connecting the two network nodes i (inlet) and j (outlet) eq. (3.3) and (3.4) become:

$$H_i - H_j = k_A \dot{V}_A^n \tag{3.7}$$

$$p_i - p_j = \hat{k}_A \dot{V}_A^n \tag{3.8}$$

Together with Kirchhoff's current law (conservation of mass)

$$\sum_{k \in inflows} \rho \dot{V}_k - \sum_{l \in outflows} \rho \dot{V}_l = 0 \tag{3.9}$$

or

$$\sum_{k \in inflows} \rho \frac{d_k^2 \pi}{4} v_k - \sum_{l \in inflows} \rho \frac{d_l^2 \pi}{4} v_l = 0 \tag{3.10}$$

for a network consisting of m nodes and n arcs this methodology leads to a non linear equation system of $m + n$ equations in the variables $p_i, i = 1...m$ and $v_j, j = 1...n$.

The system's variables are defined as two variable vectors $\mathbf{x}_v$ and $\mathbf{x}_p$ which are concatenated to the final variable vector $\mathbf{x}$:

$$\mathbf{x}_v = \begin{bmatrix} v_1 \\ v_2 \\ \vdots \\ v_n \end{bmatrix}; \quad \mathbf{x}_p = \begin{bmatrix} p_1 \\ p_2 \\ \vdots \\ p_m \end{bmatrix}; \quad \mathbf{x} = \begin{bmatrix} \mathbf{x}_v \\ \mathbf{x}_p \end{bmatrix}$$

The application of eq. (3.10) to each node is done with behalf of the incidence matrix which was introduced in section 3.3, [14]:

$$\mathbf{M} = \begin{bmatrix} \mathbf{I}_{1n} \circ \mathbf{r} \circ \mathbf{a} \\ \vdots \\ \mathbf{I}_{mn} \circ \mathbf{r} \circ \mathbf{a} \end{bmatrix} \tag{3.11}$$

with

$$\mathbf{r} = \begin{bmatrix} \rho_1 & \dots & \rho_n \end{bmatrix} \quad \text{and} \quad \mathbf{a} = \begin{bmatrix} \frac{d_1^2 \pi}{4} & \dots & \frac{d_n^2 \pi}{4} \end{bmatrix}$$

The mass conservation equation (3.10) applied to every network node then becomes:

$$\mathbf{M}\,\mathbf{x}_v = 0 \tag{3.12}$$

The hydraulic problem's equation system is due to the exponent $n \neq 1$ in eq. (3.4) non-linear. Bothe linearizes in [14] the energy conservation equation with the linear theory method proposed by Wood and Charles [92]. The variable's quadratic dependency is replaced with the linear version of the variable and an initial value, which is the result of the previous time step.

Due to possible oscillations in the solution vector, a iterative method including relaxation has to be used. For further information see [82]. A wide variety of successful applications of the linear theory method in the network context are available, for instance see [8], [64]. If the linear theory method is applied to eq. (3.4) it can be expressed as

$$\Delta p = \hat{k}\, \dot{V}^{(t-1)}\, \dot{V}^{(t)} \tag{3.13}$$

and with v being an element of the variable vector $\mathbf{x}$

$$\Delta p = \tilde{k}\, v^{(t-1)}\, v^{(t)} \tag{3.14}$$

and

$$\tilde{k} = \frac{f_D\, L\, \rho}{2\, D} \tag{3.15}$$

Applied to every pipe element inside the network follows the diagonal matrix $\mathbf{N}$:

$$\mathbf{N} = \begin{bmatrix} \tilde{k}_1\, v_1^{(t-1)} & 0 & \dots & 0 \\ 0 & \tilde{k}_2\, v_2^{(t-1)} & \dots & \vdots \\ \vdots & \vdots & \ddots & 0 \\ 0 & \dots & 0 & \tilde{k}_n\, v_n^{(t-1)} \end{bmatrix} \tag{3.16}$$

With behalf of the incidence matrix the energy conservation for a pipe network with interconnected pipes states as follows:

$$\begin{bmatrix} \mathbf{N} & (-\mathbf{I})^T \end{bmatrix} \begin{bmatrix} \mathbf{x}_v \\ \mathbf{x}_p \end{bmatrix} = \mathbf{0} \tag{3.17}$$

Note: The network constituting pipes here are assumed to be horizontally burried. Otherwise the right side of eq. (3.17) would not be zero but the hydrostatic pressure of the two adjacent network nodes.

The equation system for the hydraulic network calculation is now fully defined. To obtain other solutions than the trivial one the boundary conditions have to be provided to the system. For this purpose a vector with the boundary conditions is defined here:

$$\mathbf{b}_v = \begin{bmatrix} b_v^{(1)} \\ b_v^{(2)} \\ \vdots \\ b_v^{(n)} \end{bmatrix}; \quad \mathbf{b}_p = \begin{bmatrix} b_p^{(1)} \\ b_p^{(2)} \\ \vdots \\ b_p^{(m)} \end{bmatrix}; \quad \mathbf{b} = \begin{bmatrix} \mathbf{b}_v \\ \mathbf{b}_p \end{bmatrix}$$

The vectors $\mathbf{b}_v$ and $\mathbf{b}_p$ are the boundary condition vectors for the flow velocities and the pressures, respectively. The content of the vectors are represented as numerical values on the right-hand side of the following equation:

$$\begin{bmatrix} bc_1 & 0 & \dots & 0 \\ 0 & bc_2 & \dots & 0 \\ \vdots & \vdots & \ddots & \vdots \\ 0 & \dots & 0 & bc_{n+m} \end{bmatrix} \mathbf{x} = diag(bc_1, bc_2, \dots, bc_{n+m})\, \mathbf{x} \tag{3.18}$$

$$\mathbf{BC}\,\mathbf{x} = \mathbf{b}$$

Not every element of those vector elements has to be provided to the system. Let π be the number of network end points. An end note is a network node where water can enter or exit the system. For GCHP network systems π would be the number of heat consumers plus the number of heat suppliers plus the connection point of the BTES. The equation system is fully determined if the number of boundary conditions $\neq 0$ is not greater than π. The kind of provided boundary condition can either be a pressure value or a flow velocity value. In order to obtain absolute pressures and due to the differential pressure notation of eq. (3.4) at least one pressure boundary condition has to be provided to the system.

Usually exists in water networks at least one point with known pressure, for instance where an expansion tank is placed. It is useful to set the pressure boundary condition for that neuralgic point and a flow velocity boundary condition for each heat consumer. Due to the fact one pressure boundary condition is provided, only $\pi - 1$ flow velocity boundary conditions are necessary. The flow velocity boundary condition element for the BTES is left blank in that case. The global mass conservation equation determines in that case the last mass flow and hence the last flow velocity. The following equation shows this procedure:

$$bc_i \in \mathbf{BC} = \begin{cases} 0 & \text{boundary condition i not set} \\ 1 & \text{boundary condition i set} \end{cases} \qquad i = 1 \dots (m+n) \tag{3.19}$$

The combination of the mass conservation equation (3.12), energy conservation equation(3.17) and the boundary conditions (3.18) yields to the following equation system which is stated in the following as the *hydraulic equation system for the horizontal pipe network.*

$$\begin{bmatrix} \mathbf{M} & & 0 \\ \mathbf{N} & & (-\mathbf{I})^T \\ & \mathbf{BC} & \end{bmatrix} \mathbf{x} = \begin{bmatrix} \mathbf{0} \\ \mathbf{0} \\ \mathbf{b} \end{bmatrix} \tag{3.20}$$

This equation system is equivalent to the one with the form $\mathbf{A}\,\mathbf{x} = \mathbf{b}$ and can be solved using different solving algorithms which can be found in standard mathematics literature. In MATLAB® it is used the backslash operator (*mldivide*) to solve equation systems like the presented one. The software initially analyzes the equation system and selects the most efficient solver. Further information about the mldivide algorithm can be found in section 1.5.2 and the MATLAB® documentation.

Due to the application of the linear theory method on the energy conservation equation the

equation system (3.20) has to be solved multiple times taking into consideration a relaxation coefficient. The equation system for a distinct time step is solved if the solution vector satisfies a predefined convergence criterion. Possible oscillations in the solution are damped with the relaxation coefficient α_v and α_p. *Wood* and *Charles* suggest in [92] to use the mean value of the two last successfully computed iterations (i and ii) to assemble the final solution:

$$\mathbf{x}_v = |\mathbf{x}_v^{(ii)}| \, (1 - \alpha_v) + |\mathbf{x}_v^{(i)}| \, \alpha_v \tag{3.21}$$

$$\mathbf{x}_p = \mathbf{x}_p^{(ii)} \, (1 - \alpha_p) + \mathbf{x}_p^{(i)} \, \alpha_p \tag{3.22}$$

To avoid oscillations in the flow velocity the absolute value in (3.21) of the variable has to be taken into account.

The presented methodology does only consider pressure losses due to pipe friction inside fully flow through, horizontal pipes. *Bothe* expands in [14] the energy conservation part within this methodology to pipe networks whose nodes have different geodetic altitudes and takes into account also flow related components like valves and pumps. Due to the size and relatively simple structure of the water networks considered in this work the nodes can be assumed to lie in a horizontal plane. Sophisticated modeling of pumps and valves requires detailed data considering the underlying characteristics. The aim here is not to recalculate existing systems, but to design networks that are able to use industrial (waste) heat within a water distribution system. The pressure and flow velocity field of course depend on the used valves and pumps which are crucial parts of the system. Pumps and valves in the network context here connect the warm and the cold pipe. Therefore, two hydraulic problems are solved here, one for the warm pipe and one for the cold one. Fig. 3.6 shows a program flow chart for one time step of the network calculation. The mentioned internal loop due to linear theory is not shown in this schematic diagram but takes place inside the two hydraulic problem solving blocks.

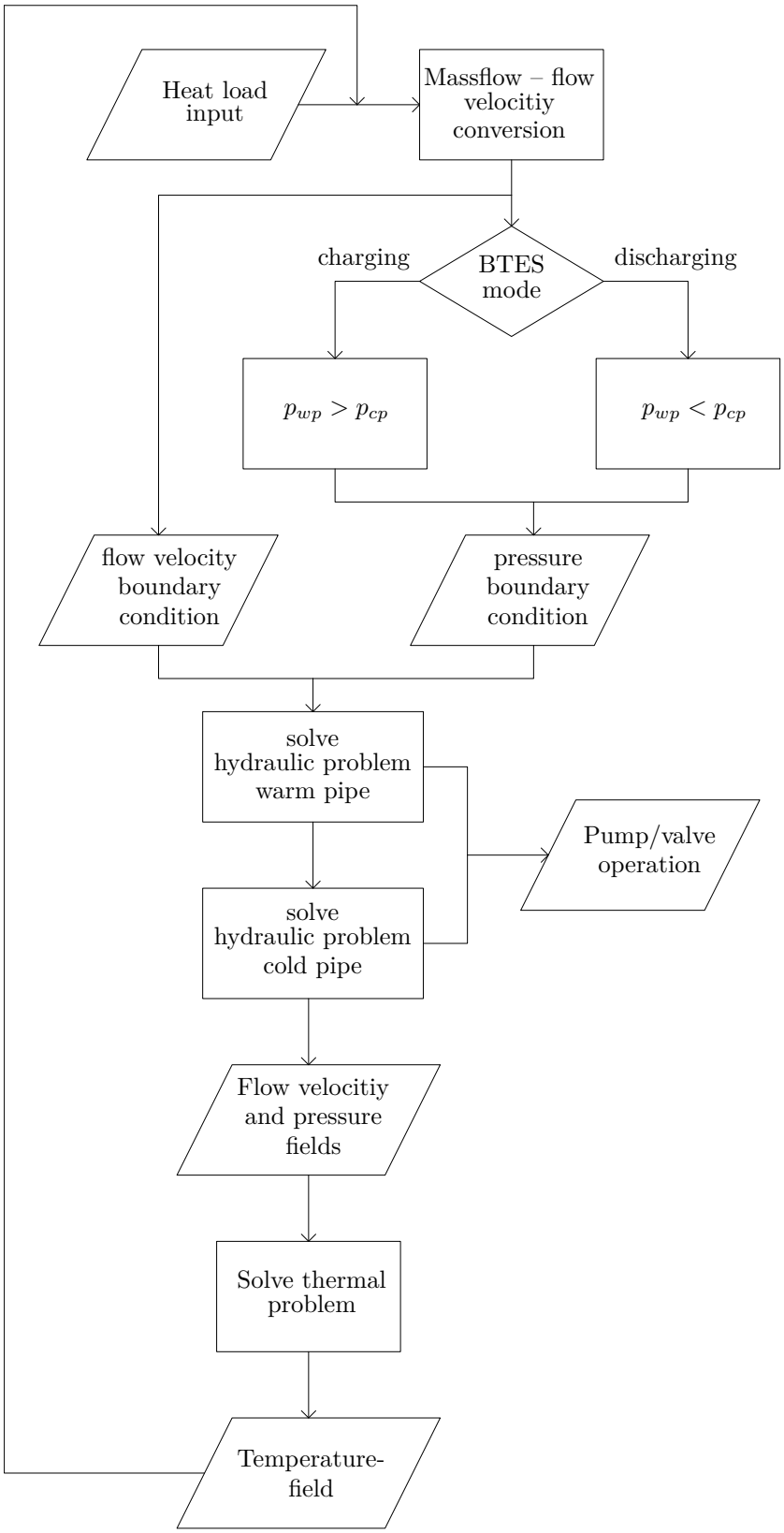

FIGURE 3.6: Thermo-hydraulic network calculation flow chart

The pressure boundary condition is calculated based on a fixed pressure in the cold pipe near the BTES and the pressure losses which accrues during water flow through the BTES' vertical pipes. Based on the two possible operating modes considering the seasonal storage the pressure boundary condition for the warm pipe is calculated. It is assumed that the expansion tank which provides the constant pressure p_e is located at the cold pipe connection point of the BTES. Fig. 3.7 shows the pressure relations for the BTES operating modes. If the network is oversupplied, that means that more water is fed into than demanded from the warm pipe network, the BTES is charged with the excess water mass flow, fig. 3.7a. The pressure in the warm tube at the BTES's connection point to the ring network is in that case greater than the pressure in the cold tube. The other situation, fig. 3.7b implies a smaller pressure in the warm pipe than in the cold one.

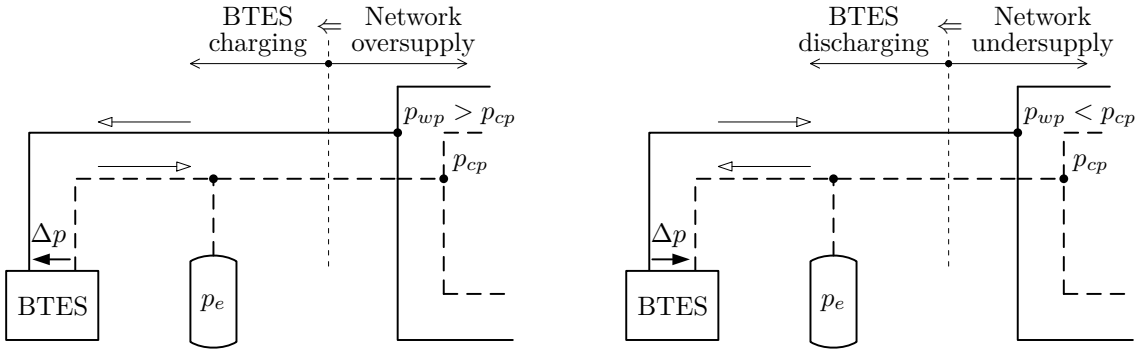

(A) Charging mode (B) Discharging mode

FIGURE 3.7: Pressure relations for BTES modes

The difference of the two boundary condition pressure values is the pressure drop along the BTES inlet and outlet pipe. It is calculated with the following equation:

$$\Delta p = \left(\frac{f_D \, L}{D} + \zeta \right) \frac{\rho \, v^2}{2} \tag{3.23}$$

ζ represents here the pressure loss coefficient for the pipe bending at the bottom of the U-pipes and the pipe junctions (distributors and connectors). The darcy friction factor f_D is calculated with respect to the flow regime. If the Reynolds number is sufficiently low the friction factor is calculated with the following equation which is also known as the *Hagen-Poiseuille* equation.

$$f_D = \frac{64}{Re} \quad \text{if} \quad Re < 2300 \tag{3.24}$$

For higher Reynold numbers it is used the *Colebrook-White* equation, (3.25), in the transition between fully turbulent flow in smooth and rough conduits.

$$\frac{1}{\sqrt{f_D}} = -2 \log_{10} \left(\frac{R_a}{3.71 \, D} + \frac{2.51}{Re \sqrt{f_D}} \right) \tag{3.25}$$

For fully turbulent flow in rough pipes the *Nikuradse* correlation is taken to determine the friction factor f_D.

$$\frac{1}{\sqrt{f_D}} = -2 \log_{10} \left(\frac{R_a}{3.71\, D} \right) \tag{3.26}$$

Depending on the result of f_D the boundary curve between eq. (3.25) and eq. (3.26) is

$$f_D = \left(\frac{200\, D}{Re\, R_a} \right) \tag{3.27}$$

As mentioned previously, the hydraulic problem is solved for the warm and the cold pipe system. The results are the flow velocities in each pipe and the pressures in each node. The pressure differences in the network end nodes between cold and warm pipe system gives the operation mode of the pressure setting device. Depending on the load profiles of heat consumers and heat suppliers either the valve or the pump has to provide a negative or a positive pressure difference between the two pipes. Depending whether warm water has to be supplied to the network or drawn from the network the pressure relations shown in fig. 3.8 are possible:

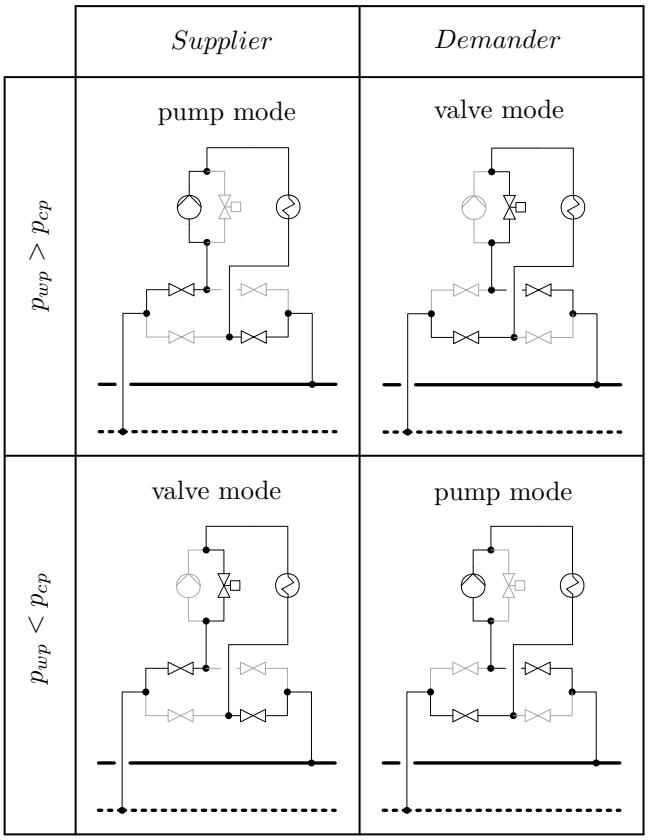

FIGURE 3.8: Pump and valve modes for the prosumer model in respect to the pressure at the connection node

As the water has to pass through different heat exchangers the pressure drops due to friction losses along those components has to be considered as well. The heat exchangers in this context are heat pump evaporators at the consumer energy centrals and plate heat exchangers for the cooling of the buildings during summer time and the suppliers heat providing facility. The component related pressure losses are added to the pipe flow induced pressure drops by adapting eq. (3.14) and eq. (3.15) in the following manner:

$$\Delta p = \tilde{k}_{tot}\, v^{(t-1)}\, v^{(t)} \tag{3.28}$$

with

$$\tilde{k}_{tot} = \frac{f_D\, L\, \rho}{2\, D} + \frac{\zeta_{hex}\, \rho}{2} \tag{3.29}$$

Every element of the matrix $\mathbf{N}$ (eq. 3.17) which represents a pipe from the ring network to a network end node is adjusted with this additional pressure drop. Half of the heat exchanger induced pressure drop is assumed to accrue in the warm pipe and cold pipe, respectively. The pressure loss coefficient ζ_{hex} is calculated with a nominal flow velocity v_N and a nominal pressure drop Δp_N before the simulation starts:

$$\zeta_{hex} = \frac{2\, \Delta p_N}{\rho\, v_N^2} \tag{3.30}$$

The numerical values of the nominal pressure drops Δp_N are assumed to be 70 kPa for heat pump evaporators and 30 kPa for plate heat exchangers. The determination of the nominal flow velocities v_N and the pressure loss coefficients ζ_{hex} is an iterative process where the network simulation is performed several times. The pressure loss coefficients are adapted continuously until the simulation results of the nominal flow velocities do not differ from the assumed ones anymore.

The main objective of the hydraulic network calculation is the determination of the necessary pumping power as well as a quantitative assessment of the necessary pump and valve characteristics in terms of hydraulic head and volume flow. The flow velocities as well as the flow directions finally are also essential parameters for the following thermal network calculation.

The pumping power is assessed with the following equation:

$$P_p = \frac{\rho\, g\, \dot{V}\, \Delta H_p}{\eta_p} \tag{3.31}$$

where, if the geodetic head difference and velocity changes are neglected

$$\Delta H_p = \frac{\Delta p_p}{\rho\, g} \tag{3.32}$$

and

$$\Delta p_p = \begin{cases} p_{wp} - p_{cp} & \text{Supplier pump mode} \\ p_{cp} - p_{wp} & \text{Demander pump mode} \\ 0 & \text{Supplier/Demander valve mode} \end{cases} \tag{3.33}$$

The pump's global efficiency η_p is set here to 0.5.

3.3.2 Temperature computation

In addition to the hydraulic network computation a thermal network calculation is performed. The methodology is based on the one described in [14]. Due to the inability to provide temperature differences between supply and return node temperatures in the methodology developed by *Bothe* the procedure is further developed to allow for temperature differential control at prosumer connection points. In the following the key features of the thermal network calculation are shown and the numerical solution process as well as the methodology for compiling the equation system for the network temperatures is given. Aim for the thermal network calculation is the determination of possible thermal heat losses as well as to provide the necessary boundary conditions for the BTES calculation.

Starting point is transport equation (1.8) from chapter 1. If the factor ϕ is replaced by other variables, the following relations can be obtained:

- $\phi = 1 \Rightarrow$ conservation of mass
- $\phi = u \Rightarrow$ conservation of momentum
- $\phi = h \Rightarrow$ conservation of energy

Conservation of mass

By setting $\phi = 1$ the diffusion term disappears and the general form of the mass conservation equation becomes

$$\frac{\partial}{\partial x_i}(\rho\, u_i) + \frac{\partial}{\partial t}\rho = S \tag{3.34}$$

If no mass sources and sinks are assumed for the considered control volume S becomes 0. The flow is further assumed to be one dimensional in x-direction and the fluid to be incompressible. If only steady changes of the pressure during time are allowed, hence no pressure shocks accrue the term $\frac{\partial \rho}{\partial t}$ becomes 0 and the conservation of mass becomes, [14]

$$\frac{\partial}{\partial x}(\rho\, u) = 0 \tag{3.35}$$

Conservation of momentum

If ϕ is replaced by the velocity in x direction, u, the equation becomes for the first direction in space, [11]:

$$\frac{\partial}{\partial t}(\rho\, u) + \frac{\partial}{\partial x_i}(\rho\, u_i\, u) = \frac{\partial}{\partial x_i}\left(\mu\, \frac{\partial u}{\partial x_i}\right) - \frac{\partial p}{\partial x} \tag{3.36}$$

with μ being the dynamic viscosity and the assumption that there are no field forces in x direction.

For the thermal network calculation the conservation of momentum equation is only of secondary importance. Hence, more detailed considerations are omitted here. In the presented methodology the conservation of momentum is simplified within the hydraulic computation with one equation that relates a pressure change with water velocities and geodetic heads. The pressure and flow velocity field of every node and arc in the network is calculated within the hydraulic network calculation in chapter 3.3.1. The results constitute an input for the thermal network calculation.

Conservation of energy

By replacing the factor ϕ in equation (1.8) with the specific enthalpy h and applying Fourier's law to the diffusion coefficient Γ the convection-diffusion equation becomes the energy conservation equation for fluid streams inside a given control volume:

$$\frac{\partial}{\partial x_i}\,(u_i\, \rho\, h) + \frac{\partial}{\partial t}(\rho\, h) = -\frac{\partial}{\partial x_i}\,(\dot{q}_i) + S \tag{3.37}$$

If the specific enthalpy is replaced by the product $T\, c_p$, which is allowed if no phase changes and only small pressure variations occur, the relation for the x direction becomes:

$$c_p\, \frac{\partial}{\partial x}\,(u\, \rho\, T) + c_p\, \frac{\partial}{\partial t}(\rho\, T) = -\frac{\partial}{\partial x}\,(\dot{q}_x) + S \tag{3.38}$$

The first term on the left hand side is the convective part of the energy transport, the second one the transient part. On the right side of the equal sign follows the diffusive part and possible energy sources or sinks.

In order to be able to solve the conservation of mass and energy differential equations, a discretization of eq. (3.35) and eq. (3.38) has to be performed. Both, a time and a spatial discretisation is applied to the mentioned equations. The accurate approach here is found to be the finite volume method. The tubes are divided into equally sized control volumes with the volume $\Delta V = \frac{D^2\,\pi}{4}\,\Delta x$.

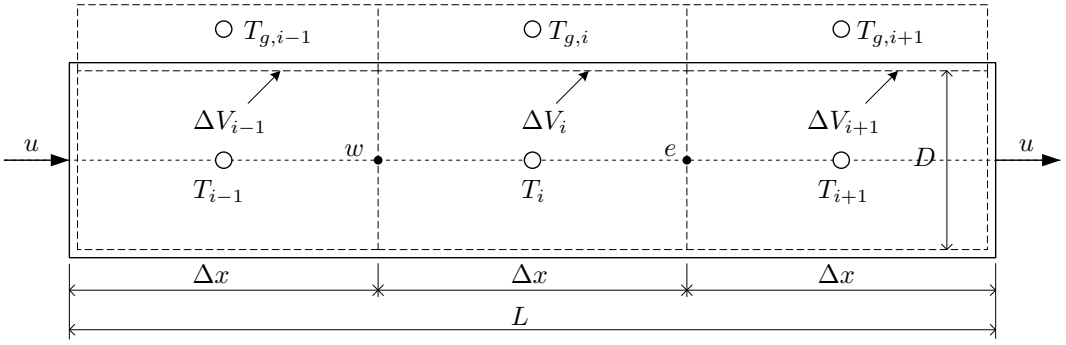

FIGURE 3.9: Spatial pipe discretization with $n = 3$ elements and $\Delta x = \frac{L}{3}$, volume element temperatures T_i and their respective direct ambient temperatures T_g

The mass conservation equation, eq. (3.35) is integrated over the control volume ΔV depicted in fig. 3.9

$$\int_{\Delta V} \frac{\partial}{\partial x} (\rho\, u)\, dV = 0 \tag{3.39}$$

if ΔV is expressed as $A\,\Delta x$ and $\Delta x \to 0$ it follows:

$$\int_{\Delta x} \frac{\partial}{\partial x} (\rho\, u)\, A\, dx = (\rho\, u\, A)|_{x=x_e} - (\rho\, u\, A)|_{x=x_w} = 0 \tag{3.40}$$

and finally

$$\dot{m}_w = \dot{m}_e = \rho(T_i, p_i)\, \frac{D^2 \pi}{4}\, u \tag{3.41}$$

For water distribution networks the mass flows are constantly high and hence the convective part in the energy transport equation dominates over the diffusive term. Due to the fact that the pipes are assumed to be buried pipes in the surrounding soil, the diffusive term has to be considered as well. The different temperatures inside the two pipes considered as supply and return legs, do cause a mutual influence, which is considered with behalf of the *Resistance Capacity model*, see chapter 4.2.1.

Integration of the energy conservation equation (3.38) yields:

$$\int_{\Delta V} c_p\, \frac{\partial}{\partial x} (u\, \rho\, T)\, dV + \int_{\Delta V} c_p\, \frac{\partial}{\partial t} (\rho\, T)\, dV = -\int_{\Delta V} \frac{\partial}{\partial x}\, (\dot{q}_x)\, dV + \int_{\Delta V} S\, dV \tag{3.42}$$

again, the finite volume ΔV is expressed as $A\,\Delta x$ and so the volume integral can be written as an integral in the flow direction x:

$$\int_{\Delta x} c_p\, \frac{\partial}{\partial x} (u\, \rho\, T)\, A\, dx + \int_{\Delta x} c_p\, \frac{\partial}{\partial t} (\rho\, T)\, A\, dx = -\int_{\Delta x} \frac{\partial}{\partial x}\, (\dot{q}_x)\, A\, dx + \int_{\Delta x} S\, A\, dx \tag{3.43}$$

The evaluation of the integral from point w to point e in fig. 3.9 and division by A yields the spacial discretized form of the energy conservation equation:

$$c_p\, u\, \rho\, (T_e - T_w) + \left(c_p\, \rho\, \frac{\partial T}{\partial t} \right)_i \Delta x = (\dot{q}_w - \dot{q}_e) + S\, \Delta V \tag{3.44}$$

The further application of Fourier's law transforms the heat fluxes through the adjacent finite volumes to temperature differences:

$$c_p\, u\, \rho\, (T_e - T_w) + \left(c_p\, \rho\, \frac{\partial T}{\partial t} \right)_i \Delta x = \frac{\lambda_f}{\Delta x}\, (T_{i-1} + T_{i+1} - 2\, T_i) + S\, \Delta x \tag{3.45}$$

The temperature of interest T_i is, as shown in eq. (3.45), dependent from the two temperatures T_w and T_e on the volume's boundary. Therefore, an assumption of the temperature profile along the pipe is necessary. *Bothe* uses in [14] the *First-order upwind scheme*, which assigns the cell temperature T_i to the boundary temperature which lies in the upstream direction. In fig. 3.9 the temperature T_w would get the value of T_{i-1} and T_e the one of T_i. Generally speaking the *First-order upwind scheme* for temperatures of a fluid inside a pipe flowing with the flow velocity u can be expressed as, [70]:

$$T_i^{n+1} = T_i^n - \Delta t\, (u^+\, T_x^- + u^-\, T_x^+) \tag{3.46}$$

with

$$u^+ = max(u, 0) \qquad u^- = min(u, 0)$$

and

$$T_x^- = \frac{T_i^n - T_{i-1}^n}{\Delta x} \qquad T_x^+ = \frac{T_{i+1}^n - T_i^n}{\Delta x}$$

If the *first-order upwind scheme* is applied to the problem from fig. 3.9, eq. (3.45) becomes:

$$c_p\, u\, \rho\, (T_i - T_{i-1}) + \left(c_p\, \rho\, \frac{\partial T}{\partial t} \right)_i \Delta x = \frac{\lambda_f}{\Delta x}\, (T_{i-1} + T_{i+1} - 2\, T_i) + S\, \Delta x \tag{3.47}$$

Possible heat losses to the environment are considered here within the source/sink term S. The heat flux to the environment through the pipe wall is proportional to the temperature difference between the cell's internal temperature T_i and the ambient Temperature $T_{g,i}$ and indirectly proportional to the thermal resistance R_{fg}:

$$S = \frac{1}{A_f}\, \frac{T_{g,i} - T_i}{R_{fg}} \tag{3.48}$$

The thermal resistance R_{fg} consists of three parts: the inner heat transfer from the fluid to the pipe, the conduction through the pipe and the heat conduction from the outer pipe diameter to the grouting material's center. Following *Bauer* in [10] it can be written as:

$$R_{pi} = \frac{1}{\pi\, Nu\, \lambda_f} + \frac{1}{2\,\pi\,\lambda_p}\,\ln\left(\frac{d_a}{d_i}\right) + x_{sg}\, R_g \tag{3.49}$$

The energy conservation equation becomes then:

$$\left(c_p\,\rho\,\frac{\partial T}{\partial t}\right)_i = \frac{c_p\, u\, \rho}{\Delta x}\,(T_{i-1} - T_i) + \frac{T_{g,i} - T_i}{R_{fg}\, A_f} + \frac{\lambda_f}{\Delta x^2}\,(T_{i-1} + T_{i+1} - 2\,T_i) \tag{3.50}$$

which is equivalent to:

$$\left(\frac{\partial T}{\partial t}\right)_i = \frac{1}{C_f}\left[\frac{c_p\,\dot{m}}{\Delta x}\,(T_{i-1} - T_i) + \frac{T_{g,i} - T_i}{R_{fg}} + \frac{A_f\,\lambda_f}{\Delta x^2}\,(T_{i-1} + T_{i+1} - 2\,T_i)\right] \tag{3.51}$$

This is the determination equation for the fluid temperature T_i representing an arbitrary fluid volume element i. For a twin-pipe element layer two of this equations (3.51) are needed: one for the supply and one for the return line. The equation for the ambient temperatures $T_{g,i}$ are created like proposed by the resistance capacity model shown in fig. 4.2, chapter 4.2.1.

For the temperature which represents the grouting material, $T_{g,i}$ it holds that there is no convective energy transport, but only heat conduction. The first term on the right hand side of equation (3.51) drops. The term for the conductive heat fluxes now has three entries (see 4.2). The heat flux parallel to the pipe axis has the same quality than the one in equation (3.51), with the difference in the thermophysical properties and geometries of the grouting material cells. The equation for the temperature of a grouting material cell becomes:

$$\left(\frac{\partial T_{g1,i}}{\partial t}\right)_i = \frac{1}{C_g}\left[\frac{T_{g2,i} - T_{g1,i}}{R_{gg}} + \frac{T_{b,i} - T_{g1,i}}{R_{gb}} + \frac{T_{1,i} - T_{g1,i}}{R_{fg}} + \frac{A_g\,\lambda_g}{\Delta x^2}\,(T_{g1,i-1} + T_{g1,i+1} - 2\,T_{g1,i})\right] \tag{3.52}$$

Again, for the second half of the grouting material, equation (3.52) yields to the temperature $T_{g2,i}$.

Like shown in [10] the borehole temperature $T_{b,i}$ is not linked to the borehole temperatures $T_{b,i-1}$ and $T_{b,i+1}$. Hence, a simple stationary approach is chosen to describe the relationship considering the borehole wall temperature:

$$\frac{T_{b,i} - T_{s1,i}}{R_{s0}} + \frac{T_{b,i} - T_{g1,i}}{R_{gb}} + \frac{T_{b,i} - T_{g2,i}}{R_{gb}} = 0 \tag{3.53}$$

The five equations (3.51) (2x), (3.53) (2x) and (3.53) of the layer i form an equation system in the six variables T_1, T_2, T_{g1}, T_{g2}, T_b and T_{s1}. One more equation is needed to obtain a fully determined equation system. This missing equation is provided as a heat flux boundary condition. The heat flux passing the borehole wall is set with an additional relationship.

Franz provides in [31] a relation to calculate the soil related heat transfer coefficient R_{bc} in respect to the pipe's installation depth h_p:

$$R_{bc} = \frac{\operatorname{arcosh}(\frac{h_p}{r_p})}{2\,\pi\,\lambda_s} \tag{3.54}$$

It satisfies the relation

$$\dot{q}_{bhw} = \frac{\Delta T}{R_{bc}}$$

The propelling temperature difference ΔT is assumed here to be $T_b - T_{amb}$. As ambient temperature the soil temperature in a depth of 10 cm is taken. The heat flux which is obtained by this formula corresponds to a heat flux which would accrue if a cylinder with diameter d_b and uniform temperature T_b would have been buried in soil with temperature T_{amb}. The missing equation for the equation system then becomes:

$$\frac{T_{b,i} - T_{s1,i}}{R_{s0}} = \frac{T_{b,i} - T_{amb}}{R_{bc}} \tag{3.55}$$

To get rid of the time derivative the equation is integrated over time. Here a fully implicit approach is used which has the advantage to be unconditionally stable. For time independent variables the integration over time is as follows:

$$\int_t^{t+1} \alpha\,T^t\,dt = \alpha\,T^{t+1}\,\Delta t \tag{3.56}$$

And for the first term of eq. (3.50)

$$\int_t^{t+1} \alpha \left(\frac{\partial T}{\partial t}\right)_i dt = \alpha\,(T_i^{t+1} - T_i^t) \tag{3.57}$$

In this way an equation system is obtained which contains all the volume temperatures as variables. The equation system for the vertical layer i has then the following appearance:

$$EQS_{twinpipe,i}: \begin{cases} \alpha_1^{(1)}\,T_{1,i-1} + \alpha_2^{(1)}\,T_{1,i} + \alpha_3^{(1)}\,T_{1,i+1} + \alpha_4^{(1)}\,T_{g1,i} = \beta_1 \\ \alpha_1^{(1)}\,T_{2,i-1} + \alpha_2^{(1)}\,T_{2,i} + \alpha_3^{(1)}\,T_{2,i+1} + \alpha_4^{(1)}\,T_{g2,i} = \beta_2 \\ \alpha_1^{(2)}\,T_{1,i} + \alpha_2^{(2)}\,T_{g1,i-1} + \alpha_3^{(2)}\,T_{g1,i} + \alpha_2^{(2)}\,T_{g1,i+1} + \alpha_4^{(2)}\,T_{g2,i} + \alpha_5^{(2)}\,T_{b,i} = \beta_3 \\ \alpha_1^{(2)}\,T_{2,i} + \alpha_2^{(2)}\,T_{g2,i-1} + \alpha_3^{(2)}\,T_{g2,i} + \alpha_2^{(2)}\,T_{g2,i+1} + \alpha_4^{(2)}\,T_{g1,i} + \alpha_5^{(2)}\,T_{b,i} = \beta_4 \\ \alpha_1^{(3)}\,T_{g1,i} + \alpha_1^{(3)}\,T_{g2,i} + \alpha_2^{(3)}\,T_{b,i} + \alpha_3^{(3)}\,T_{s1,i} = 0 \\ \alpha_1^{(4)}\,T_{b,i} + \alpha_2^{(4)}\,T_{s1,i} = \beta_6 \end{cases} \tag{3.58}$$

The factors $\alpha_e^{(f)}$ and β_e are listed in appendix B.

Since the temperatures $T_{1,i}$, $T_{2,i}$, $T_{g1,i}$ $T_{g2,i}$ and $T_{s1,i}$ are coupled with their neighbors in the

adjacent layers, 10 more equations are necessary to obtain a fully determined equation system. No equations are provided for the first and the last layer. Therefore, there is also a need for two more equations for $T_{b,i}$. If a twin pipe element is divided into n elements further boundary conditions for the first layer $i = 1$ and the last layer $i = n$ are needed:

$$BC_{twinpipe} : \begin{cases} T_{1,1} = T_{inlet,1} \\ T_{1,n} = T_{1,n-1} \\ T_{2,n} = T_{inlet,2} \\ T_{2,1} = T_{2,2} \\ T_{g1,1} = T_{g2,1} = T_{b,1} = T_{s1,1} = T_{g1,n} = T_{g2,n} = T_{b,n} = T_{s1,n} = T_{amb} \end{cases} \tag{3.59}$$

Lets assume a twin pipe with a number of axial discretization elements n, hence, $i = 1 \dots n$. The variable vector $\mathbf{T}^{tp}$ is then $[T_{1,i}\, T_{2,i}\, T_{g1,i}\, T_{g2,i}\, T_{b,i}\, T_{s1,i}\, \dots\, T_{1,n}\, T_{2,n}\, T_{g1,n}\, T_{g2,n}\, T_{b,n}\, T_{s1,n}]^\intercal$ and has the size $6\,n \times 1$. Let $\mathbf{A}$ be the matrix containing all the coefficients α_k^j from the equation system (3.58) with size $6\,(n-2) \times 6\,n$. Together with the matrix $\mathbf{BC}$ which contains the 12 boundary conditions and the vector $\mathbf{b}$ containing all the inhomogeneous elements β_k from equation system (3.58) the linear equation system for the twin pipe temperatures becomes:

$$\begin{bmatrix} \mathbf{A} \\ \mathbf{BC} \end{bmatrix} \mathbf{T}^{tp} = \mathbf{b} \tag{3.60}$$

or for an arbitrary network twin pipe s:

$$\mathbf{TP}_s\, \mathbf{T}_s^{tp} = \mathbf{b}_s \tag{3.61}$$

Departing from the equation system for one single twin pipe, in further consequence a whole network of pipes is build up. All the single pipes which compose the whole network are connected with network nodes. The mathematical description with the incidence matrix was given in chapter 3.3. The network variables for the pipes are the inlet temperatures $T_{inlet,1}$, $T_{inlet,2}$ and the outlet temperatures for both pipes of all the twin pipe elements. Node temperatures can be calculated in respect to pipe outlet temperatures. Pipe inlet temperatures are always equal one particular node temperature. The general form of the node temperature calculation equation is as follows:

$$T_n = \frac{\sum_{i=1}^{j} \dot{m}_i\, c_{p,f}\, T_i}{\sum_{i=1}^{j} \dot{m}_i\, c_{p,f}} \tag{3.62}$$

The subscript $i = 1 \dots j$ represents the inflowing water streams towards the node. Here it is assumed that the node itself doesn't have a volume. Therefore this simplified relation can be taken. Each node is assumed to be a perfect mixing point where the temperature weighted inflowing mass flows compose the temperature of the out flowing streams. The water temperatures

of the whole network inside the warm and cold pipe systems do not differ significantly, therefore the equation simplifies to

$$T_n = \frac{\sum_{i=1}^{j} \dot{m}_i \, T_i}{\sum_{i=1}^{j} \dot{m}_i} \tag{3.63}$$

or for the usage in the equation system the equation can also be written as

$$T_n - \sum_{i=1}^{j} e_i \, T_i = 0 \tag{3.64}$$

with

$$e_i = \frac{\dot{m}_i}{\sum_{i=1}^{j} \dot{m}_i} \tag{3.65}$$

Let's now assume a network with $j = 1 \dots m$ nodes and $i = 1 \dots n$ arcs/twin pipes. Each arc is divided into $l_i,\ i = 1 \dots n$ volume elements whose temperatures need to be calculated. The vector with the number of volume elements for the arcs $i = 1 \dots n$ is: $\mathbf{l} = [l_1 \, l_2 \, \dots \, l_n]^\intercal$.

All the network temperatures, i.e. node temperatures $T^k_{nj},\ j = 1 \dots m;\ k = h, c$ for the hot and the cold pipe system and arc's volume temperatures $\mathbf{T}^{tp}_i, i = 1 \dots n$ are collected in the vector $\mathbf{T_{nw}}$

$$\mathbf{T_p} = \begin{bmatrix} T^{tp}_1 \\ T^{tp}_2 \\ \vdots \\ T^{tp}_n \end{bmatrix}; \quad \mathbf{T^h_n} = \begin{bmatrix} T^h_{n1} \\ T^h_{n2} \\ \vdots \\ T^h_{nm} \end{bmatrix}; \quad \mathbf{T^c_n} = \begin{bmatrix} T^c_{n1} \\ T^c_{n2} \\ \vdots \\ T^c_{nm} \end{bmatrix}; \quad \mathbf{T_{nw}} = \begin{bmatrix} \mathbf{T_p} \\ \mathbf{T^h_n} \\ \mathbf{T^c_n} \end{bmatrix} \tag{3.66}$$

with the size $\sum_{i=1}^{n} 6\, l_i + 2\, m \times 1$.

Given the mass flow vector $\dot{\mathbf{m}}_{\mathbf{nw}} = [\dot{m}_{a1} \, \dot{m}_{a2} \, \dots \, \dot{m}_{an}]^\intercal$ derived from the flow velocities as results of the hydraulic network calculation and the incidence matrix $\mathbf{I}$ which was introduced in section 3.3 the node and arc volume elements temperatures for the whole network can be calculated.

As mentioned before, the described networks here are temperature differential controlled. That means that every heat consumer and heat supplier receives exactly that amount of water that he needs to realize a temperature difference of ΔT_c between cold and warm pipe. For the equation system this means, that the cold and warm pipe system are coupled. Instead of providing given or constant return temperatures, as it is sometimes done in conventional district heating network calculations, here the return temperatures are equal the supply temperatures plus or minus the customer's temperature difference. For the equation system this means that at a customer node the hot and the cold node temperatures are coupled. Let the matrix $\mathbf{N}$ be a matrix with size $2\, m \times 2\, m$ representing the network nodes for the hot and the cold pipe

network.The entries in $\mathbf{N}$ follow the following rule:

$$n_{i,j} \in \mathbf{N}, i = 1 \dots 2\,m; j = 1 \dots 2\,m \;= \begin{cases} 1 & \text{if } \; i = j \\ -1 & \text{if node } i \text{ is a customer node and } j = m \pm i \\ 0 & \text{otherwise} \end{cases} \tag{3.67}$$

There is also an inhomogeneous part for the coupled node temperatures (customer nodes). The elements b_i^{nodes} of the vector $\mathbf{b}^{nodes}$ with the size $2\,m \times 1$ are

$$b_i^{nodes} \in \mathbf{b}^{nodes}, i = 1 \dots 2\,m = \begin{cases} \Delta T_c & \text{if node } i \text{ is a customer node and supplier} \\ -\Delta T_c & \text{if node } i \text{ is a customer node and consumer} \\ 0 & \text{otherwise} \end{cases} \tag{3.68}$$

To couple the pipe's outlet and inlet temperatures and to calculate the node temperatures a few more matrices have to be created. To this end the incidence matrix $\mathbf{I}$ is divided based on the results of the hydraulic calculation into $\mathbf{I^{in}}$ and $\mathbf{I^{out}}$:

$$\mathbf{I^{in}} = (i_{n,i}^{in}) = \frac{|\mathbf{I}| + \mathbf{I}}{2} \tag{3.69}$$

$$\mathbf{I^{out}} = (i_{n,i}^{out}) = \frac{|\mathbf{I}| - \mathbf{I}}{2} \tag{3.70}$$

with $\mathbf{I^{in}}$ representing all the input nodes for each arc (output nodes for each node) of the network and $\mathbf{I^{out}}$ for the output nodes for each arc (input nodes for each node). Each arc's inlet and outlet temperature corresponds to a node temperature. Since only node inlet temperatures are relevant for finding the mixing temperatures inside the nodes, the arc's inlet and outlet temperatures are divided here in $\mathbf{T_a^{in}} \subseteq \mathbf{T_p}$ and $\mathbf{T_a^{out}} \subseteq \mathbf{T_p}$. The coefficients e_i in eq. (3.64) for the warm and the cold network can be determined using the following formulas:

$$\mathbf{E}^f = (e_{mn}^f) = -diag\left(\left(\mathbf{I}_f^{\mathbf{out}}\,\dot{\mathbf{m}}_{\mathbf{nw}}^f\right)^{-1}\right)\,\mathbf{I}_f^{\mathbf{out}}\,diag\left(\dot{\mathbf{m}}_{\mathbf{nw}}^f\right) \quad f = h, c \tag{3.71}$$

and ultimately

$$\mathbf{EE} = \begin{bmatrix} \mathbf{E}^h & 0 \\ 0 & \mathbf{E}^c \end{bmatrix} \tag{3.72}$$

Based on the arc's outlet temperatures, which are node inlet temperatures, the equation system for the node temperatures follows:

$$\begin{bmatrix} \mathbf{EE} & \mathbf{N} \end{bmatrix} \begin{bmatrix} \mathbf{T_a^{out}} \\ \mathbf{T_n^h} \\ \mathbf{T_n^c} \end{bmatrix} = \mathbf{b}^{nodes} \tag{3.73}$$

Due to the fact that $\mathbf{T_a^{out}} \subseteq \mathbf{T_p}$, a transformation has to be applied on $\mathbf{EE}$. In order to get an equation system for the network temperatures with respect to the variable vector $\mathbf{T_{nw}}$ introduced in eq. (3.66), the matrix $\mathbf{EE}$ has to be reallocated to have the same column number like $\mathbf{T_p}$. The target size is $2\,m \times \sum_{i=1}^{n} 6\,l_i$. As mentioned previously, the node inlet flow temperatures correspond to the temperatures of the last volume element in flow direction of the connected pipe which carries water towards the node. These temperatures are the last elements of the vector entries in $\mathbf{T_p}$, respectively. Therefore, the new matrix's $\tilde{\mathbf{EE}}$ columns k are created by extracting the proper columns from $\mathbf{EE}$ as follows:

$$(\tilde{ee}_{jk})_{j=i;\, k=\sum_{f=1}^{s-1} l_f+\delta\, i_{h,out}+(1-\delta)\, i_{c,out}} = (ee_{is})_{i=1\ldots 2\,m; s=1\ldots 2\,n} \tag{3.74}$$

with

$$\delta = \begin{cases} 1 & \text{if } s \geq n \\ 0 & \text{otherwise} \end{cases} \tag{3.75}$$

and $i_{h,out}$ and $i_{c,out}$ being the column indices of the temperatures in $\mathbf{TP}_s$ which represent the warm and cold pipe outlet temperatures, respectively, see eq. (3.59).

Last step is the link from pipe inlet temperatures to the corresponding node temperatures. The matrix $\tilde{\mathbf{A}}^f$ links the pipe inlet temperatures with the node temperatures obtained by the incidence matrix $\mathbf{I^{in}}$. For the subset $\mathbf{T_a^{in}}$ the following applies:

$$\mathbf{A}^f = (a_{ij}^f) = (\mathbf{I}_f^{\mathbf{in}})^\intercal \quad f = h, c \tag{3.76}$$

and

$$\mathbf{AA} = \begin{bmatrix} \mathbf{A}^h & 0 \\ 0 & \mathbf{A}^c \end{bmatrix} \tag{3.77}$$

$\mathbf{AA}$ has double the size of the transposed input incidence matrix $\mathbf{I^{in}}$, thus $2\,n \times 2\,m$. Every row in $\mathbf{AA}$ represents the link for the input temperature for each arc of the network. Given the variable vector $\mathbf{T_{nw}}$, the matrix $\mathbf{AA}$ needs to have the size $\sum_{i=1}^{n} 6\,l_i \times 2\,m$ to fit into the equation system (3.80). Therefore a new matrix $\tilde{\mathbf{AA}}$ is introduced, whose rows (which represent the node outlet temperatures) correspond to the rows of the matrix $\mathbf{AA}$. The rule for the row distribution is as follows:

$$(\tilde{aa}_{jk})_{j=\sum_{f=1}^{i-1} l_f+\delta\, i_{h,in}+(1-\delta)\, i_{c,in};\, k=s} = (aa_{is})_{i=1\ldots 2\,n; s=1\ldots 2\,m} \tag{3.78}$$

with

$$\delta = \begin{cases} 1 & \text{if } i \geq n \\ 0 & \text{otherwise} \end{cases} \tag{3.79}$$

and $i_{h,in}$ and $i_{c,in}$ being the row indices of the inlet temperature boundary condition of the hot and the cold pipe, respectively, in $\mathbf{TP}_s$, eq. (3.59).

The equation system for the temperature vector $\mathbf{T_{nw}}$ then looks like this:

$$\begin{bmatrix} \mathbf{TP}_1 & 0 & \dots & 0 & \\ 0 & \mathbf{TP}_2 & \dots & 0 & \\ \vdots & \vdots & \ddots & \vdots & \mathbf{\tilde{A}A} \\ 0 & 0 & \dots & \mathbf{TP}_n & \\ & & \mathbf{\tilde{E}E} & & \mathbf{N} \end{bmatrix} \mathbf{T_{nw}} = \begin{bmatrix} \mathbf{b}_1 \\ \mathbf{b}_2 \\ \vdots \\ \mathbf{b}_n \\ \mathbf{b}^{nodes} \end{bmatrix} \tag{3.80}$$

Within the networks considered in this work the coupling condition at the consumer nodes is always $\Delta T_c = 4\,\mathrm{K}$. The equation system has still one open inlet and outlet node, respectively. This is the node where the seasonal heat storage is connected to the system. Depending whether the BTES is charged or discharged, it's inlet node is either added at the warm pipe network's or the cold pipe network's connection node. The BTES's outlet node corresponds then to the last open node of the equation system. If the BTES is charged, it provides water to the cold pipe network, therefore the BTES outlet temperature is linked to the specific node in $\mathbf{T_n^c}$. For the discharging operating mode the linking element is set in $\mathbf{T_n^h}$. The equation system for the network temperatures expanded with the BTES model looks then like the following:

$$\begin{bmatrix} \mathbf{TP}_1 & 0 & \dots & 0 & & \\ 0 & \mathbf{TP}_2 & \dots & 0 & & \\ \vdots & \vdots & \ddots & \vdots & \mathbf{\tilde{A}A} & \mathbf{BA} \\ 0 & 0 & \dots & \mathbf{TP}_n & & \\ & & \mathbf{\tilde{E}E} & & \mathbf{N} & \\ & & \mathbf{BE} & & & \mathbf{BT} \end{bmatrix} \mathbf{T_{nw}} = \begin{bmatrix} \mathbf{b}_1 \\ \mathbf{b}_2 \\ \vdots \\ \mathbf{b}_n \\ \mathbf{b}^{nodes} \\ \mathbf{b}^{btes} \end{bmatrix} \tag{3.81}$$

For further information about the BTES model and the determination of **BT**, **BA**, **BE** and $\mathbf{b}^{btes}$ see section 4.2.3.

The solution vector $\mathbf{T_{nw}}$ of the linear equation system (3.81) is found using the *mldivide* command in MATLAB®. (see 1.5.2)

Chapter 4

Seasonal Thermal Energy Storage

The proposed system allows for the usage of low temperature industrial, commercial and/or residential waste heat. In general the time period of the accruing of such low-grade thermal energy doesn't meet necessarily the demand of thermal useful energy. Therefore, a seasonal thermal energy storage is connected to the ring network. The objective is to bridge the gap between the different time intervals of demand and usage of low temperature waste heat and to allow for an energy efficient cooling during summer months. Cooling in that case doesn't need effort in terms of electrical energy (except the hydraulic pumps), but takes place by simply dumping thermal energy into the TES. This kind of cooling is named in the following *free cooling*. Although there are several different ways in achieving seasonal thermal energy storage the system chosen in this work is a borehole thermal energy storage system (BTES).

In this chapter the methodology in simulating the proposed seasonal thermal energy system is presented. First, a general overview of the available tools is stated. It follows the presentation of a numerical finite volume approach to handle the local heat transfer in BTES rapidly in the framework of district heating network simulations. Finally the connection between local and global problem, which is the thermal interaction between vertical heat exchangers placed in a quadratic borehole field is presented.

4.1 Overview

Borehole thermal energy storage systems (BTES) are widely used as seasonal heat storage systems and well described in literature. The behavior of duct heat storage when heat exchange processes accrues are described both analytically [68, 37] as well as numerically [10, 20]. There are existing models for simulation environments, for instance TRNSYS, [69] which have been tested and validated on existing systems.

Research considering the systemic approach of BTES coupled with ground-source heat pump (GSHP) is proceeding recently. Yuan et al. states in Ref. [93] the deterioration of a GSHP-

system if the heat injected into and extracted from the underground is imbalanced in long terms. Hence, the authors propose a control strategy for the BTES with borehole free cooling to restore the ground storage system. In this work it is paid particular attention to the heat balance of the underground to avoid deterioration processes on a long term scale. The necessary amount of low temperature heat supply to the system and therefore to the BTES for the operating years is investigated in the following chapters.

A methodology for the design of BTES systems is presented by *Zhang et al.* in Ref. [95]. In this systemic approach the authors make use of g-functions to simulate the BTES performance. Together with the Hooke-Jeeves pattern search algorithm they find the optimal combination of the distance between boreholes, borehole depth and borehole number under a given annual heat load.

Groundwater flows can have a noticeable impact on BTES performance. *Choi et al.* investigate in [17] the effects of groundwater flows on various BHE configurations using a two-dimensional coupled heat conduction-advection model. The results show that especially L-type and single line arrays are affected significantly by the ground water's flow direction and flow rate. For groundwater flow velocities of less than $1\frac{m}{a}$ the groundwater effect on the system's performance was found to be negligible. In this work the considered BTES fields are assumed to have a quadratic densely packed appearance, hence the effect of groundwater flows on the BTES can be neglected.

Eskilson presents in [68] the there called Δ-Model, fig. 4.1, which constitutes a steady state heat circuit including the downstream and upstream pipes of a single U-pipe and the pipe surrounding material. Heat flows between the two pipes and between each pipe and the surrounding material are calculated using the *mulipole method*. The Δ-Model thus is able to handle bypass heat flows between the two pipes, which in fact behave like a counterflow heat exchanger as well as the net heat flow to/from the surrounding grout/soil material. *Hellström* proposes in [37] the so called duct storage systems (DST) which gives accurate (analytical) results for densely packed ground heat exchangers. The analysis of the storage material involved in heat transfer processes is divided into two parts. One is the direct surrounding of the buried pipes (local process) and the second one constitutes the volume outside the enclosed drilled volume (global process). The results of these two coupled processes are obtained by applying a two-dimensional finite difference method on the global process and by solving the Δ-Model circuit on the local scale process.

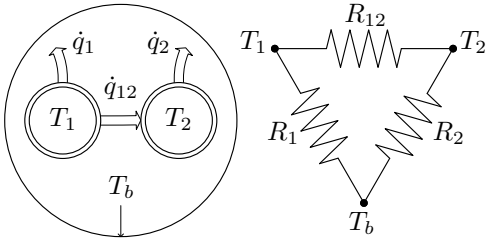

FIGURE 4.1: Cross-section of the borehole, left and Δ-Model, right [37]

DST are suitable for a large number of distinct boreholes which are densely packet in a rectangular or circular cross section. *Hellström* is using in [37] the Δ-Model and handles short-term responses due to step changes in heat rejections/injections from/into the ground heat exchanger with a Laplace transformation. The obtained solutions which contain Bessel functions of the first and second kind are difficult and time-consuming to evaluate. Hence, an approximation, called the line source approximation, is used instead of the Laplace transform method. The author provides a time threshold where the relative error of the line source approximation in respect to the exact solution falls below 10%, which is specified as the time limitation for the Δ-Model:

$$t > t_b = \frac{5\, r_b^2}{a}$$

For reasonable values of the thermal diffusivity a with the magnitude $10^{-6}\, m^2/s$ and the pipe radius' magnitude $10^{-1} - 10^{-2}\, m$ the simulation time minimum step size is in the range several minutes to quite a few hours. For investigations of heat pump's performances and network issues this time limitation is too extensive. Another method in describing the influence of vertical heat exchangers on the surrounding soil material are g-functions, [68]. *Lamarche* mentiones in [48] the g-functions to determine the temperature difference $T_b - T_0$:

$$T_b - T_0 = \frac{\dot{q_0}}{2\,\pi\, k}\, g\left(\frac{t}{t_s}\,,\, \frac{r_b}{H_b}\,,\, borefield\ geometry\right) \tag{4.1}$$

with

$$t_s = \frac{H_b^2}{9\, a} \tag{4.2}$$

T_0 in this case is the temperature at $t = 0$, H_b stands for the borehole height.

Different g-functions for different BTES array configurations can be found in the literature, [68].

Bauer developed in [10] a model to avoid the time step size limitation as well as the necessary stationary condition of the Δ-Model. These so called *resistance capacity models* allow for the investigation of short time related changes in ground heat exchangers by adding a thermal capacity on elements which participate in the heat exchanging process.

4.2 BTES Model

This work aims for the simulation of a low temperature energy distribution network with attached seasonal heat storage. This section contains an overview over the seasonal heat storage simulation which takes part in the thermal network calculation. Firstly the governing equation is found by editing the transport equation (1.8) from chapter 1.5.1. The replacement of ϕ with the specific enthalpy h in eq. (1.8) and replacing the diffusion term results in the energy conservation equation for a finite volume element:

$$\frac{\partial}{\partial x_i}\left(u_i\, h\right) + \frac{\partial h}{\partial t} = \frac{\partial}{\partial x_i}\left(k\,\frac{\partial T}{\partial x_i}\right) + S \tag{4.3}$$

For small pressure variations and ideal fluids and solids the simplification $dh = c_p\, dT$ is feasible:

$$c_p\left(\frac{\partial}{\partial x_i}\left(u_i\, T\right) + \frac{\partial T}{\partial t}\right) = \frac{\partial}{\partial x_i}\left(k\,\frac{\partial T}{\partial x_i}\right) + S \tag{4.4}$$

If there is no heat source/sink and if the thermal properties are assumed to be constant the general form of the heat transport equation yields to

$$\frac{1}{a}\,\frac{\partial}{\partial x_i}\left(u_i\, T\right) + \frac{1}{a}\,\frac{\partial T}{\partial t} = \frac{\partial^2 T}{\partial x_i^2} \tag{4.5}$$

with

$$a = \frac{k}{c_p} = \frac{\lambda}{\rho\, c_p} \tag{4.6}$$

For heat transport processes in the underground assumed to take place by heat conduction only the first term disappears and the governing equation becomes

$$\frac{1}{a}\,\frac{\partial T}{\partial t} = \frac{\partial^2 T}{\partial x_i^2} \tag{4.7}$$

Within the heat storage model heat transport not only takes place by heat conduction. For the heat transfer from the fluid to the surrounding solid material the governing equations is eq. (4.5). The equations for the usage in the equation system are already defined by the resistance-capacity model from chapter 3.3.2. The heat transport process is divided here into two parts. The first one, which describes the heat transfer process from the fluid to the U-tube is called in the following *Local Process*. The determination of the interaction from the U-tube with the surrounding soil and the associated temperature differences are stated as *Global Process*. An overview over the two processes is given here. It follows then the formulation of a simulation model for vertical ground source heat exchangers for single U-pipes. The accuracy of the model for both the local and the global processes is examined by calibrating the simulation model. The BTES simulation model is then embedded into the thermal network calculation which yields to

an integrated network-storage simulation model.

4.2.1 Local Process

The aim of solving the local problem is to obtain the water outlet temperature and the heat supplied to/from the underground. The conduction/convection heat transfer problem is solved with a finite volume methodology. The heat flow circuit of one horizontal layer is shown in the following fig. 4.2:

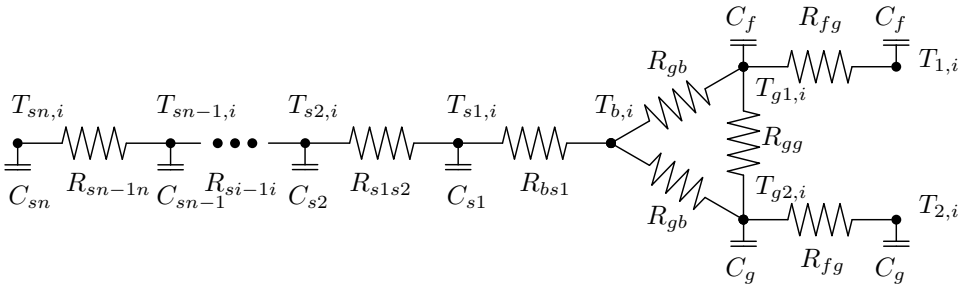

FIGURE 4.2: Resistance Capacity Model for a single horizontal layer i, [10]. Every volume element with the capacity symbol is also coupled with the adjacent cells in z direction

The water temperature in the downward pipe is $T_{1,i}$ and $T_{2,i}$ in the upward pipe. The thermal resistances R_i and the thermal capacities C_i are all normalized with the borehole's depth and satisfy the relations:

$$\dot{q}_i = \frac{\Delta T_i}{R_i}, \qquad \dot{q}_i = C_i \frac{\partial T_i}{\partial t}$$

The heat transport problem is solved using a two dimensional finite volume method. The annular volumes are concentrated into singular points as shown in Fig. 4.3. The discretization is carried out in axial direction Δz and in radial direction.

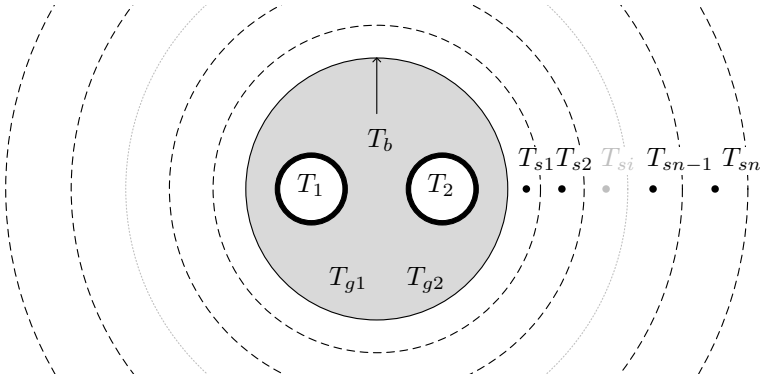

FIGURE 4.3: Horizontal borehole section, discretization cells in respect to the resistance capacity model, grey: grouting material

The thermal resistances R_i are given in [10]. Energy transport from the fluid to the grouting material takes place by convection and conduction. The thermal resistance R_{fg} in (4.2) is a combination of these two processes:

$$R_{fg} = R_{convection} + R_{pi} + R_g \tag{4.8}$$

The resistance R_g is usually found by using the *Multipole Method*, [12]. *Bauer* proposes in [10] an empirical, simulation based relation for the thermal resistance between the pipe's outer wall and the borehole's wall. For single U-pipes the equation for the thermal resistance is given by:

$$R_g \approx \frac{\operatorname{arcosh}\left(\frac{d_b^2+d_a^2-s^2}{2\,d_b\,d_a}\right)}{2\,\pi\,\lambda_g}\left(1.0601 - 0.888\,\frac{s^2}{d_b^2}\right) \tag{4.9}$$

with d_b and d_a being the borehole diameter and the outer pipe diameter. s is the single u-pipe's tube spacing. For the other thermal resistances R_{gg}, R_{gb}, R_{bs1} and R_{sisj} and the capacities C_i see [10].

4.2.2 Global Process

For the global process the heat sink term in equation (4.4) is different from zero. There is no convective contribution for the heat transport from the borehole to the surrounding ground. Starting from equation (4.4) the general form of the heat conduction in cylindrical coordinates is:

$$\frac{\partial^2 T}{\partial r^2} + \frac{1}{r}\,\frac{\partial T}{\partial r} + \frac{1}{r^2}\,\frac{\partial^2 T}{\partial \varphi^2} + \frac{\partial^2 T}{\partial z^2} = \frac{1}{a}\,\frac{\partial T}{\partial t} \tag{4.10}$$

Here, as usual in the literature the angular dependence of the temperature is neglected and the heat transfer is assumed to be a radial and axial heat conduction problem. The equation (4.10) simplifies to

$$\frac{\partial^2 T}{\partial z^2} + \frac{\partial^2 T}{\partial r^2} + \frac{1}{r}\,\frac{\partial T}{\partial r} = \frac{1}{a}\,\frac{\partial T}{\partial t} \tag{4.11}$$

with the boundary conditions (see also [44]):

$$\begin{aligned} -2\,\pi\,r_b\,\lambda\,\frac{\partial T}{\partial r} &= \dot{q_b}\;|_{r=r_b\;0\le z\le H} \\ T - T_0 &\to 0\;|_{r\to\infty} \\ T - T_0 &= 0\;|_{t=0} \end{aligned}$$

$\dot{q_b}$ is the heat flow per unit length. Two solutions for a temperature distribution which satisfy equation (4.11) if a step function in the heat flow $\dot{q}(t) = \dot{q}_0\,u(t)$ is applied at t are shown here: The

cylindrical heat source method (CHSM), [16] and the much simpler solution known as Kelvin's infinite line-source theory, [44]. The heat source is applied in the first case at the borehole radius r_b and at $r = 0$ in the latter case.

Cylindrical heat source method

$$T(\tilde{r}, \tilde{t}) - T_0 = \frac{\dot{q}}{\lambda \pi^2} \int_0^\infty \frac{e^{-z^2 \tilde{t}} - 1}{z^2 \left(J_1^2(z) + Y_1^2(z)\right)} \left(J_0(\tilde{r}z)\, Y_1(z) - J_1(z)\, Y_0(\tilde{r}z)\right) dz \tag{4.12}$$

with the dimensionless radius $\tilde{r} = \frac{r}{r_b}$ and the Fourier number $\tilde{t} = Fo = \frac{a\,t}{r_b^2}$.

Kelvin's infinite line-source theory

$$T(\tilde{r}, \tilde{t}) - T_0 = \frac{\dot{q}}{4\,\pi\,\lambda} \int_{\frac{\tilde{r}^2}{4\,a\,\tilde{t}}}^\infty \frac{e^{-u}}{u} du \tag{4.13}$$

Lamarche shows in [48] that the error in the solutions for the CHSM and the infinite line-source theory are small for $Fo > 20$. Due to the more practical mathematical handling of the solution obtained by the Kelvin's infinite line-source theory this equation is used in the actual work to solve the global temperature process. The evaluation of equation (4.13) and hence the adjusting of the local processes radial boundary condition is executed periodically in every time step that fulfills the following condition:

$$t_n - t_{n-1} > 20\, \frac{r_b^2\, c_p\, \rho}{\lambda}$$

Due to the linearity of the conduction equation (4.10) the superposing of the temperature responses of m multiple boreholes with the heat flows $q_1 \ldots q_m$ results in the global temperature field:

$$\Delta T(x, y, \tilde{t}) = \sum_{i=1}^{m} \frac{\dot{q}_i}{4\,\pi\,\lambda} \int_{\frac{\tilde{r}_i^2}{4\,a\,\tilde{t}}}^\infty \frac{e^{-u}}{u}\, du \tag{4.14}$$

where $\tilde{r}_i$ is the distance from the center of he borehole i and the coordinates of the point of interest x, y in respect to the borehole diameter r_b. For a probe i the influence of the eight adjacent probes are additionally taken into account. The methodology in obtaining the boundary condition's temperature is shown in fig. 4.4.

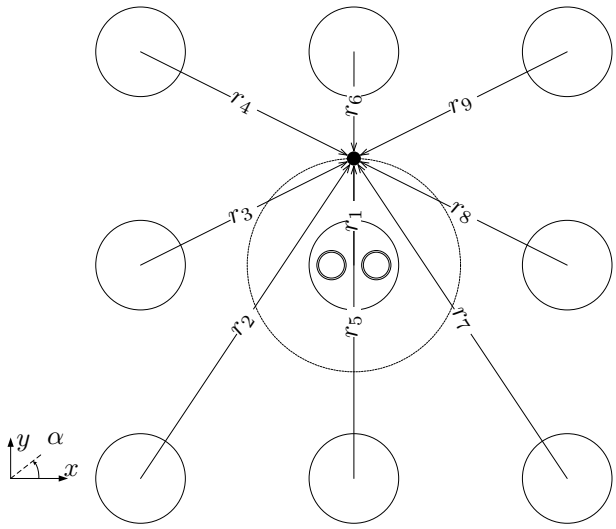

FIGURE 4.4: Scematic representation of the methodology for calculating the boundary temperature at d_{bc} for the center probe with consideration of the adjacent boreholes. Influence of all the 9 boreholes for the point at $\alpha = \frac{\pi}{2}$

The heat flow $\dot{q}$ in the previous equations comes from the local process (chapter 4.2.1) and is equal the heat flow moving over the boreholes wall located at $r_b = \frac{d_{bc}}{2}$. The effect of eq. (4.14) is rather small for small temperature differences between ground and water and short time steps. Due to the Fourier number limitation the global process, hence, the influence of the interaction between adjacent probes, is only evaluated if $Fo > 20$. The time span for this condition with the selected thermopysical soil data and the borehole diameter is found to be appropriate with 24 hours. The mean temperature difference at time t when the global process is evaluated is then equal the mean value of the temperature differences of all the points describing the diameter where the temperature boundary condition specification is set, see chapter 4.2.3 and fig. 4.5.

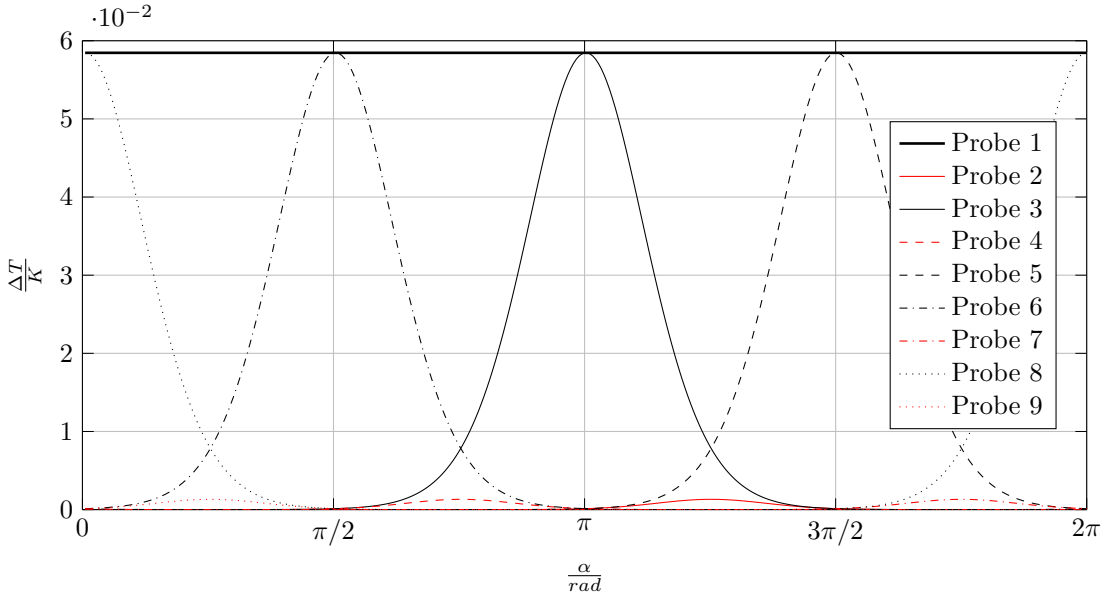

FIGURE 4.5: Radial temperature differences caused by the probes 1-9 at the diameter d_{bc} for the center borehole from fig. 4.4 with $\dot{q} = 10$ W/m and $\Delta t = 240$h

Since only the probes that are located in the center of the borehole field have eight adjacent probes, the borehole heat exchangers that are located on the border and the edges of the borehole field perform differently than the center ones. This is the reason why more than one single probe have to be simulated within the network simulation. The effects of the thermal interaction of vertical heat exchangers within the heat supply network and the associated change in waste heat energy supply is investigated in the following chapters. The borehole distance within the borehole field is chosen here to be equally sized in x and y direction. This yields to a quadratic borehole field. For simulation speed reasons not every borehole is simulated. The necessary number of borehole simulations is determined by the exploitation of the four symmetry axes as shown in the following figure:

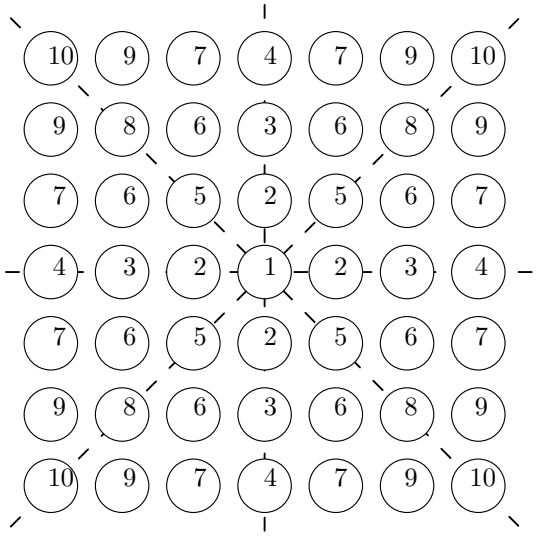

FIGURE 4.6: 7×7 Borehole field symmetry for equally sized borehole distances

For the borehole field shown in fig. 4.6 the number representative boreholes is $n_{rb} = 10$. In that case the BTES simulation model accounts for 10 single probes. For a quadratic borehole field with the side length z_b, hence $n_b = z_b^2$, n_{rb} can be determined with behalf of the triangular number:

$$n_{rb} = \frac{z^* \left(z^* + 1\right)}{2} \tag{4.15}$$

with

$$z^* = \begin{cases} \frac{z_b}{2} & \text{if } \frac{z_b}{2} \in \mathbb{Z} \\ \frac{z_b+1}{2} & \text{otherwise} \end{cases} \tag{4.16}$$

For large numbers z_b the number of probes located within the borehole field rises rapidly. If the amount of necessary boreholes is much smaller than the possible numbers prescribed by $n_b = z_b^2$ the borehole number is adjusted by cutting off the corners, hence by omitting the simulation of borehole 10 and/or 9 etc. from fig. 4.6.

4.2.3 Simulation Model

The methodology shown in section 4.2.1 and 4.2.2 is applied to a simplified BTES model. For that purpose an equation system based on a finite horizontal and vertical local discretization is performed. In this section the methodology in compiling the equation system and setting the corresponding boundary conditions is shown. Aim is to find the missing matrices **BT**, **BA**, **BE** and $\mathbf{b}^{btes}$ from chapter 3.3.2.

In the following it is assumed, that the soil which, together with the single u-tubes, constitute a single BTES element is divided into $i = 1 \dots m$ horizontal layers, with the vertical dimension

$\Delta z = \frac{H}{m}$. In the radial direction according to the *resistance capacity model* proposed by *Bauer* in [10] the BTES consists of $7 + n$ cells, if the number of the radial finite soil cells is $j = 1 \dots n$. The variable vector for the temperatures of one horizontal layer is

$$\mathbf{T}_{1L} = \begin{bmatrix} T_1 & T_2 & T_{g1} & T_{g2} & T_b & T_{s1} & T_{s2} & \dots & T_{sn} \end{bmatrix}^\intercal \tag{4.17}$$

In order to obtain an equation system which describes the heat conduction problem between adjacent volume elements as well as the heat transfer between water and the grouting material a few equations have to be defined. The presented equations here are based on the work by *Bauer* described in [10]. For further insight considering the factors C_i and R_i see the literature. Referring to the capacity resistance model, fig. 4.2 the radial heat transport problem inside one horizontal layer requires the following relations:

- heat transfer water - grouting material
- heat conduction grouting material - borehole wall
- heat conduction borehole wall - 1^{st} soil volume element
- heat conduction surrounding soil volume elements

Since the resistance capacity model was already used in the determination of the twin pipe model in chapter 3.3.2, the equations (3.51) - (3.53) are also used for the BTES simulation model. The soil as a participant in the heat transfer problem was not considered within the pipe model. Therefore, two more equations are defined here. The first one handles the heat transfer from the borehole wall to the first soil volume element. $T_{s1,i}$ stands for the temperature of the first soil element outside the borehole wall. The heat transport processes for this cell have the same phenomenology and directions like the heat transport terms in equation (3.52). Hence, the equation for $T_{s1,i}$ follows with:

$$\left(\frac{\partial T_{s1,i}}{\partial t}\right)_i = \frac{1}{C_{s1}} \left[\frac{T_{s2,i} - T_{s1,i}}{R_{s1}} + \frac{T_{b,i} - T_{s1,i}}{R_{s0}} + \frac{A_{s1}\,\lambda_s}{\Delta x^2} \left(T_{s1,i-1} + T_{s1,i+1} - 2\,T_{s1,i}\right) \right] \tag{4.18}$$

The second equation is the general equation for an arbitrary soil element $j = 2 \dots n$ in radial direction:

$$\left(\frac{\partial T_{sj,i}}{\partial t}\right)_i = \frac{1}{C_{sj}} \left[\frac{T_{sj+1,i} - T_{sj,i}}{R_{sj}} + \frac{T_{sj-1,i} - T_{sj,i}}{R_{sj-1}} + \frac{A_{sj}\,\lambda_s}{\Delta x^2} \left(T_{sj,i-1} + T_{sj,i+1} - 2\,T_{sj,i}\right) \right] \tag{4.19}$$

To assure a fast and straight-forward applicability to a equation system based on the variable vector shown in eq. (4.17) the equations and factors are prepared to have the form $T_k + \sum \alpha_i\, T_i =$

β_i. After the integration in time, in analogy to chapter 3.3.2, an equation system for a horizontal layer i is obtained with:

$$EQS_{btes,i}: \begin{cases} \alpha_1^{(1)} T_{1,i-1} + \alpha_2^{(1)} T_{1,i} + \alpha_3^{(1)} T_{1,i+1} + \alpha_4^{(1)} T_{g1,i} = \beta_1 \\ \alpha_1^{(1)} T_{2,i-1} + \alpha_2^{(1)} T_{2,i} + \alpha_3^{(1)} T_{2,i+1} + \alpha_4^{(1)} T_{g2,i} = \beta_2 \\ \alpha_1^{(2)} T_{1,i} + \alpha_2^{(2)} T_{g1,i-1} + \alpha_3^{(2)} T_{g1,i} + \alpha_2^{(2)} T_{g1,i+1} + \alpha_4^{(2)} T_{g2,i} + \alpha_5^{(2)} T_{b,i} = \beta_3 \\ \alpha_1^{(2)} T_{2,i} + \alpha_2^{(2)} T_{g2,i-1} + \alpha_3^{(2)} T_{g2,i} + \alpha_2^{(2)} T_{g2,i+1} + \alpha_4^{(2)} T_{g1,i} + \alpha_5^{(2)} T_{b,i} = \beta_4 \\ \alpha_1^{(3)} T_{g1,i} + \alpha_1^{(3)} T_{g2,i} + \alpha_2^{(3)} T_{b,i} + \alpha_3^{(3)} T_{s1,i} = 0 \\ \alpha_1^{(4)} T_{b,i} + \alpha_2^{(4)} T_{s1,i-1} + \alpha_3^{(4)} T_{s1,i} + \alpha_2^{(4)} T_{s1,i+1} + \alpha_4^{(4)} T_{s2,i} = \beta_6 \\ \alpha_1^{(k)} T_{sj-1,i} + \alpha_2^{(k)} T_{sj,i-1} + \alpha_3^{(k)} T_{sj,i} + \alpha_2^{(k)} T_{sj,i+1} + \alpha_4^{(k)} T_{sj+1,i} = \beta_k; \quad k = 7\,(1 \ldots n) \end{cases} \tag{4.20}$$

The factors $\alpha_e^{(f)}$ and β_e are listed in appendix B.

On the edges of the considered volume some boundary conditions have to be specified. Fig. 4.7 gives an insight into the boundary conditions, whose appearance inside the equation system is shown below. The boundary conditions, BC consist either in temperature specifications or in a no heat flux condition on the edges, as shown in the figure. For the BC_{top} it is assumed, that the geothermal probes of the BTES are thermally insulated on the top layers in that way that temperature influences of the ground surface can be neglected. Due to possible strong dependence of groundwater flows (see section 4.1) on the performance of the borehole heat storage it is assumed here that no groundwater flows accrue below the zero level of the BTES.

The lateral boundary condition, denoted $BC_{lateral}$ in fig. 4.7, is the gateway to the global process. If the global process from chapter 4.2.2 is applied to the probe the prescribed temperatures are not constant anymore, but vary along the timeline according to the single probe's relative configuration and the way they exchange thermal energy with the surrounding soil. In that case a lateral boundary condition (temperature prescription) is applied at the outer diameter D_{bc}.

The dashed lines in fig. 4.7 show the borehole diameter D_b inside which the single u-tube is placed. After inserting the u-tube, the borehole is filled with a high thermal conductivity grouting material, with the thermophysical properties ρ_g, λ_g and c_g.

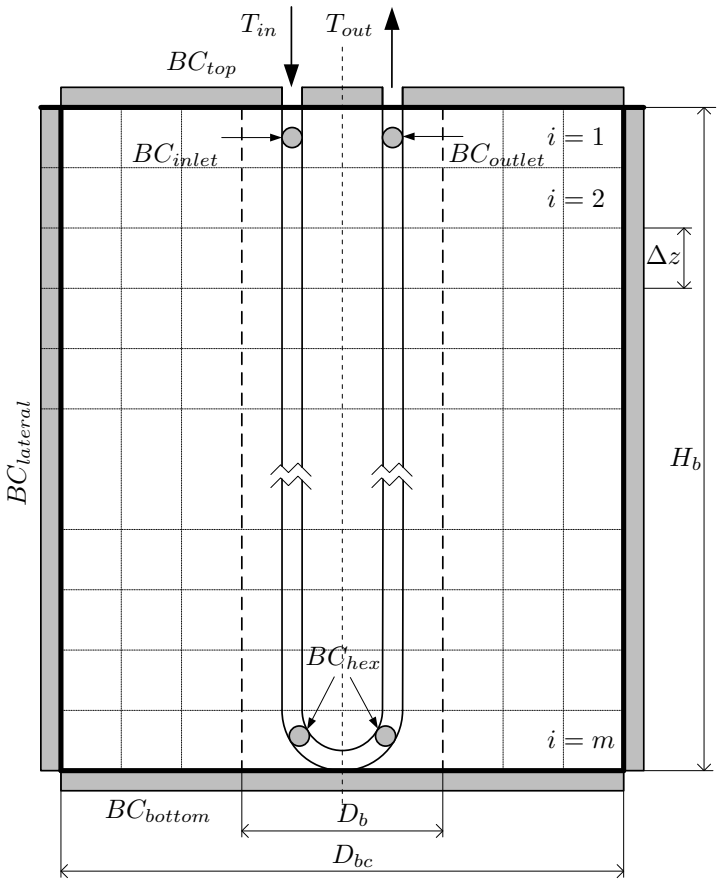

FIGURE 4.7: BTES horizontal layers $i = 1 \dots m$ and boundary conditions

For the smallest possible BTES model, hence $m = 3$ horizontal layers, of which one equipped with the resistance-capacity model, and $n = 1$ soil elements the equation system (4.20) has the following appearance:

$$\begin{bmatrix}
\alpha_1^{(1)} & 0 & 0 & 0 & 0 & 0 & 0 \\
0 & \alpha_1^{(1)} & 0 & 0 & 0 & 0 & 0 \\
0 & 0 & \alpha_2^{(2)} & 0 & 0 & 0 & 0 \\
0 & 0 & 0 & \alpha_2^{(2)} & 0 & 0 & 0 \\
0 & 0 & 0 & 0 & 0 & 0 & 0 \\
0 & 0 & 0 & 0 & 0 & \alpha_2^{(4)} & 0 \\
0 & 0 & 0 & 0 & 0 & 0 & \alpha_2^{(7)} \\
0 & 0 & 0 & 0 & 0 & 0 & 0 \\
\alpha_2^{(1)} & 0 & \alpha_1^{(2)} & 0 & 0 & 0 & 0 \\
0 & \alpha_2^{(1)} & 0 & \alpha_1^{(2)} & 0 & 0 & 0 \\
\alpha_4^{(1)} & 0 & \alpha_3^{(2)} & \alpha_4^{(2)} & \alpha_1^{(3)} & 0 & 0 \\
0 & \alpha_4^{(1)} & \alpha_4^{(2)} & \alpha_3^{(2)} & \alpha_1^{(3)} & 0 & 0 \\
0 & 0 & \alpha_5^{(2)} & \alpha_5^{(2)} & \alpha_2^{(3)} & \alpha_1^{(4)} & 0 \\
0 & 0 & 0 & 0 & \alpha_3^{(3)} & \alpha_3^{(4)} & \alpha_1^{(7)} \\
0 & 0 & 0 & 0 & 0 & \alpha_4^{(4)} & \alpha_3^{(7)} \\
0 & 0 & 0 & 0 & 0 & 0 & \alpha_4^{(7)} \\
\alpha_3^{(1)} & 0 & 0 & 0 & 0 & 0 & 0 \\
0 & \alpha_3^{(1)} & 0 & 0 & 0 & 0 & 0 \\
0 & 0 & \alpha_2^{(2)} & 0 & 0 & 0 & 0 \\
0 & 0 & 0 & \alpha_2^{(2)} & 0 & 0 & 0 \\
0 & 0 & 0 & 0 & 0 & 0 & 0 \\
0 & 0 & 0 & 0 & 0 & \alpha_2^{(4)} & 0 \\
0 & 0 & 0 & 0 & 0 & 0 & \alpha_2^{(7)} \\
0 & 0 & 0 & 0 & 0 & 0 & 0
\end{bmatrix}^{\mathsf{T}}
\begin{bmatrix}
\mathbf{T}_{1L}^{(i=1)} \\
\mathbf{T}_{1L}^{(i=2)} \\
\mathbf{T}_{1L}^{(i=3)}
\end{bmatrix} =
\begin{bmatrix}
\beta_1 \\ \beta_2 \\ \beta_3 \\ \beta_4 \\ 0 \\ \beta_6 \\ \beta_7
\end{bmatrix} \tag{4.21}$$

or

$$\boldsymbol{\alpha}\,\mathbf{T}^{btes} = \boldsymbol{\beta} \tag{4.22}$$

The equation system consists of $6 + n$ equations for the $m\,(7 + n)$ variables. By setting the boundary conditions properly, a fully defined equation system is obtained. The number of additional equations which are provided to the equation system in form of boundary conditions are listed below.

- BC_{top} and BC_{bottom}: $2\,(4 + n)$ equations for the soil elements of the top/bottom layer

$$T_{g1,1} = T_{g2,1} = T_{b,1} = T_{s1,1} = \ldots = T_{sn-1,1} = T_{soil}^{top} \tag{4.23}$$

$$T_{g1,m} = T_{g2,m} = T_{b,m} = T_{s1,m} = \ldots = T_{sn-1,m} = T_{soil}^{bottom} \tag{4.24}$$

- $BC_{lateral}$: m equations for the lateral soil cells

$$T_{sn+2,i} = T_{soil}^{lateral} \qquad i = 1 \ldots m \tag{4.25}$$

- BC_{inlet}: One equation for the water inlet temperature T_1 at the top layer

$$T_{1,1} = T_{BTES,inlet} = T_n^{inlet} \tag{4.26}$$

- BC_{outlet}: One equation for the water outlet temperature T_2 at the top layer

$$T_{2,1} = T_{2,2} \tag{4.27}$$

- BC_{hex}: Two equations for the heat transfer water - soil on the probe's bottom layer

$$\alpha_1^{(BC)}\, T_{1,m} + \alpha_2^{(BC)}\, T_{g1,m} + \alpha_3^{(BC)}\, T_{1,m-1} + \alpha_4^{(BC)}\, T_{2,m} = 0 \tag{4.28}$$

$$\alpha_1^{(BC)}\, T_{2,m} + \alpha_2^{(BC)}\, T_{g2,m} + \alpha_3^{(BC)}\, T_{1,m} + \alpha_4^{(BC)}\, T_{2,m-1} = 0 \tag{4.29}$$

$$\alpha_2^{(BC)} = -\frac{1}{R_{fg}} \quad \alpha_3^{(BC)} = -\frac{\lambda_f\, A_f}{dz^2} - \frac{\dot{m}\, c_{p,f}}{dz} \quad \alpha_4^{(BC)} = -\frac{\lambda_f\, A_f}{dz^2}$$

$$\alpha_1^{(BC)} = -\alpha_2^{(BC)} - \alpha_3^{(BC)} - \alpha_4^{(BC)}$$

All the boundary conditions are collected within the matrix $\boldsymbol{\alpha}^{bc}$ and the vector $\boldsymbol{\beta}^{bc}$ which results in a matrix with the size $(2\,(4+n)+m+4) \times (m\,(7+n))$ and a vector with $(2\,(4+n)+m+4)$ rows. For the usage in the network thermal calculation procedure the matrices are merged to fit into eq. (3.81). The final equation system for the BTES then is obtained with:

$$\mathbf{BT}\,\mathbf{T}^{btes} = \mathbf{b}^{btes} \tag{4.30}$$

with

$$\mathbf{BT} = \begin{bmatrix} \boldsymbol{\alpha} \\ \boldsymbol{\alpha}^{bc} \end{bmatrix} \tag{4.31}$$

and

$$\mathbf{b}^{btes} = \begin{bmatrix} \boldsymbol{\beta} \\ \boldsymbol{\beta}^{bc} \end{bmatrix} \tag{4.32}$$

The two coupling matrices **BA** and **BE** link the BTES's outlet and inlet with the corresponding network node. Let's assume the BTES connection point is the node n_b. Depending whether the BTES is charged or discharged, $be_{i,j} \in \mathbf{BE} = -1$ for the row i which represents the boundary condition (4.26) and the column j which represents the node n_b^h (charging) or n_b^c (discharging). All the other elements of **BE** are = 0. The matrix **BA** couples the probe's outlet temperature with the corresponding network point, hence with n_b^c if the seasonal heat storage is charged or with n_b^h for the discharging mode.

The equation system (4.30) constitutes a single probe of a BTES system. For the investigation how an array of probes interact with each other the lateral boundary condition $BC_{lateral}$ is

modified. The BTES considered within this work have a depth of $H = 150$m. This limitation is due to increasing specific drilling costs with increasing depths. For rather shallow BTES like the ones used for systems described within this work the geothermal gradient is negligible and the boundary condition in eq. (4.25) is satisfied for one boundary temperature for every layer $1 \dots m$. For design calculations only one representative borehole is calculated. For a number of n_{bh} boreholes the calculated probe receives the fraction $\frac{1}{n_{bh}}$ of the total incoming mass flow.

If the probes are located within a borehole field, the assumption that every probe behaves the same way is no longer true. Probes located in the borehole field's center perform in long term differently than the ones on the edges or corners. In that case it is necessary to simulate a number of boreholes.

4.3 Model Calibration

To determine the quality of the results obtained by the numerical models explained above a model calibration is carried out. For both the processes, local and global a calibration is done. The local process is calibrated with the results of a thermal response test (TRT), which was done for a potential BTES site in Vienna. Before the results of the local problem's model are compared with the measured values obtained by the TRT, a few studies considering the discretization size of both time and space are investigated in detail. Based on different simulation time steps and a varying number of discretization elements in radial and axial direction the systematic error in simulation results is studied.

The calibration of the global process here is done based on a few simulations. Through the comparison of simulation results obtained from models with different boundary conditions the proper functioning of the global process is affirmed.

4.3.1 Local process calibration

For the investigation on the impact of different simulation time steps Δt as well as a different number of axial and radial discretization elements m and n a model of a single BTES probe is simulated with a given test function. This test function is a prescription of inlet temperature and mass flow. Originating from the undisturbed soil temperature which was found by the TRT to be $T_{soil} = 13.1\,°\text{C}$ the BTES is charged first with a temperature of $T_{soil} + 4\text{K}$ and $T_{soil} + 8\text{K}$, respectively. In the following the BTES is discharged in the same way, hence, with $T_{soil} - 4\text{K}$ and $T_{soil} - 8\text{K}$, respectively. The duration of the two cycles is 3h. The water mass flow during the two processes is constant. After the charging mode the mass flow's sign changes from positive to negative, because switching from charging to discharging mode means also a change in flow direction. As the probe's outlet during storage charging is coupled with one node of the cold pipe network, it switches to a node of the warm pipe network when the BTES is discharged.

The test function for the determination of the simulation step size and the number of spacial discretization elements is shown in the following fig. 4.8.

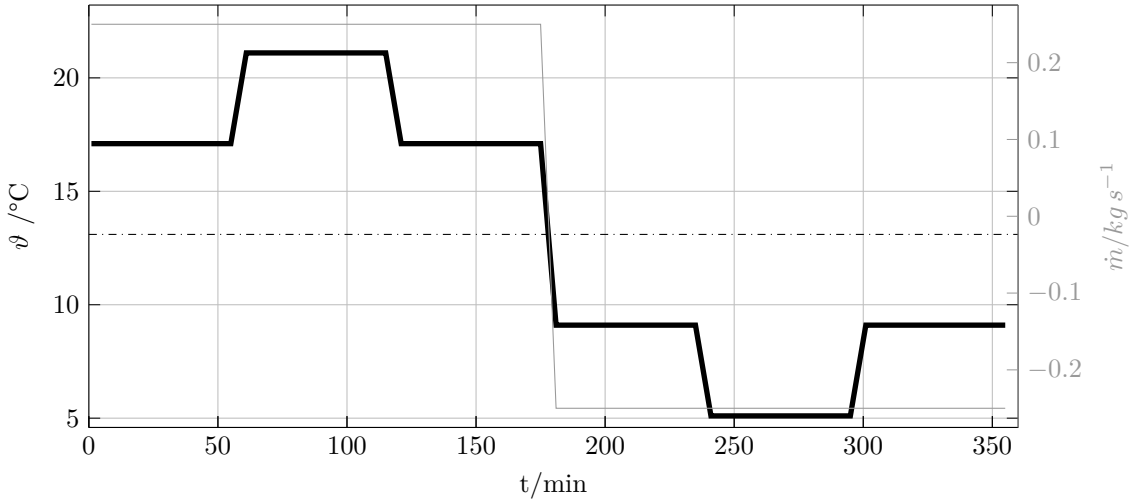

FIGURE 4.8: Test function and undisturbed soil temperature for the determination of the simulation step size and the number of discretization elements

The simulation results heat flux through the pipe wall and outlet temperature are shown for a series of BTES simulations with different time steps Δt. The heat flux is shown in fig. 4.9:

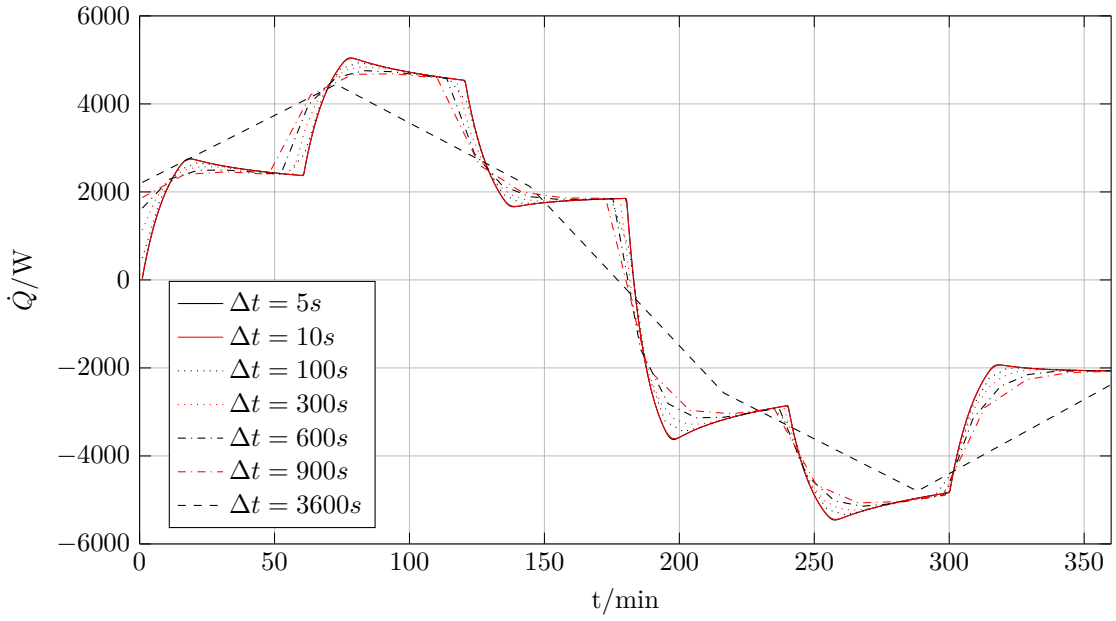

FIGURE 4.9: Storage heat flux through the pipe wall for different simulation time steps and depth $H = 150$m

The probe's outlet temperature for the given test function with respect to the simulation step size Δt is outlined in fig. 4.10. In addition, the error evolution in respect to the most detailed

simulation, hence for the one with $\Delta t = 5$s is shown in the figure.

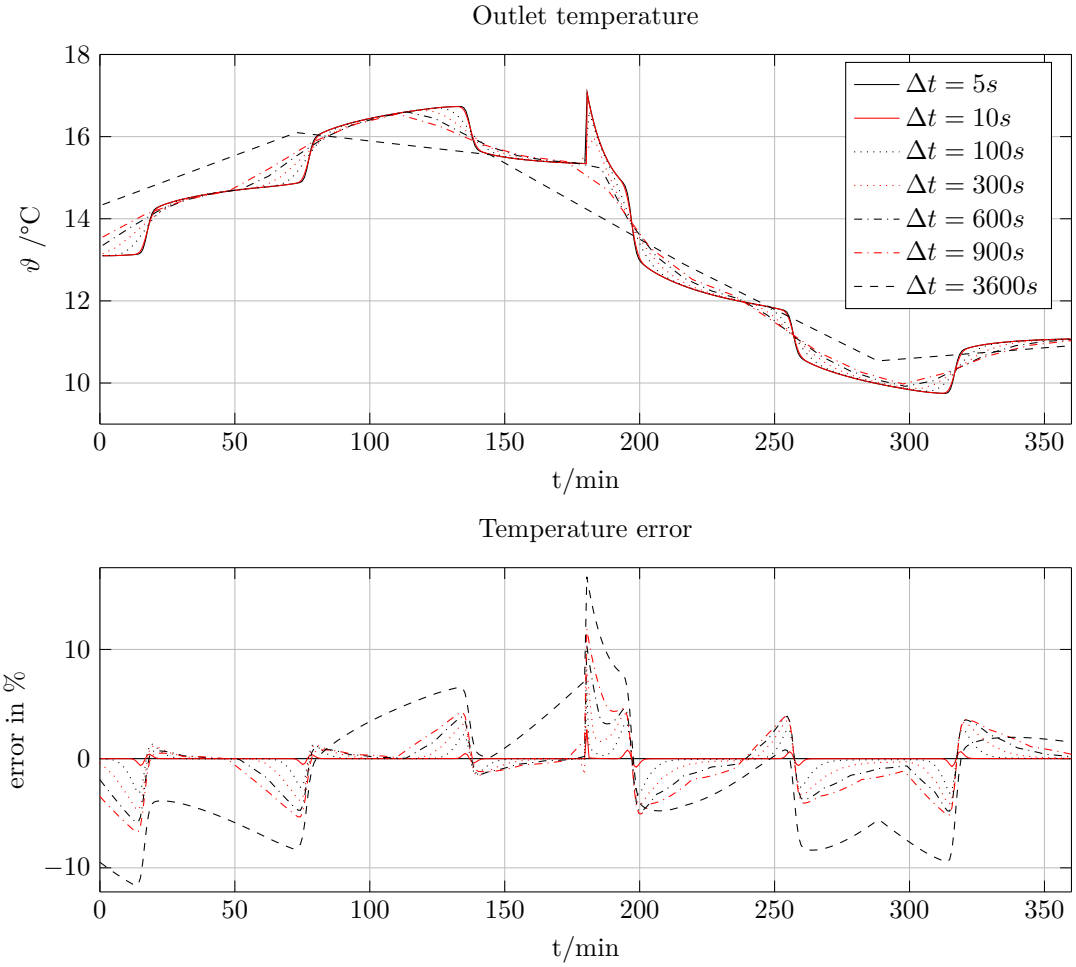

FIGURE 4.10: error in outlet temperature for different simulation time steps

The temperature step which accrues at the time when the BTES's operating mode switches from charging to discharging is due to the change of flow direction. Only the models with a simulation time step $\Delta t < 300$s are able to detect this detail at the given mass flux rate.

The mean error percentages in heat flux as well as in the outlet temperature in respect to the simulation with $\Delta t = 5$s are summarized in the following fig. 4.11:

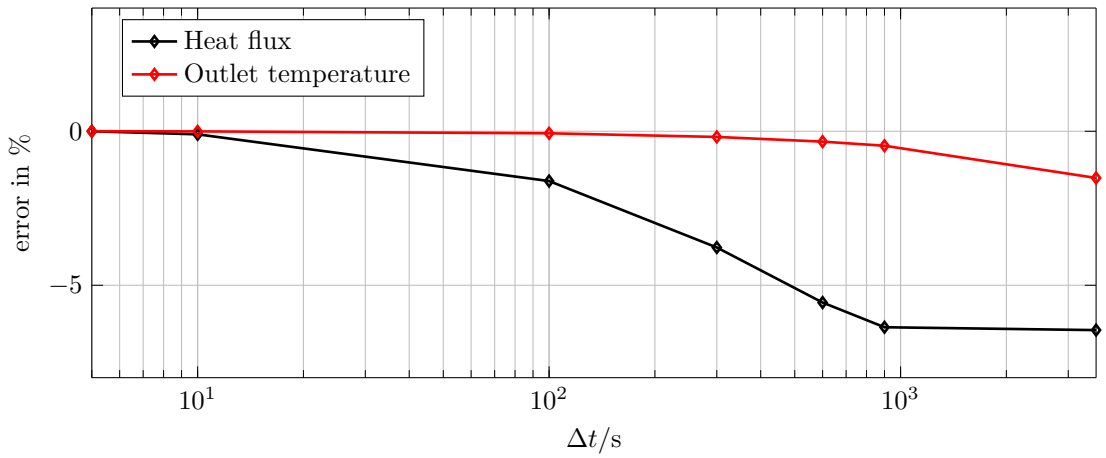

FIGURE 4.11: mean error percentage in heat flux and outlet temperature for different simulation time steps

Note that the heat flux error at $\Delta t = 3600$s seems to remain static. This is due to the BTES operating mode which switches form charging to discharging at half the simulation time. Due to this fact the error evolution averages the mean error percentage out and it remains almost constant in respect to the simulation with $\Delta t = 900$s.

The simulation with $\Delta t = 300$s has a heat flux error percentage of approx. -4% and yields to affordable simulation times for yearly network simulations. Therefore, the simulation time step is set for the following simulations to $\Delta t = 300$s.

The number of discretization elements in both directions, radial and axial is still to define. To do this, the test function is applied again to the BTES model. This time the simulation time step remains constant, the number of discretization elements n in radial direction and m in axial direction is modified. The mean error percentage for the value pairs (n/m) in respect to the most detailed simulation, hence $n = m = 400$ is shown in fig. 4.12.

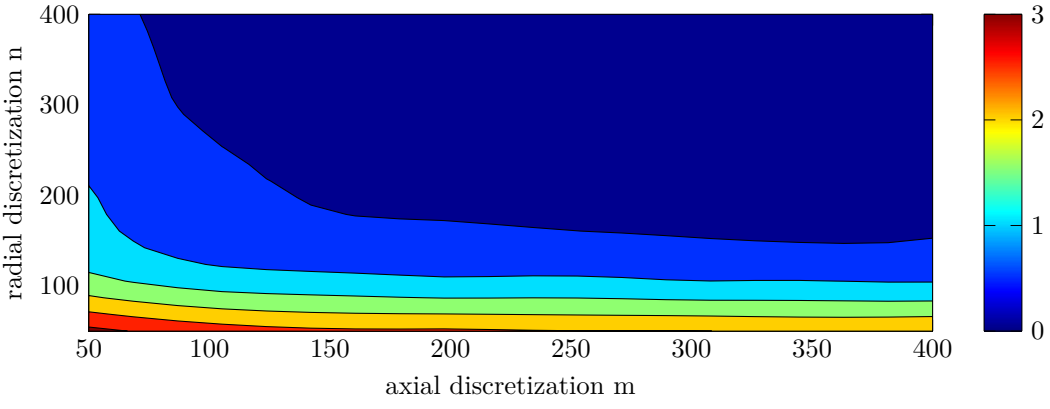

FIGURE 4.12: Mean error percentage in heat flux for $\Delta t = 300$s in respect to the number of discretization elements in radial and axial direction

The mean error percentage shows a stronger dependency on the axial discretization then on the radial one. The selected values for n and m are 100 elements with a mean error percentage of approx. 2%. The following table 4.1 gives a summary over the parameters found by the local process calibration.

TABLE 4.1: Simulation parameters identified by local process calibration

Parameter			expected error percentage
time step	Δt	300s	-3.7727%
axial discretization	m	100	1.8478%
radial discretization	n	100	
total			-1.9249%

The BTES model with the parameters determined by the calibration process is used in further consequence to perform a model validation. The validation aims for getting a BTES model which fits the measurement data obtained by the TRT. This is done by a fine-tuning of the BTES's thermophysical properties and it's geometry. The following fig. 4.13 displays the validation results in the outlet temperature and the table 4.2 lists the BTES properties obtained by the TRT matching process.

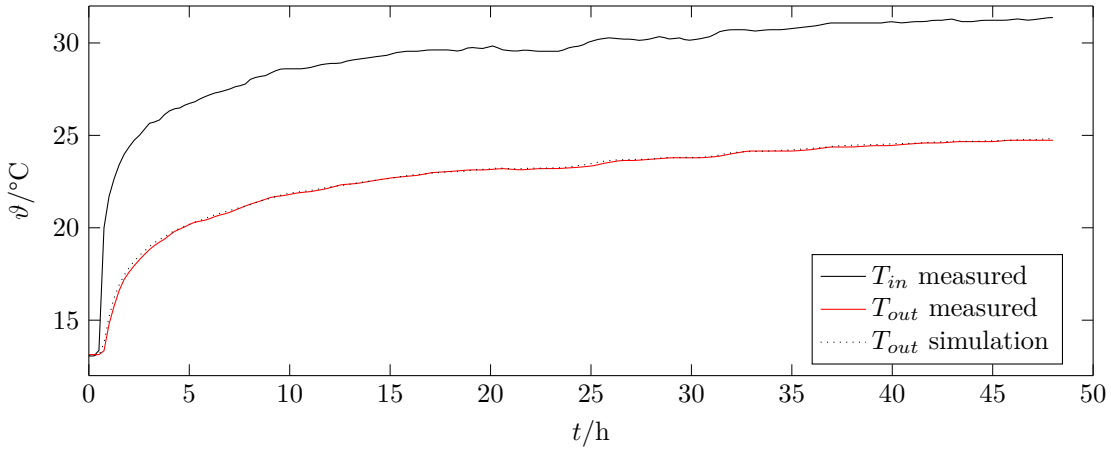

FIGURE 4.13: Temperature measurement (TRT) and simulated outlet temperature

TABLE 4.2: BTES Geometric and thermophysical properties

geometric property			thermophysical property		
pipe inner diameter	d_i	32.6mm	th. conductivity grouting	λ_g	1.5 $\mathrm{Wm^{-1}K^{-1}}$
pipe outer diameter	d_a	40mm	vol. heat capacity grouting	$c_{p,g}\,\rho_g$	$2.00E6\mathrm{Jm^{-3}K^{-1}}$
pipe distance	s	60mm	th. conductivity soil	λ_s	$2.1\mathrm{Wm^{-1}K^{-1}}$
borehole diameter	d_b	127mm	vol. heat capacity soil	$c_{p,s}\,\rho_s$	$1.76E6\mathrm{Jm^{-3}K^{-1}}$

4.3.2 Global process calibration

The aim of the global process as shown in chapter 4.2.2 is to find the temperature specification on the lateral boundary of the simulation model, see 4.7. If the temperature on a specified diameter d_{bc} is known, the influence of adjacent boreholes can be taken into account. The simulation of single boreholes then allows for the investigation of the behavior of a borehole field.

The global process with behalf of Kelvin's infinite line-source theory is used here to find the temperature specification on the lateral temperature boundary condition. In order to assure the accuracy of this methodology some simulations are performed. A network simulation for a whole year is executed with three different BTES models (i-iii):

- *i*: The temperature specification is set at a diameter d_{bc}^{i} which is assumed to be that large that the heat flow on the last radial layer has a negligible impact on the last radial cell's temperature. The temperature specification is here assumed to be constant over the whole simulation period.
- *ii*: The lateral boundary condition is set to a no heat flux boundary condition. That means that the last two cell temperatures are equal in every time step, no thermal energy leaves or enters the BTES simulation space. The boundary condition's diameter here is $d_{bc}^{ii} = d_{bc}^{i}$.
- *iii*: The temperature specification is set at the diameter d_{bc}^{iii} which is equal to the borehole field's single probe spacing. The boundary temperature specification is calculated and adjusted every 24h with Kelvin's infinite line-source theory.

Here no borehole field is simulated, the influence of adjacent boreholes is neglected. The mass flow for the probe simulation is given with the fraction $\frac{1}{n_{bh}}$ of the total mass flow flowing to/from the BTES system. This simulations serve only to assure the model's *iii* accuracy which is used in further consequence to represent the borehole field.

The energy balance for a single probe has to be fulfilled in every simulation time step. The heat flux through the pipe wall towards the first soil layer equals the heat flux that evokes a temperature change in the whole BTES system. If the model uses a specified temperature boundary condition also heat fluxes through the boundary cells have to be taken into account. That means for model *i*:

$$\dot{Q}_1 + \dot{Q}_{bc} = \dot{Q}_{soil} \tag{4.33}$$

since for the model ii $\dot{Q}_{bc} = 0$ applies, the first two simulations have the purpose to justify the selected boundary diameter $d_{bc}^{i} = d_{bc}^{ii}$. The BTES temperature result of the models *i* and *ii* at the diameter $d_{btes}^{i} = d_{bc}^{iii}$ and $d_{btes}^{ii} = d_{bc}^{iii}$ then is compared with the boundary temperature of model *iii* at d_{bc}^{iii}.

The simulation results of the soil temperatures at the diameter d_{bc}^{iii} for the three simulation models *i*-*iii* are shown in the following fig. 4.14:

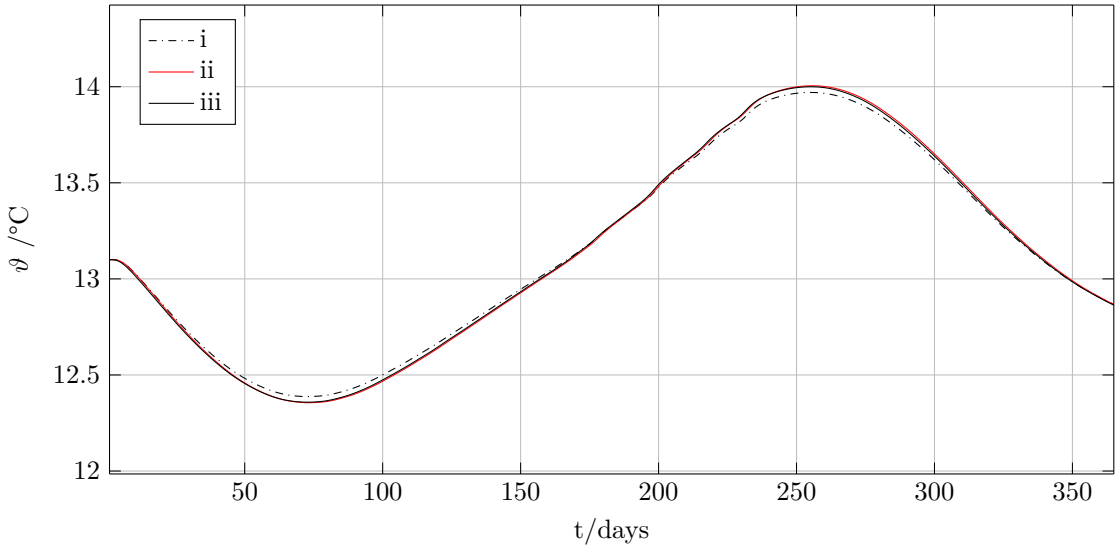

FIGURE 4.14: Temperatures at d_{bc}^{iii} for the models *i-iii*

Input for the determination of the boundary temperature is the specific heat flux to the borehole wall. The accumulated thermal energies in the storage $E(t_i) = \sum_{t=0}^{t_i} \dot{Q}(t)\,\Delta t$ during the simulation period for the three models $i - iii$ are shown in fig.4.15

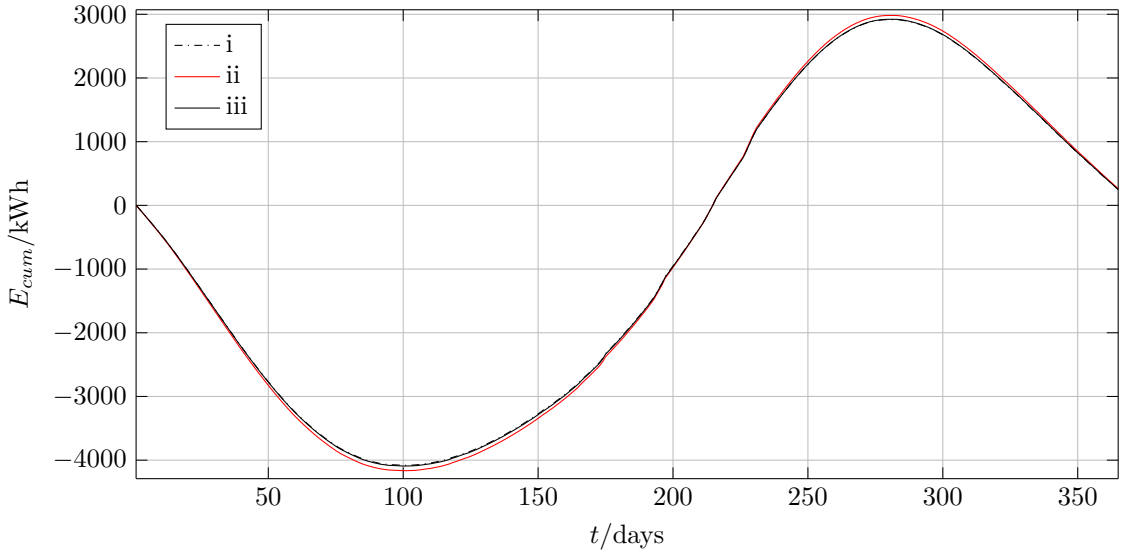

FIGURE 4.15: Cumulative heat flux (thermal energy) through the borehole wall for the models *i-iii*

Chapter 5

Feasibility Study

To provide a further facet of the presented heat distribution networks a feasibility study is performed. Aim for this is to achieve a relative measurement for comparing the systems with different features like energy demand, degree of decentralization and population density. The required cost data for being able to achieve a reasonable feasibility study are sometimes hard to find if there is no real application planned. The cost data used for the feasibility study is a result of literature survey and expert interviews. Professionals in HVAC-systems and energy economics estimated the cost data based on their personal experience. Objective here is not to calculate heat production costs that are as precise as possible, but more their relative development if certain boundary conditions are changed. The estimation in heat production costs is for sure also an indicator if the presented technology is able to compete with the conventional technologies for heat generation and distribution systems. The following table lists, based on [5], the specific costs for heating for different technologies and building qualities:

TABLE 5.1: specific costs for different heating technologies in Austria based on full costs, [5], Efficiency=60%

specific costs in € kWh^{-1}	gas boiler	ASHP	GSHP	DH	oil boiler
old building	0.128	0.133	0.149	0.151	0.165
refurbished building	0.231	0.249	0.290	0.273	0.300
new building	0.310	0.312	0.374	0.370	0.382

For other European countries the specific cost rate can be found in [35]. The data are from 2013, but give at least an estimation.

TABLE 5.2: specific costs for different heating technologies, [35], in the EU

specific costs in € kWh^{-1}	gas boiler	ASHP	GSHP	DH	el.boiler
min	0.115	0.161	0.199	0.066	0.118
max	0.180	0.216	0.249	0.163	0.284

For existing district heating systems one main aspect in economic feasibility studies is to determine if the decreasing heat sales due to enhanced buildings can be overcompensated by new house connections, [1]. The systems described here are not existing yet, hence it is assumed here that possible heat demand reductions have a direct impact on the building's cooling demand. Since selling cooling energy to the customers generates the same revenues than heating energy, this assumption is feasible at least for the economic feasibility study.

5.1 Heat Production Costs

The specific energy cost in €/MWh is calculated using the levelized cost of heat (LCOE). This economic assessment of costs includes all the cost which accrue over the system's lifetime, hence initial investments and cost for operation and maintenance (replacement investments). All the costs that will arise in the future are broken down to the first year by applying a net present value calculation. The seasonal heat storage determines the lifetime of the project and is set here equal to 40 years. In accordance to [58, 32, 40] the LCOE is calculated using the following relation:

$$LCOE = \frac{I_0 + \sum_{i=1}^{n} \frac{CF_i}{(1+r)^i}}{\sum_{i=1}^{n} \frac{E}{(1+r)^i}} = \frac{I_0 + \sum_{i=1}^{n} (CRC_i^{ri} + DRC_i + ORC_i)}{\sum_{i=1}^{n} \frac{E}{(1+r)^i}} \tag{5.1}$$

The revenues are achieved by selling energy to the customers. This is thermal energy for heating and domestic hot water and cooling energy during the summer months. It is assumed that the heat supplier provides the energy for zero costs. Depending on the supplier it could also be a business-model to achieve further revenues from the supplier, which receives cooling energy from the network. The variable $LCOE$ here indicates the levelized cost of energy, whereas in literature it is often used as an indicator for the levelized cost of electricity.

The cost of energy both electricity and consumer's demand are assumed to increase over the system's lifetime. This is taken into account with a price-dynamic cash value factor. The price increase of replacement investments that accrue after the components reach it's service life is regarded with the inflation rate. The rates for the price dynamics are shown in tab. 5.3.

TABLE 5.3: Yearly interest rates for the feasibility study

rate		Percentage
calculation interest rate	r	5%
inflation rate	r_i	1%
price-increase rate thermal energy	r_h	1.5%
price-increase rate electricity	r_{el}	2%

5.2 Cost structure

The methodology in finding the heat generation costs is in accordance with VDI 2067, [88] and ÖNORM M 7140. The costs are subdivided into capital-related, demand-related, operation-related and other costs.

5.2.1 Capital-related costs

The capital related costs are the initial investments I_0 and the replacement investments. Information about the cost functions and the component's service life is presented in tab. 5.4.

TABLE 5.4: Capital related costs (ei: expert interview), service life t^N in years and share from initial investment for yearly service and maintenance r_{sm}

component	type	source	t^N	r_{sm}
hot water storage tank for heating and dhw	cost function	fig.5.1	20	1%
heat exchanger for cooling (houses and supplier)	cost function	fig.5.1	20	10%
heat pump units	cost function	fig.5.2	20	1.5%
hydraulic pumps	manufacturer data	[34]	10	-
BTES drilling costs	45 € m^{-1}	ei	50	1%
piping ring network including elbows and branches	1250 € m^{-1}	ei	40	-
BTES connection pipes	1250 € m^{-1}	ei	40	-
piping energy centrals (house connections)	1250 € m^{-1}	ei	40	-
piping to/from supplier	2000 € m^{-1}	ei	40	-
electrical grid connection	90.26 € kW^{-1}	[85]	40	-
pressure compensation vessel	5000 €	ei	15	1%

The cost function for hot water storage is extracted from [46] which is a guideline for waste heat utilization and seems to represent the Austrian market. The cost function includes installation, taxes and transport and has been validated with manufacturer's data [52]. It's appearance can be found in fig. 5.1. The plate heat exchanger's cost function is taken form a comprehensive work considering cost functions in the framework of the energy technology sector and is also shown in 5.1.

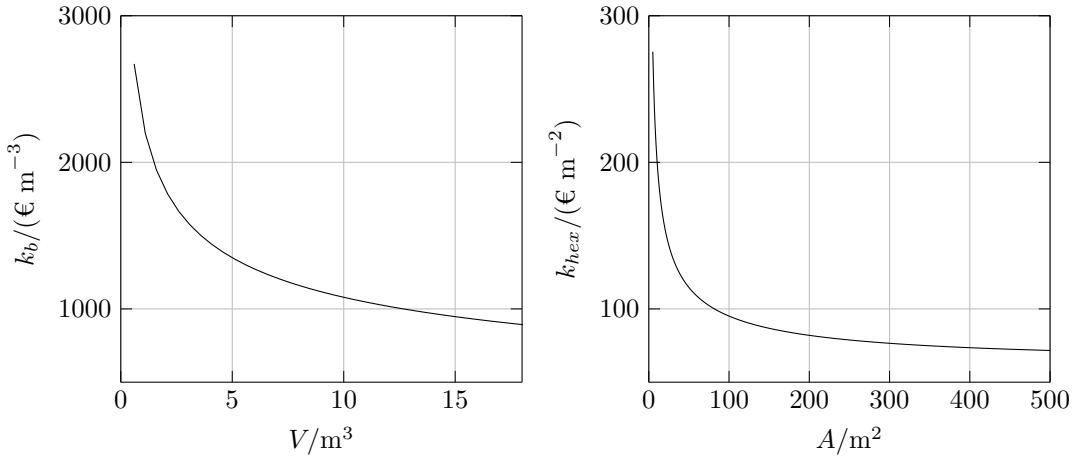

FIGURE 5.1: Cost function for buffer storages k_b (left), [46] and plate heat exchanger k_{hex} (right), [42]

Cost functions for heat pumps are subject to large fluctuations, see fig 5.2. Depending on the sources and associated countries the price spread can be double-digit. The literature is also fuzzy about the cost function's elements (installation, maintenance, heat source). Cost functions for large heat pumps are hard to find, because they are mostly not standard products. Therefore reliable price data can only be found in presence of specific offers. For this study the cost function from [46] is chosen.

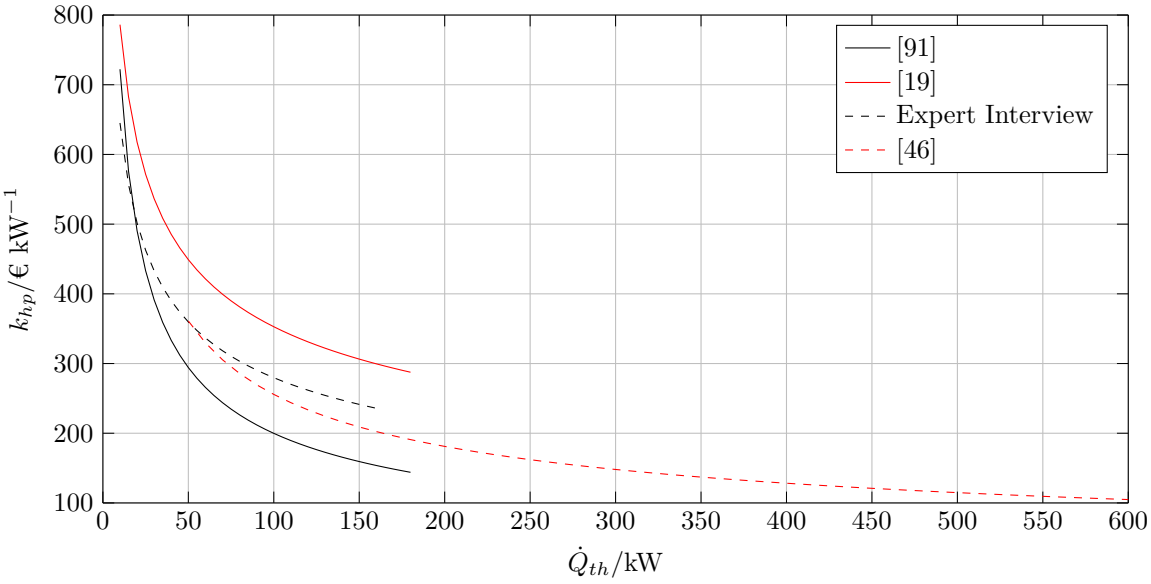

FIGURE 5.2: Cost function for heat pump units k_{hp} according to literature

5.2.2 Demand-related costs

Electricity for the heat pumps and hydraulic pumps is provided by the local energy supplier. Considering all the cost elements regulated by the electricity acts a table of the energy rates, demand rates and flat fees can be provided as shown in the following:

TABLE 5.5: Electricity prices for Vienna and the Austrian network level 5

		Energy	Grid	Taxes & fees	sales tax	total
Energy rate	€ MWh^{-1}	55.28	11.79	17.72	16.96	101.75
Demand rate	€ kW^{-1}	20	45.72	9.6	17.06	102.39
flat fee	€	0	0	14159	2831.8	16991

The indicated energy rate is an offer by the local electricity supplier, whereas the demand rate is just an estimated value. All the other grid taxes and other fees can be found in [85] and [62]. For a system with an energy demand of 2200 MWh and a delivery rate of 650 kW the values shown in table 5.5 result in a full cost based energy rate of 136.2 €/MWh which corresponds to a typical value for industry customers within the Austrian market, [67].

5.2.3 Operation-related costs

Service and maintenance costs are the main components of the operation-related costs. The costs are calculated with respect to the cost rates for service and maintenance in tab. 5.4 and the inflation rate r_i.

Chapter 6

Results

This chapter is an attempt to summarize the network simulation results. The key features of the results are shown here. Due to the relatively large result data extend it is not possible to show the results entirety, hence some key characteristics are listed in the following. The impact of the four system boundary conditions which have been defined in section 1.2, namely network structure, population density, network size and building quality is outlined for every results subsection. The subdivision of the present chapter is based on the system design and it's performance during operation. Finally an estimation about the economic feasibility is given at the end of the chapter.

6.1 System Design

The network design includes the dimensioning of all the components that make up the presented GCHP systems. Also the heat loads which are derived from climate data are part of the system design. They are the main influence factor for the heat pump and storage tank sizing procedure. For heating dominated systems like the ones proposed in this work the external heat supplier is an important element for the system. It's required size in term of yearly provided energy at the required temperature level are shown. The BTES size is indicated with the necessary number of probes. With the given probe spacing the space requirement for a square borehole field can be calculated easily. Finally the pressure conditions are shown for the two extreme cases in winter and summer.

6.1.1 Heat loads

The methodology shown in chapter 2 yields the heat loads for the buildings that are connected to the ring network. The network simulation requires the heat pump's heat loads that are subject to lower fluctuations due to the buffer storage tanks. Fig. 6.1 shows the evolution from building to

HP heat loads. Note that the minimum heating HP's part load is equal to 25% of it's maximum (nominal) load.

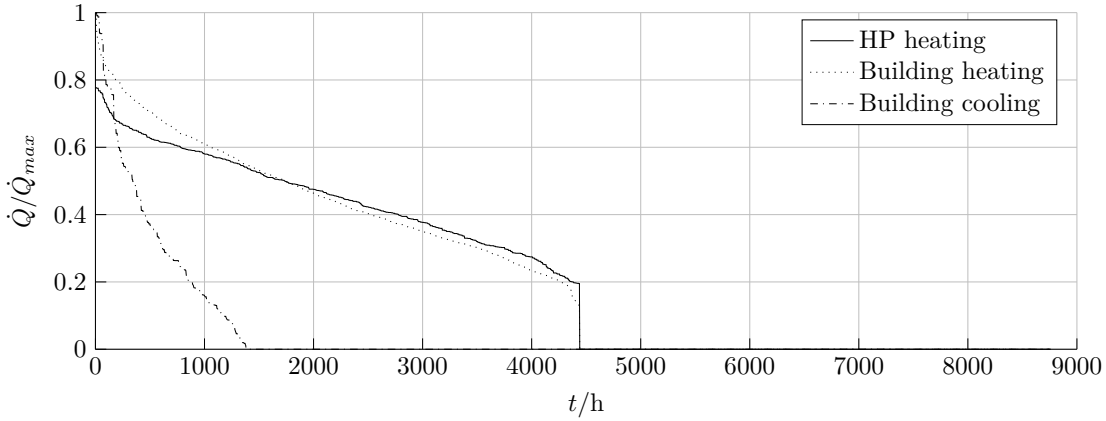

(A) building quality V

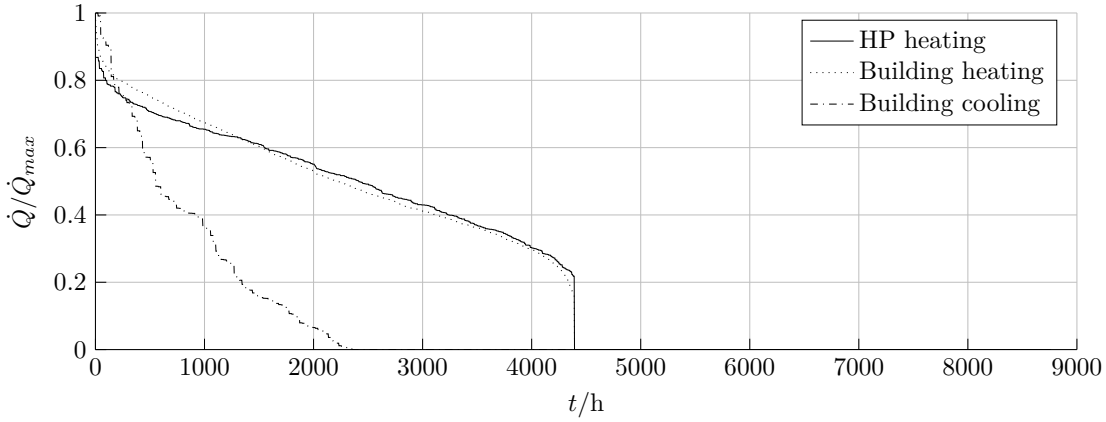

(B) building quality S

FIGURE 6.1: Relative cumulative heat load curves for building heating with heat pump and hot water storage, building heat load and building cooling load for the two building qualities

The comparison of the two building qualities shows that the combination of HP and water storage tanks allows for a peak load reduction of 22.3% for building quality V and 13.2% for building quality S. This is due to the limitation of the storage tank volumes. The convolution of the building heat loads (chapter 2.1.1), which results in the heat loads for building quality S, yield to a smoother cooling load. This can be seen in fig. 6.1B. The hours of the cooling system in service increases from 1489 to 2353 hours, the cooling peak load decreases by 40.5% (not shown in the figure). Note that the two heating curves have been related to the maximum value of the heating load and the cooling curve is relative to to the maximum cooling load. The ratio of the maximum values heating to cooling is 1.09 for fig. 6.1A and 1.63 for 6.1B.

6.1.2 Supplier cooling demand

The external supplier size in term of yearly supplied thermal energy to the ring network and the corresponding temperature level allows for a fast suitability assessment of an available industrial or commercial waste heat source. The necessary energy demand to achieve a yearly even BTES energy balance is shown in fig. 6.2. The hourly heat load resolution in therms of power was found in chapter 2.6. When assessing a potential supplier it has to be evaluated if it's seasonal variations fit to the required heat load curve.

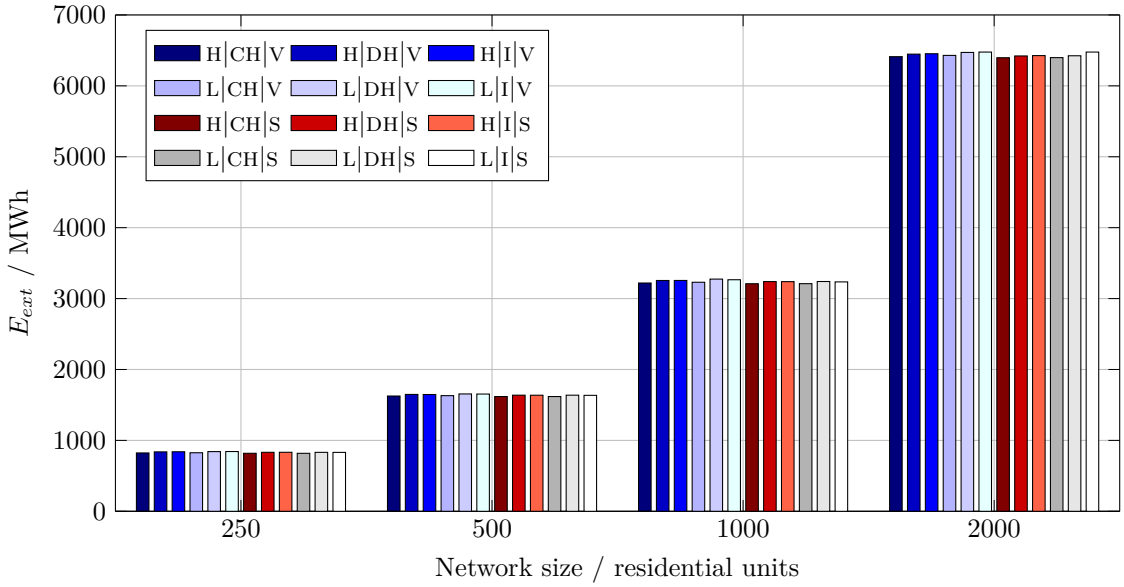

FIGURE 6.2: Necessary supplier's cooling demand for balanced yearly BTES

The different scenarios according to tab. 1.2 for one network size do not show significant variations. Tough, the decentral homogen versions DH require between 0.39% and 1.97% more energy in respect to the central versions, at the decentral inhomogen versions the range is inbetween 0.47% and 2.08%.

As a thumb rule it can be stated that the external heat supplier has to provide approx. 2/3 of the aggregated consumer's yearly heating energy demand for heating and domestic hot water preparation. As the cooling during summer contributes to the BTES regeneration, another rough design rule is that the necessary external energy contribution E_{ext} is approx. 3/4 of the net aggregated energy demand. The consumer energy demand is reduced in that case by the expected cooling energy.

6.1.3 Supplier temperature level

If a potential heat supplier is evaluated to fit into the system, the statement about the yearly energy contribution in terms of MWh is not sufficient. The temperature level at which the energy

is provided to the system is the second important influence factor. If the temperature level of the heat distribution system is sufficiently low, industrial or commercial waste heat can find an application in the presented GCHP systems. The temperature ranges of the supply water temperatures at the supplier node are shown in fig. 6.3. The colored bar's heights label the mean temperature, whereas the vertical lines denote the range of 90% of the hourly temperature values.

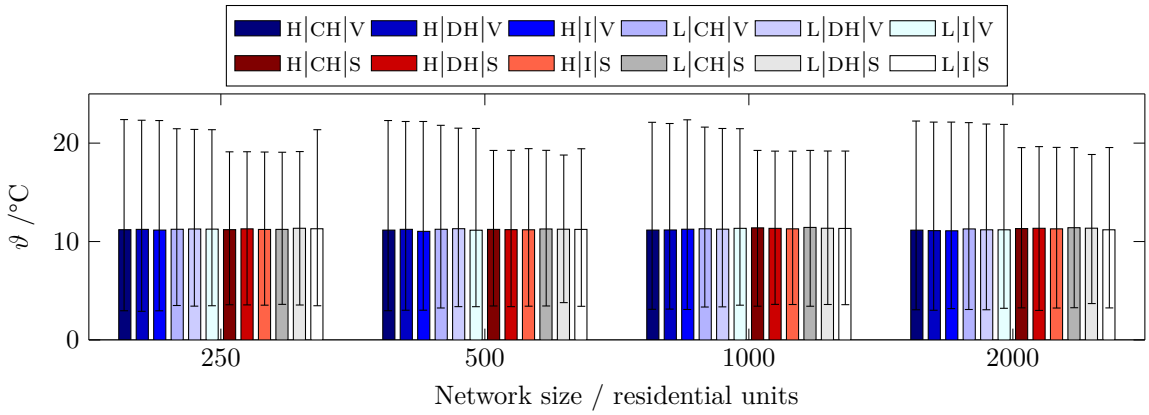

FIGURE 6.3: Average, minimum and maximum network temperatures with 5% and 95% quantiles

It can be observed that the maximum temperatures are lower for the building quality S. This is due to the the lower peaks in the building cooling loads during summer months. For persistent building cooling loads the network temperature is about to rise because the BTES power is limited by relatively slow heat conduction in the surrounding soil material. This temperature rise holds for the cold pipe network too and therefore also for the supplier's necessary supply temperature. If the external energy source is a sensitive facility, as e.g. a server cooling farm, this fact should be taken into account when designing such a network.

6.1.4 BTES size

The determination of the necessary number of BTES probes is done here by adjusting the number in that way that the minimum network temperature in the design stage does not fall below a temperature of 3.5 °C during the first operational year. The result for each scenario is shown in fig. 6.4. The storage size here is given in water equivalent volume. For square BTES fields the volume is calculated as shown below:

$$V_{we} = V_s \frac{c_{p,s}\,\rho_s}{c_{p,w}\,\rho_w} \approx n_b\, s^2\, L_b \frac{c_{p,s}\,\rho_s}{c_{p,w}\,\rho_w}$$

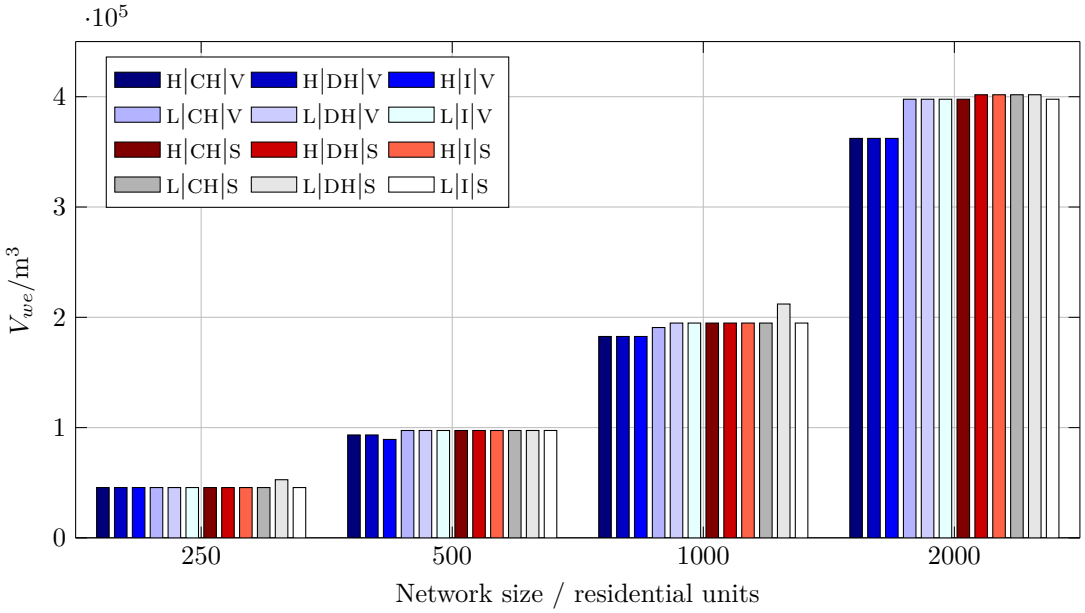

FIGURE 6.4: Number of probes within the BTES field

Apart from some outliers the size of the BTES field does not show big dependencies from network structure, building quality and population density. The required BETS volume increases slightly for low population density and the building quality S.

6.1.5 Network pressure

The hydraulic network calculation yields the pressure in every network node. As shown in chapter 3 the pressure expansion vessel and therefore the node with fixed pressure is located at BTES cold pipe connection node. The figures considering network pressures shown in the following show the results from one scenario only. It is chosen a representative one to provide general information about the issues to pay attention when designing a GCHP system. Two extreme cases are shown in fig. 6.5. The vertical distance between the solid and the dashed line is proportional to the pressure difference between the warm and cold network pipes. The dots at the pipe endings denote the outlet node of each pipe. The seasonal extreme cases show that the hydraulic load is higher for the cooling mode during the summer months. This is also due to the fact that the supplier can only provide warm water and is not intended to consume it. That means that the seasonal heat storage is the only cooling energy source during summer and has to supply the whole network. During the heating season the network has two suppliers. The external heat supplier and additionally the BTES. This results in smaller pressure differences as shown in fig. 6.5a.

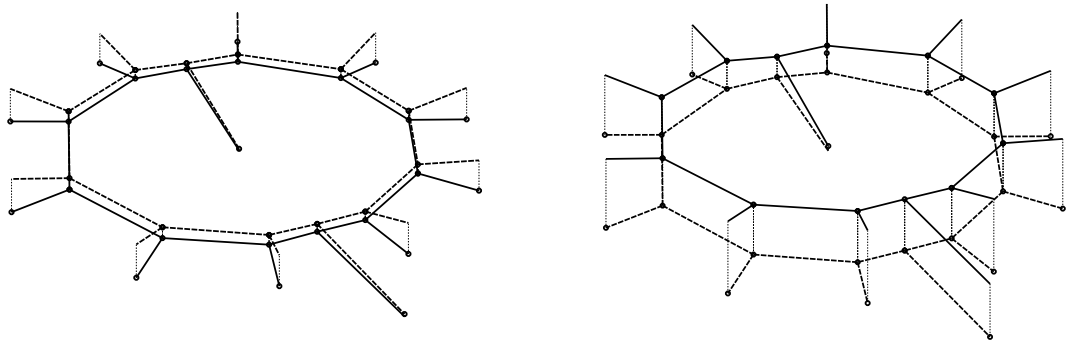

(A) highest winter heating load (B) highest summer cooling load

FIGURE 6.5: Qualitative network pressure field during the maximum load hours for scenario H|2000|I|V. Solid line: warm pipe network, dashed line: cold pipe network. The fixed pressure point is located in the center.

The reason why the pressure compensation vessel is located in the cold network can be derived from the extreme cases shown above. The vessel's function is to preload the network's static pressure to prevent cavitation at the hydraulic pump's suction side. The 2D version of fig. 6.5 with the quantitative pressure values is shown in the following fig. 6.6. The vertical lines show the pressure drop in the connection pipes from the ring network towards the buildings. It can be seen that the water mass flows during winter are higher than the ones for the summer extreme case. Also the two suppliers during winter are seen immediately considering the ring network's pressure lines. The absolute pressures are the lowest for the summer case in the cold network pipes at the hydraulic pump's suction nodes. Depending on the relative location of the customers to the BTES connection node the minimal pressure for each house connection varies from 1.9 to 1.3 bars. That means that the location within the network determines the individual pump's cavitation risk.

If the pressure expansion vessel is connected to the warm pipe network the minimal suction pressures would be about the BTES's pressure drop lower than shown in fig. 6.6. The reduction of the cavitation risk can take place by either enlarging the ring networks pipe diameters or increasing the expansion vessel's pressure during summer periods.

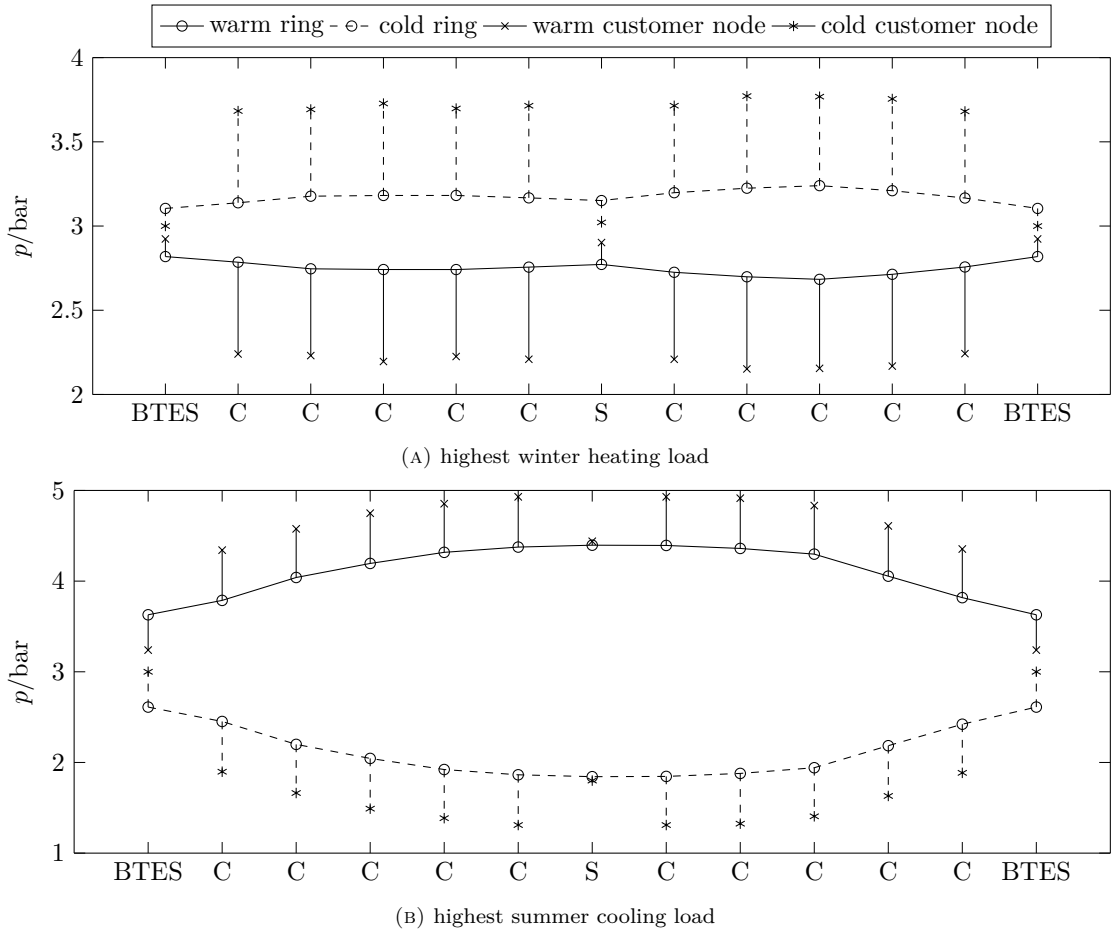

(A) highest winter heating load

(B) highest summer cooling load

FIGURE 6.6: Pressure values during the maximum load hours for scenario H|2000|I|V. C: Customer, S: Supplier. For symmetry reasons the BTES is added at both sides

For the low population density scenarios the network pressure differences in high load hours are expected to grow even further. This is due to the longer ring network and customer connection pipes. This fact has to be taken into account when designing the pipe diameters and choosing the appropriate hydraulic pumps. The scenarios considering the building's storage capacity (building quality S) show due to the smoothed peaks in the heat loads smaller mass flows in peak hours. This leads to smaller pressure differences and hence to a lower cavitation risk.

For the sake of completeness the yearly electricity expense for the hydraulic pumps is shown in fig. 6.7. Note that the values are estimated values, because no detailed model for the hydraulic pump with efficiencies in respect to the operating conditions (Q/H) is used for their determination.

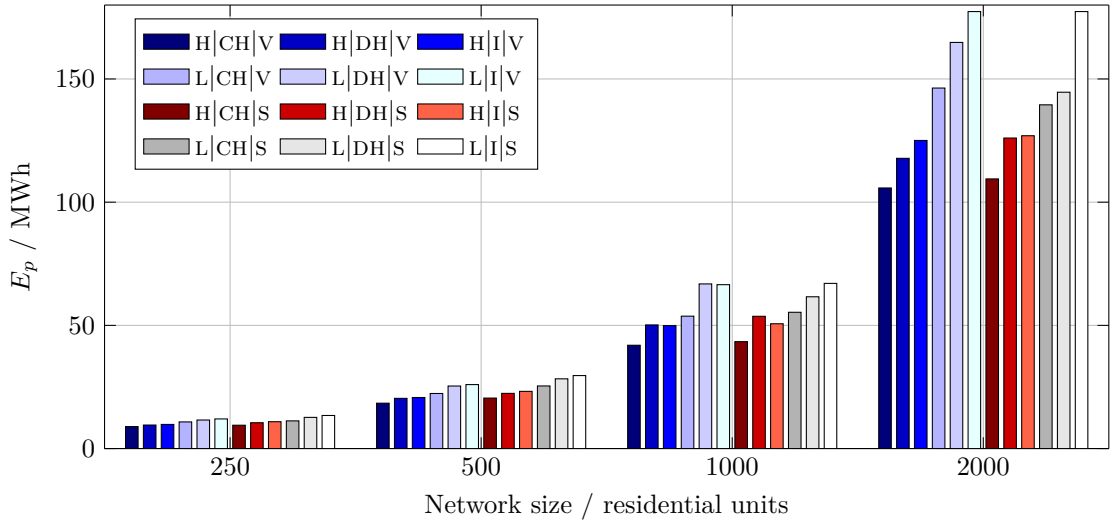

FIGURE 6.7: Yearly pumping energy effort

6.2 System Performance

This section covers the operating conditions for a GCHP system in operation. Once such a system has been designed it should be operating for a number of years. Here some aspects considering the yearly and monthly energy flows and the seasonal thermal energy storage are shown. Planners in the field of energy supply sometimes face the problem that the heat demand assumed during the design stage does not necessarily meet the real heat demand in operation. The implications for the case that the real energy demand is lower than the expected values is covered in this section.

6.2.1 Energy flows

To have an idea about the relative relation of the energy flows entering and leaving the system some figures about the supply and demand flows are presented in this section. The system boundary is placed at the heat transfer units, hence heat pumps and heat exchangers. To assure the system's functionality electricity for the hydraulic pumps and heat pumps has to be provided from external. Additionally, the system requires thermal energy. This is allocated from the supplier and the buildings during summer cooling operation. The seasonal thermal energy storage has a prosumer functionality, that means that it can act like a thermal energy consumer and supplier. Therefore, the BTES's energy flow is divided into charging and discharging portion. Due to the required yearly even energy balance the storage contributes with approx. half of it's energy conversion to supply the system with warm water, throughout the other half consumes warm water to regenerate itself. According to this fact the storage's energy conversion is redundant for the system's global energy consideration. Due to the temporal mismatch of

storage charging and discharging the storage energy portions are nevertheless crucial, especially if the timescale of the energy flow consideration is refined. The yearly energy conversion for a representative network scenario is shown in fig. 6.8. Of course, the absolute energy values change for the other scenarios, the qualitative relations between the distinct energy values are similar to the ones shown in the figure.

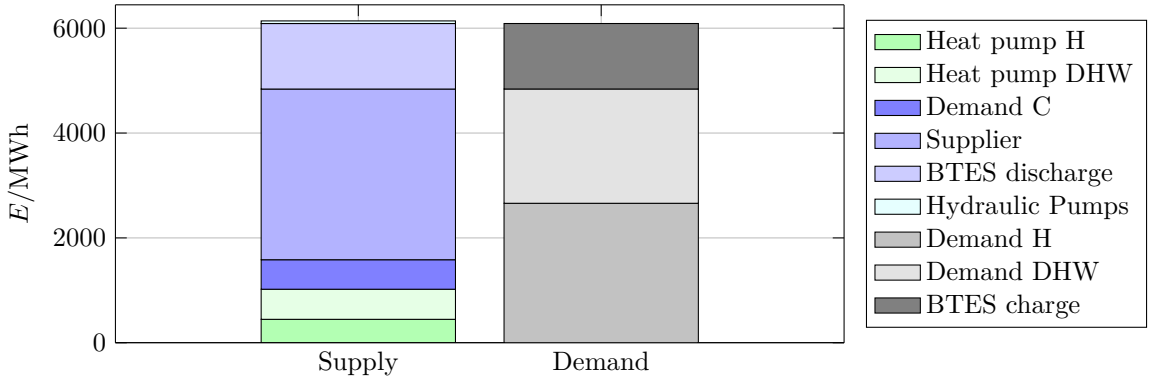

FIGURE 6.8: Yearly energy supply and demand for scenario H|1000|I|V

Although the cooling of the building is a service for the customers it contributes to regenerate the storage, therefore this position is located at the supply side. The storage's supply portion contributes with approx. 25% of the heating demand (heating and domestic hot water) to satisfy the necessary external thermal energy needs.

The share of required electrical energy for the system is 22.1 % of the total heating energy demand. The relations are shown in a sankey diagram in fig. 6.9.

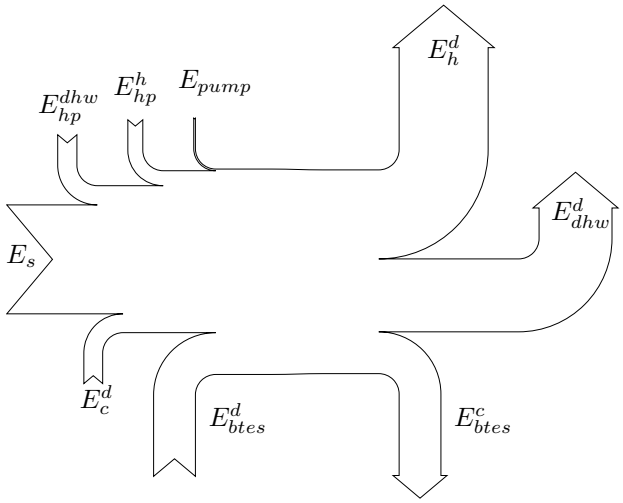

FIGURE 6.9: Yearly energy flows; top: electricity, left: thermal energy (supply), right: thermal energy (demand), bottom: building cooling demand and BTES

On a monthly and daily basis view it becomes obvious in which seasons the aggregated positions from fig. 6.8 accrue. The seasonal heat storage is discharged during the heating seasons and recharged in summer by the cooling of the buildings. The difference between the sum of the electrical inputs plus the cooling demand and the heat demand charges the storage if it is positive of discharges it if negative. Fig. 6.10a and 6.10b show this circumstances for every month and day of the year. Keep in mind that building cooling does not require a heat pump (free cooling).

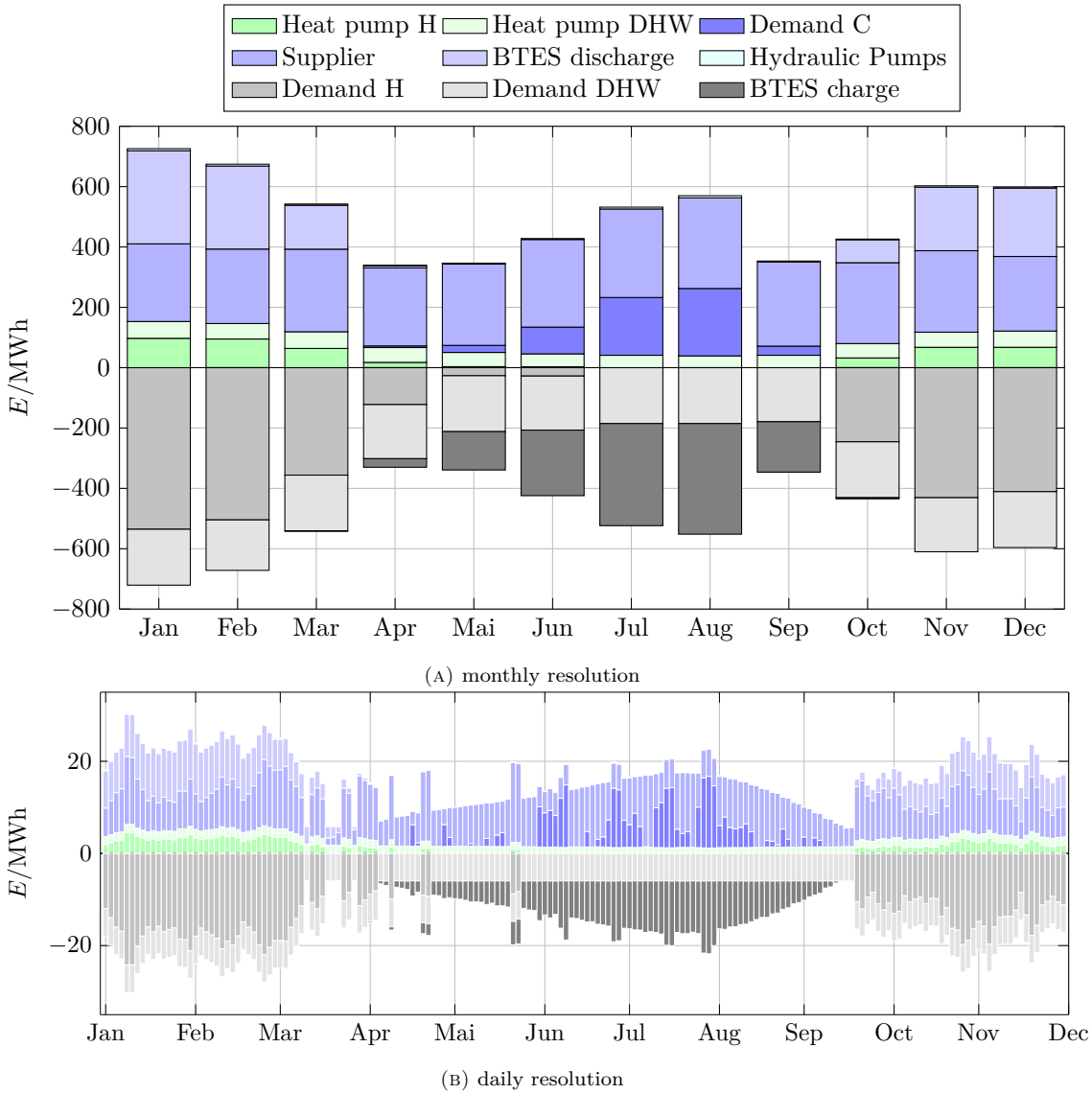

(A) monthly resolution

(B) daily resolution

FIGURE 6.10: Energy supply and demand for scenario H|2000|I|V with different time resolution

6.2.2 Seasonal thermal energy storage

The BTES system as a crucial system element stores between 31.4% and 33.3% of the incoming heating energy (external supplier and cooling of the buildings).The accumulated energy stored in the BTES system during one year of operation shows an oscillation with a period of one year, see fig. 6.11. This due to the methodology shown in chapter 2.6 in finding the external supplier's hourly heat load.

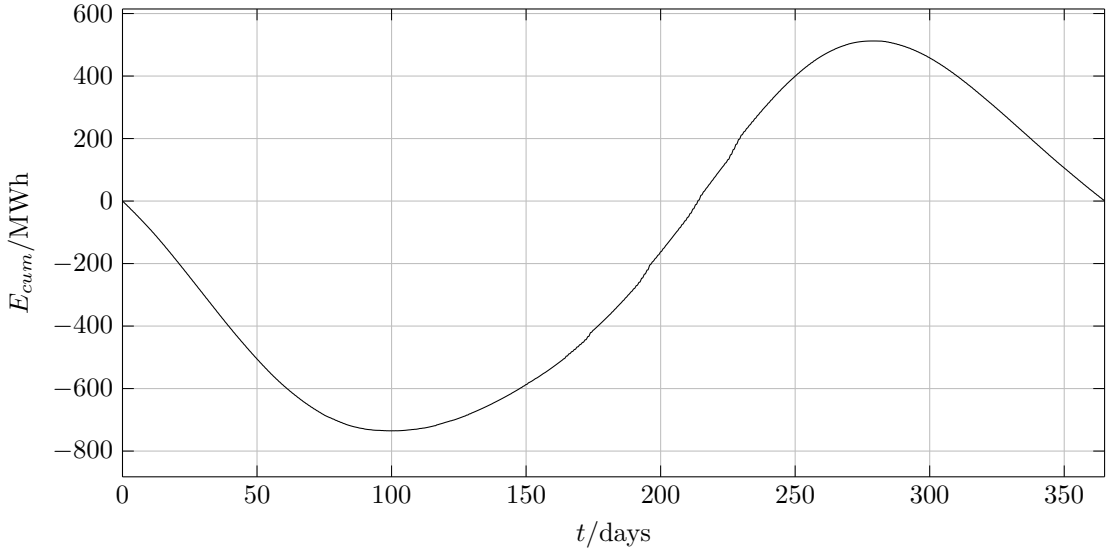

FIGURE 6.11: Cumulative storage energy state during the first operational year of scenario H|2000|I|V

The vertical distance between the maximum and the minimum point in the cumulative storage curve equals the yearly energy amount the storage is discharged respectively charged. The curve's slope sign indicates whether the storage is charged (> 0) or discharged (< 0), the slope's value is an index for the storage's heat flow. The cumulative storage curve describes the sum of all individual probe storage curves. The probes located at the field's borders and corners contribute less to the field's energy conversion than the ones located in the center. This is due to the fact that the adjacent boreholes influence the single borehole's boundary temperature and hence also it's performance. The absolute value ranges of the probe's specific heat fluxes are shown in fig. 6.12.

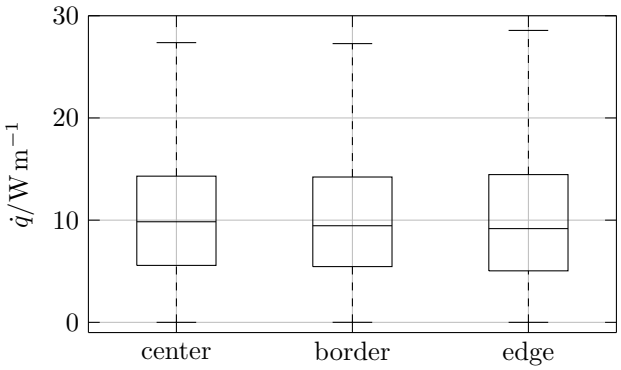

FIGURE 6.12: heat flux distribution during the first operational year for a borehole field with 19^2 boreholes. Median, 25th and 75th percentiles and whiskers

As shown in chapter 4.2.2 the BTES field calculation requires the mean boundary temperature at the diameter which equals the probe's spacing. This value is calculated periodically considering the Fourier-number restriction. The impact of the single probe's position within the borehole field on the prescribed boundary temperature is shown in fig. 6.13

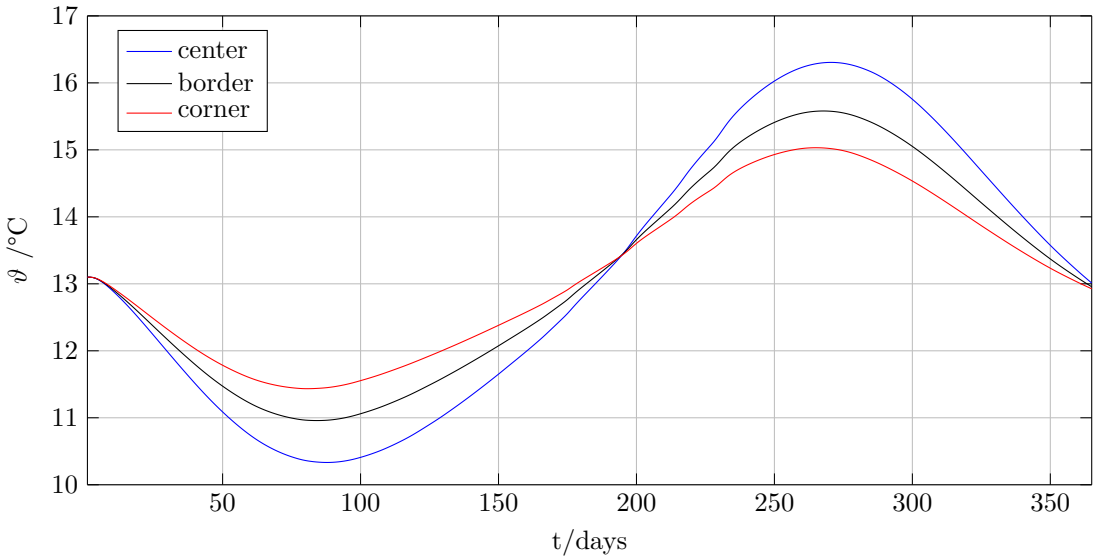

FIGURE 6.13: Boundary temperatures during the first operational year for a borehole field with 19^2 boreholes

Although the whole temperature field is not calculated by the proposed method, it is estimated here with Kelvin's infinite line-source theory. The soil's chemistry and biology is affected by temperature changes. Therefore, the expected range of the soil temperature throughout the operational time can be of interest. A temperature distribution estimation for BTES fields used

in this work is shown in fig. 6.14.

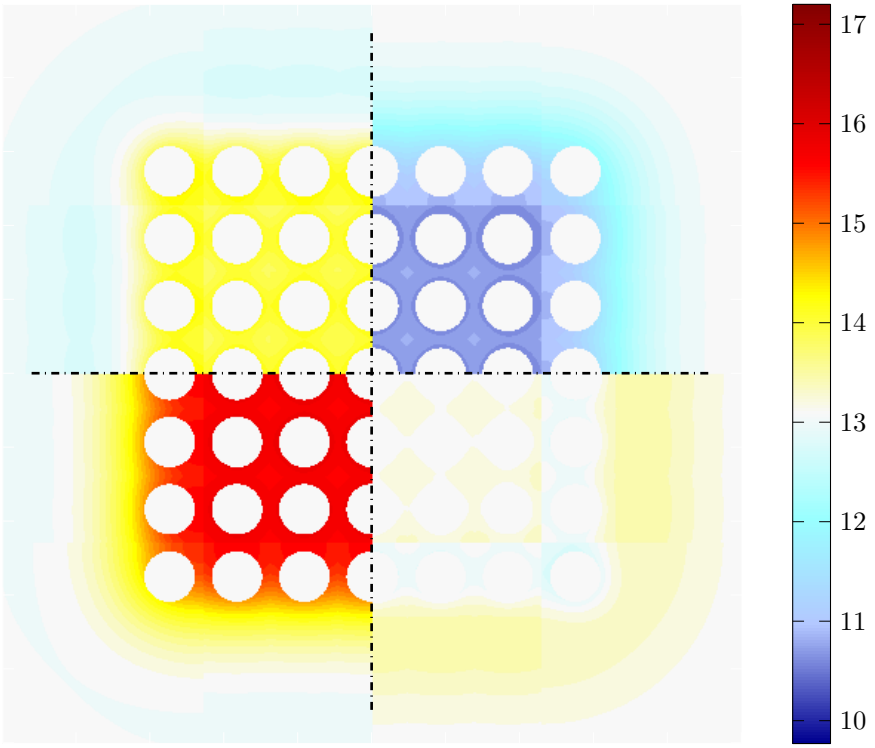

FIGURE 6.14: Temperature distribution for a BTES field with $n = 7^2$ boreholes. Top right: coldest field state; top left: mid season; bottom left: warmest field state; bottom right: regenerated

6.3 Economic feasibility

The following statements about the economy of the presented networks consider the ring network and the connected installations. The secondary side of the single energy centrals which includes the piping from the energy central to the single dwellings as well heat meters and secondary side hydraulic pumps is not part of the economic feasibility study. This is due to the fact that the construction of the secondary side has to take place in a similar manner if an alternative heat distribution system with conventional technologies replaces the proposed heat generation and distribution system. Therefore, the economic feasibility is limited to the ring network itself, the heat generation plants (heat pumps) and the related hydraulic network components, as defined in chapter 5. The BTES system and the pipe installation were identified as the main cost drivers of the systems and are also included in the economic feasibility assessment. Two economic aspects are highlighted in the following. Firstly, the expected heat production costs in €/MWh and the required initial investment for each simulation scenario. Remember that no funding from public

entities is taken into account.

6.3.1 Heat production costs

The heat production costs were calculated with the consideration of all the cash flows which accrue during the system's life time and the discounted amount of delivered heating and cooling energy to the customers. The provision of cooling energy for the external heat supplier is assumed here to create no cash flow, that means that the external heat supplier receives the cooling energy for a price of zero €/MWh. With this assumption the heat production costs are higher than they would be if the cooling energy is sold to the external heat supplier. Anyways, this cost item is a degree of freedom when it comes to pricing policy. The heat production costs for each scenario are shown in fig. 6.15.

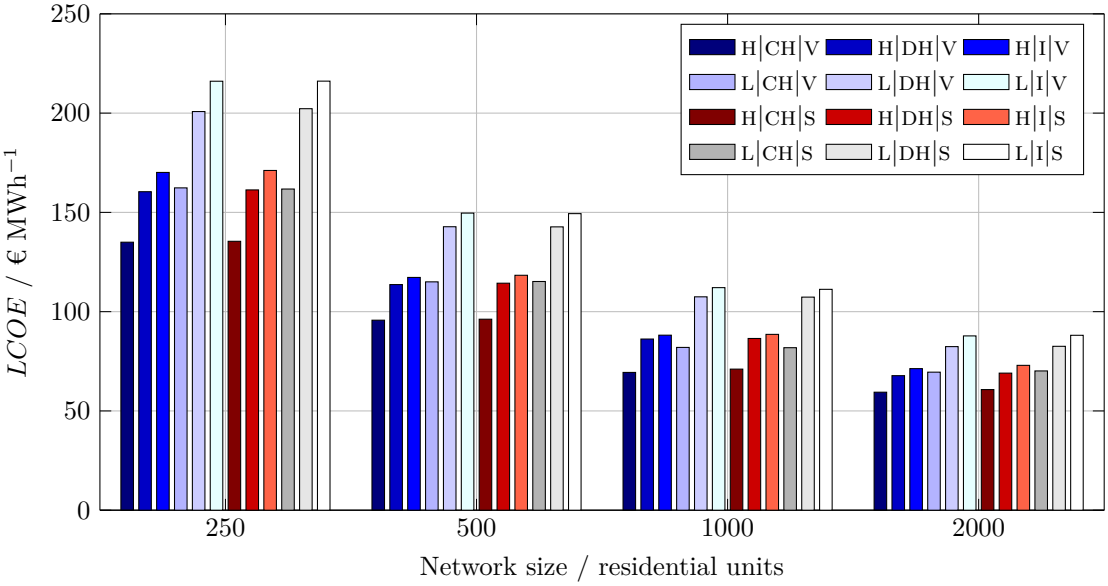

FIGURE 6.15: *LCOE* value for the different scenarios

Due to the larger amount of energy centrals in the decentralized network structures DH and I the heat production costs rise with increasing number of heat pumps in the system. The increased pipe length in the low population density scenarios L affects the heat production costs significantly. Apart from the network size, the population density is identified to be the strongest influence factor among the system boundary conditions, whereas the building quality has only a minor effect on the heat production costs.

The system allows for different pricing policies. One possible scenario is that only heating energy is offset. This can be justified with the fact that the cooling energy is required anyway to regenerate the seasonal thermal energy storage. In that case the heat production costs are about to rise by 11.3% to 11.8%. This percentage range corresponds more or less to the fraction

of delivered cooling energy to the total energy delivery. Another possibility is to request a price for the delivery of cooling energy to the external heat supplier. This will cause a decline in the heat generation costs.

6.3.2 Initial investment

The sum of the capital related costs which accrue at/until the system's start-up are stated here as initial investment. The initial investment for the simulation scenarios are shown in fig. 6.16.

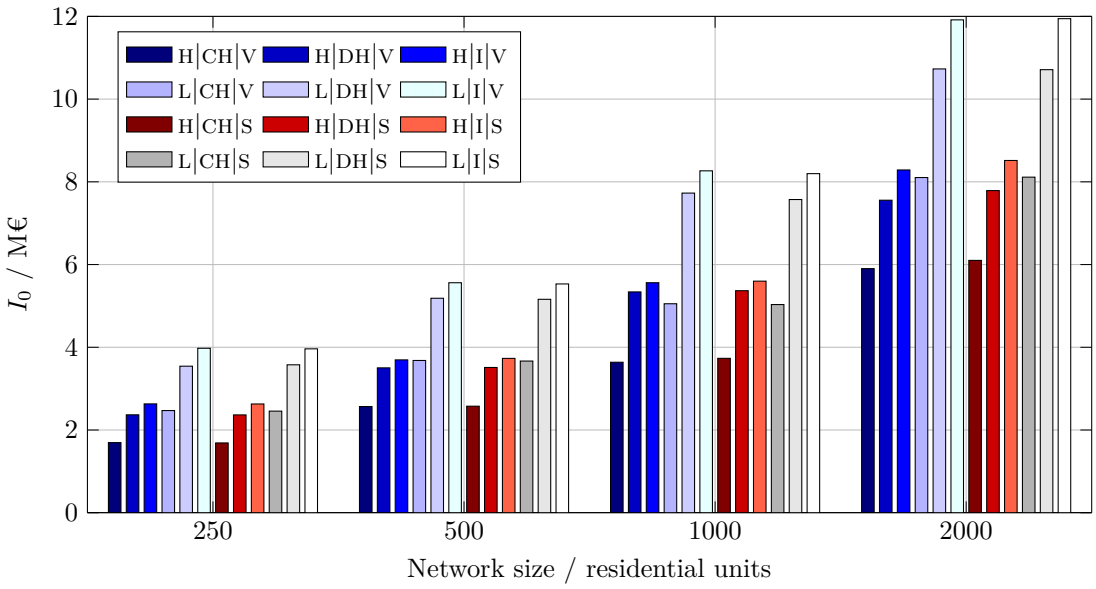

FIGURE 6.16: Initial investment for the different scenarios

The relative relationships between the different network structures and population densities follow the same rules like the heat generation costs. The initial investment is again strongly dependent on the network size, the network structure and the population density.

The main cost positions are the BTES system and the piping of the ring network and the connection to the external heat supplier. Their relative fraction on the initial investment depends on the network structure and the population density. For the network size 1000 the initial investment distribution with respect to the network structure and population density is shown in fig. 6.17.

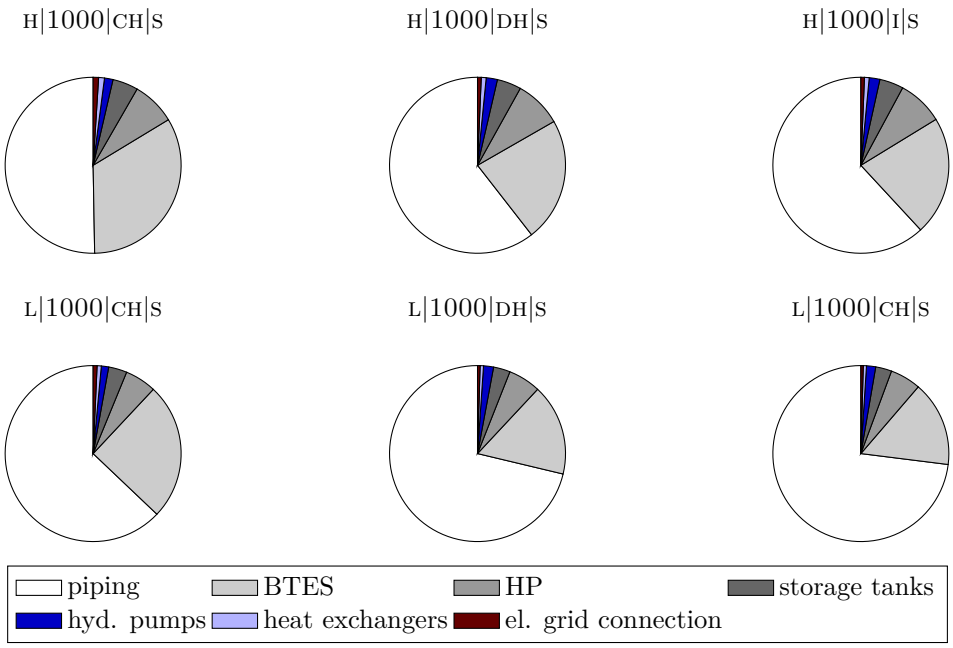

FIGURE 6.17: Initial investment cost breakdown

6.3.3 Sensitivity analysis

As the future evolution of electricity price is subject to high fluctuations a sensitivity analysis for this cost element is performed. A second possible source of uncertainty is the future energy demand for heating. The time span for the economic feasibility study is 40 years, therefore, the impact of global warming can have a significant impact on the demanded heating energy. For simplicity reasons it is assumed here that a possible reduction in heating energy affects the demanded cooling energy directly. With this assumption the net offset energy amounts (heating plus cooling) remains constant throughout the whole year.

For the economic feasibility base case scenario a yearly electricity price increase of 2% was set. The sensitivity of the LCOE for the scenarios on the rate of electricity price increase is shown in fig. 6.18. It can be seen that large networks can quite compete with conventional heat generation technologies also when the electricity prices rise more than 2% per year. The reference values for other heat generation technologies can be found in chapter 5, tab. 5.1.

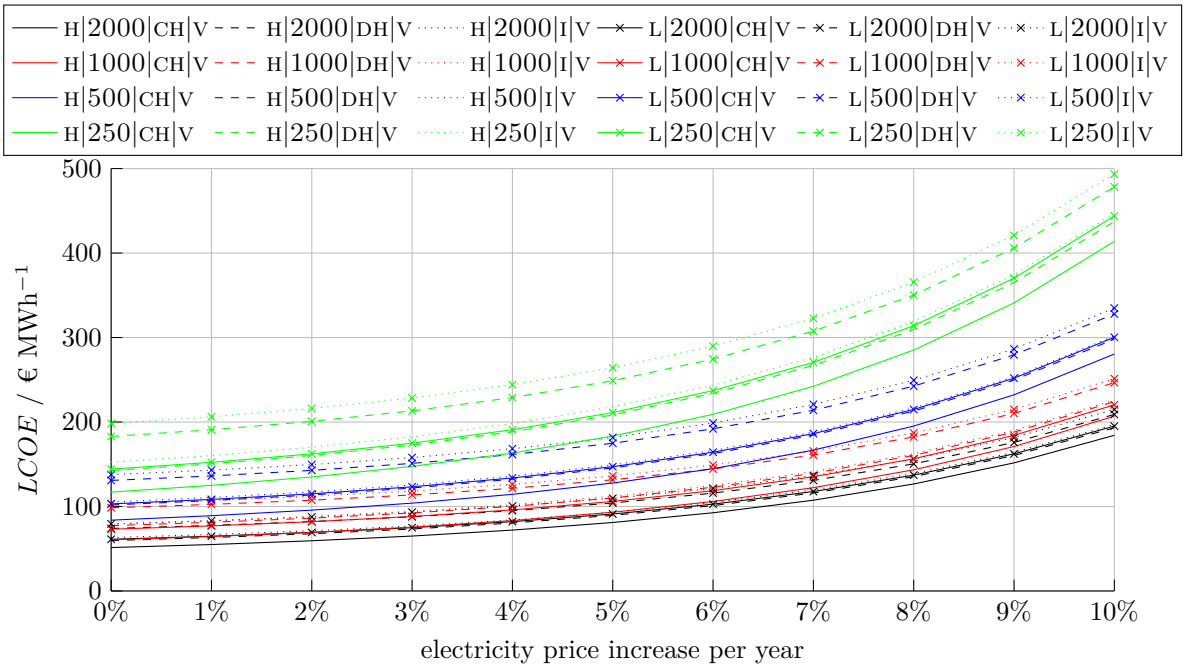

FIGURE 6.18: Impact of the electricity price increase on the LCOE of the scenarios with building quality V

6.4 Energy demand uncertainty

This section treats the effects related to a smaller effective energy demand then assumed in the design stage. The related simulations and results are stated as *off design*. The energy demand for heating, domestic hot water preparation and cooling of the buildings was set for the off design case to be 90% of the design values. The network components and the BTES size were not changed. As the energy demands decrease, the BTES is not operating as assumed in the design stage, therefore, the maximum and minimum temperatures are expected to change. Due to the smaller energy conversions during summer and winter time the accumulated energy curve 6.11 will show smaller amplitudes. As a consequence the network temperatures will change. Fig. 6.19 shows the sorted mean network temperatures for one operational year and the design and off design case. Due to the lower BTES utilization the network temperatures for the off design will rise during winter and decline for the summer operation.

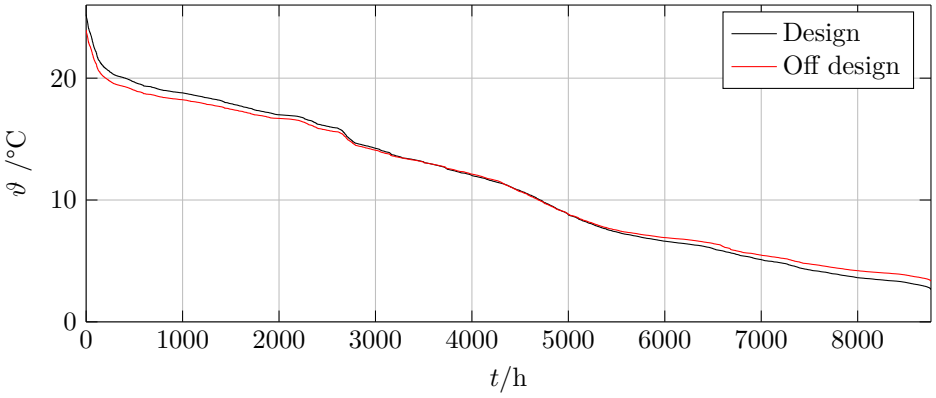

FIGURE 6.19: Sorted network temperatures for one year, scenario H|2000|CH|V

The decline of the maximum network temperatures in summer is stronger for the scenarios with building quality V (1.0-1.25°C) and only about half of this range for the heat loads with building quality S. The increase of the minimum network temperature is about 0.4 to 0.7°C and does not show significant building quality or network structure dependencies.

Water mass flows and related pressure drops are lower and therefore the necessary hydraulic pumping power will decrease by approx. 25 to 27% for all the scenarios. The higher network temperatures in winter affect the heating HP's COP positively, the temperature decline during summer assures better cooling of the buildings but affects the domestic hot water HP negatively. In total the necessary electricity demand is going to drop by more than the off design decrease percentage. This is shown in fig. 6.20.

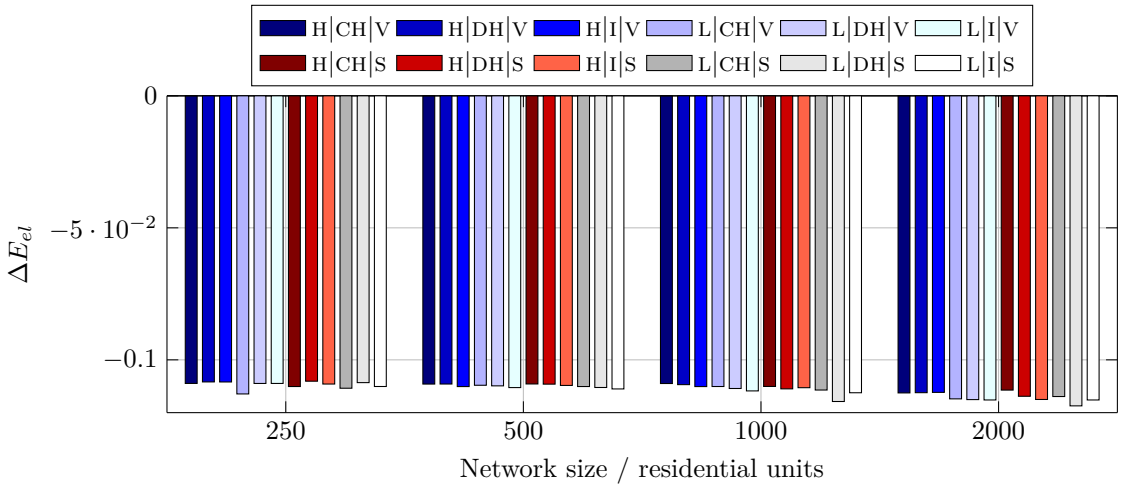

FIGURE 6.20: Change in total electricity demand for the off design scenarios in respect to the design cases

The decrease in electricity demand shows a weak network structure dependency and decreases

with increasing network sizes.

As the consumer's energy demand in the off design scenarios is only 90% of the one for the design cases, the required thermal energy delivery by the external heat supplier to assure a even yearly BTES balance is going to decline as well. The reduction rate of thermal energy needs from outside correlates directly with the off design percentage and lies between 9.5 and 10.5% for all the scenarios.

The reduction in energy sales to the customers and the related savings in electricity purchases bias the specific cost of energy. The implication of the off design scenario on the *LCOE* with respect to the design base cases is shown in fig. 6.21.

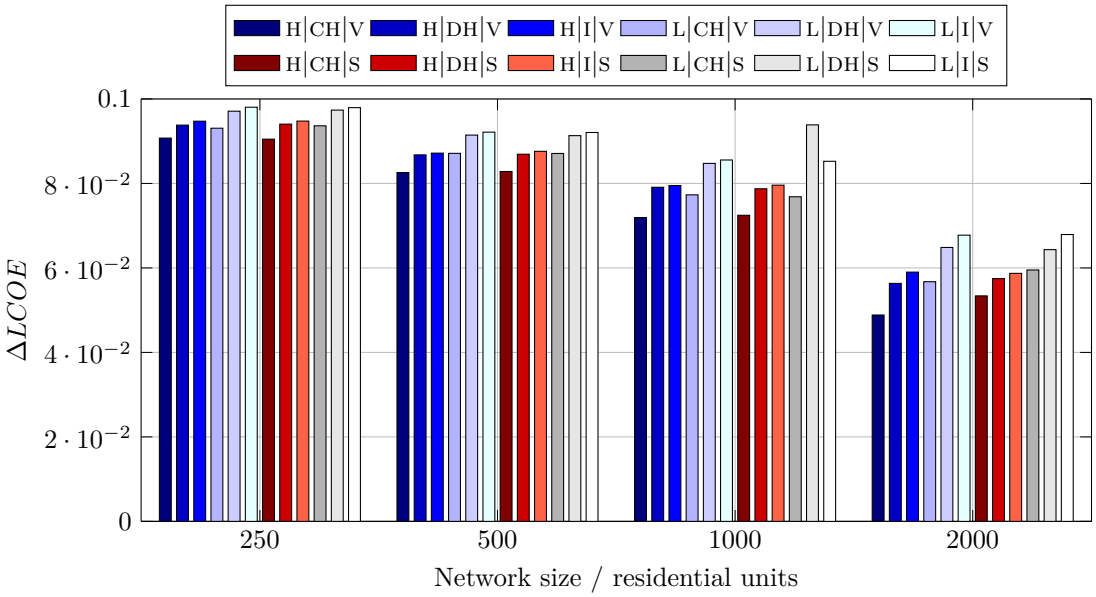

FIGURE 6.21: Change in *LCOE* for the off design scenarios with respect to the design cases

The increase in *LCOE* is slightly lower than the off design percentage for small networks. This is due to the lower relative electricity demand because of the altered network temperatures. With increasing network sizes the *LCOE* additional costs are decreasing. Therefore, the network size is the most important influence factor in the robustness of the systems for demand fluctuations.

Chapter 7

Discussion & Outlook

It's in the nature of network simulation that a few assumptions and estimations in the system boundary conditions and equations have to be made. Aim of this chapter is to discuss the most important assumptions and their related effects on the simulation results.

7.1 Design assumptions

The pipes were designed here with respect to a specific pressure loss of 60 Pa/m. In the results section it was shown that the maximum summer cooling load is more critical for the network and the hydraulic pumps than the maximum winter heating load. This is due to the fact that the external heat supplier supports the BTES system in providing warm water to the network during winter. In the simulation scenarios it was assumed that the external heat supplier is located on the opposite side of the ring network. This resulted in a relatively constant pressure difference at every consumer connection point. During summer mode there is only one supplier of the required energy, the external heat supplier is not intended to supply the network with cold water. This fact causes an inequality of the individual buildings' differential pressures. This is caused by higher pressure losses in the ring network. Although the required electricity to drive the pumps is quite small in relation to the HP's electricity demand this fact has to be accounted for the pump design and in evaluating the related cavitation risk. Especially for networks in low population density areas the ring network pipe diameter near the BTES storage connection point should be chosen larger then the one for the rest of the ring network. Fig. 7.1 shows this issue for three different ring network pipe diameters highlighted with different colors.

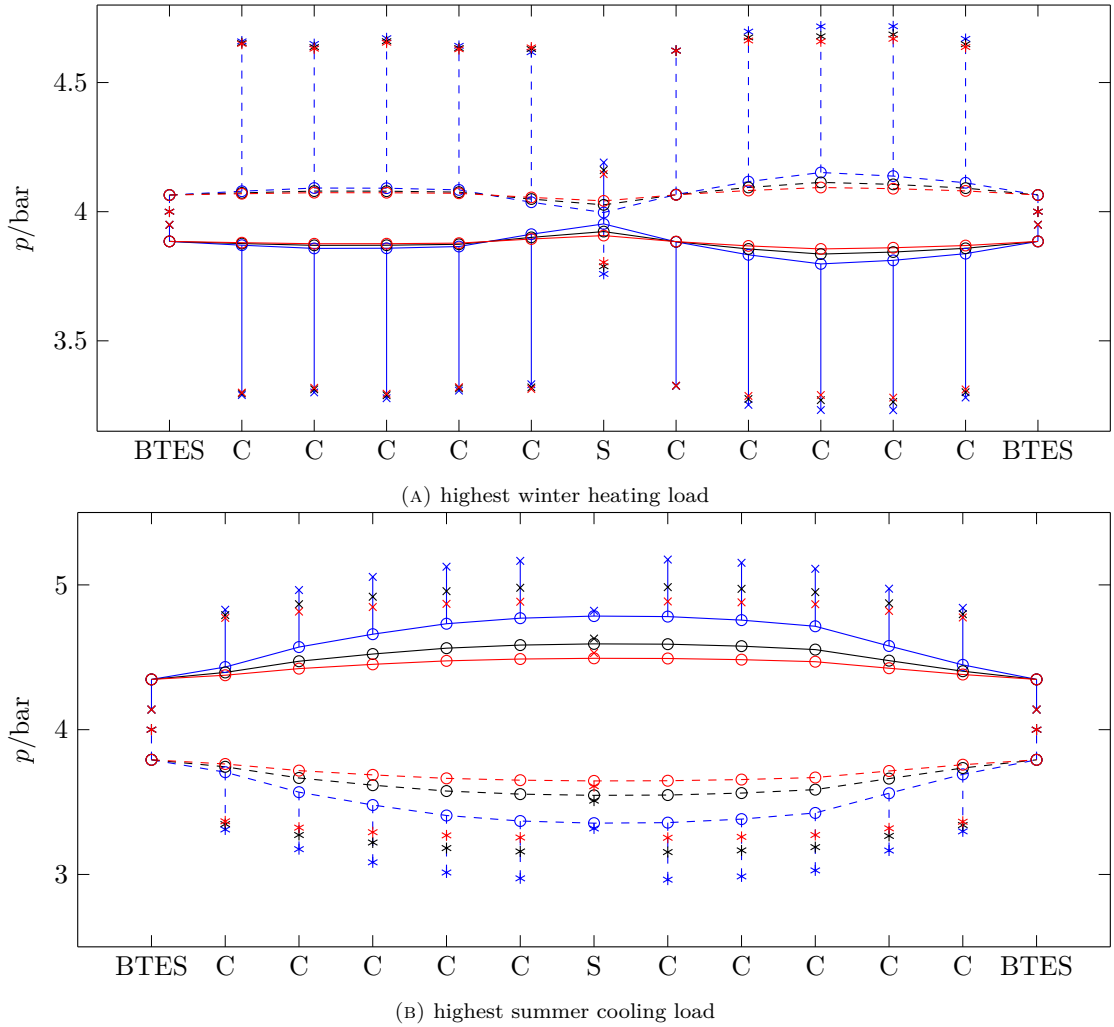

(A) highest winter heating load

(B) highest summer cooling load

FIGURE 7.1: Network pressures for different ring network pipe diameters for scenario H|2000|I|V. red: $D = 0.25$m, black: $D = 0.225$m, blue: $D = 0.2$m

The heating HP's heat loads were determined by applying the equation systems shown in chapter 2.3.1. The optimization procedure assures efficient HP operation by ensuring that the hot water storage tank has a preferably small temperature boundary layer between the cold and hot stratified water volume elements at the end of each day. The following fig. 7.2 shows the vertical storage tank temperature distribution and the related heat loads for the building and the heating HP. Note that the HP heat load is the result of the optimization procedure presented in chapter 2.3.1.

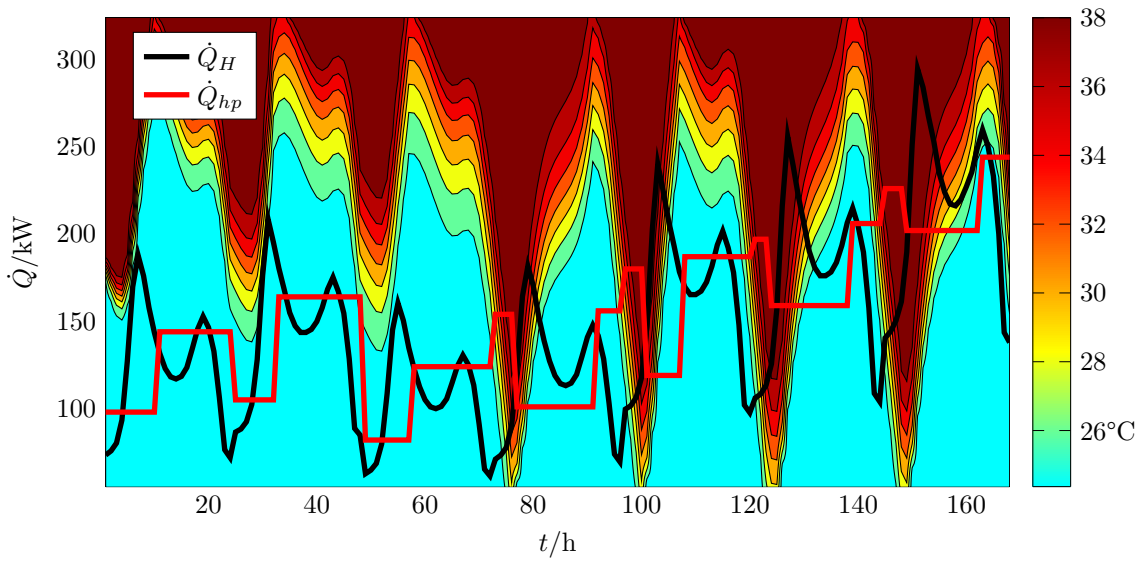

FIGURE 7.2: Storage tank vertical temperature distribution and heat loads during one operational week

Due to the fact that in reality the actual heat demand for the future is not known, another HP control strategy has to be taken. This will result in different HP heat loads and therefore change the simulation results. As long as the HP operation has a high energy efficiency and the gradients in the HP's heating load are similar as shown in the figure, the results are not expected to change significantly. Another issue considering the HP-storage tank combination is the space requirement for the hot water storage tanks. The HP's electrical power consumption is the lower the lower the target temperature for room heating is. A small temperature difference between supply and return temperature on the house side (floor heating) limits the hot water storage tank's storage capacity for a given storage volume. This leads possibly to large storage volumes. The economic feasibility study does not consider related opportunity costs for storage tank space requirements. In fact this issue presents an optimization problem considering storage tank volumes and the related opportunity costs for storage space requirement and the HP's supply temperature which can of course be greater than the maximum required supply temperature. In that case the expected mean COP over the year will be lower.

The comparison of the specific cost of energy (LCOE) calculated in the results section with the ones from conventional heat generation is only allowed if the building side of energy distribution is similar for both cases. As the presented systems here allow for floor heating and possibly also for ceiling cooling the additional construction costs have to be taken into account when comparing LCOE's for different technologies.

In the LCOE calculation it was assumed that the net energy consumption is not expected to change during the whole life time of the system. The possibly reduction in heating energy needs due to global warming was averaged out with a proportional increase of cooling demand. This

assumption is only feasible for rough economical investigations. It does not consider the fact that the BTES is operating under different conditions when altering the building's cooling to heating energy fraction. If the heating energy demand is reduced, the yearly temperature difference inside the BTES is about to decline as well, the lowest BTES temperatures in winter will rise. This affects the heat pumps' COP. Since higher COPs change the fraction of electricity needs to required evaporator powers this might also affect the system's mass flows. When designing a GCHP-system this phenomenon should be considered.

7.1.1 Seasonal thermal energy storage

The performance of a single probe located within the quadratic BTES field was calculated with consideration of the eight adjacent boreholes. In the results chapter it was shown that the boreholes that are located on the edges and borders of the field have slightly lower specific heat fluxes than the ones located in the center. This is due to the lower number of direct adjacent boreholes. A single probe is possibly also affected by other boreholes than the direct neighbors. Fig. 4.5 from chapter 4.2.2 shows that the influence of the diagonal neighborhood (probe 2, 4, 7 and 9) is about a magnitude lower compared to the impact of the center probe and it's horizontal and vertical neighbors. Therefore, it is not necessary for the BTES field simulation to consider more than the eight adjacent boreholes.

For GCHP-System planners one key issue is to determine the necessary number of boreholes for a supply area with given heating (and cooling) energy demands. A rough estimation can be done by using the accumulated energy curve presented in the results section in fig. 6.11. With an estimation about the specific BTES heat fluxes in W/m (e.g. fig. 6.12) a necessary accumulated BTES length can be obtained by considering the minimum and maximum point of the accumulated energy curve.

Due to the BTES specification to extract and feed the same amount of energy within a year, it is not expected to obtain temperature drifts in long term. For the case that temperature drifts are accruing, it is still possible to react by adjusting the external thermal energy supply. In designing the external thermal energy supplier's components and connection pipes it should be accounted for possible additional future loads.

Another issue associated with seasonal heat storage is a possible BTES control strategy. In this work the BTES was considered as a hydraulic passive element. With respect to the actual load state the hydraulic network pumps are discharging or charging the storage. The actual BTES heat flux is a function of it's geometry, the water temperatures and mass fluxes. By using valves which enable for the control of distinct probe flows it is possible to adjust the BTES' heat flux. By applying adequate control strategies on different fractions of the BTES field it could be possible to control water temperature within small boundaries and optimize the BTES operation.

7.1.2 Thermal Energy Supply

Due to the buildings' higher heating energy demand with respect to the cooling demand there is a necessity of an external thermal energy supplier. The cooling of the buildings during the summer months does only contribute with a minor fraction to the total system's needs for heat energy. In the results section it was assumed that the water temperatures during summer are always low enough to ensure cooling of the buildings. In reality the maximum allowed temperature has to be considered together with the cooling facility's surface and it's heat transfer coefficient. The maximum temperatures for cooling in summer are higher than indicated in fig. 6.3. Especially for buildings with the building quality V the system planner has to evaluate carefully if cooling of the buildings can still take place with the maximum water temperatures during summer. By enlarging the BTES' volume the water temperature difference between winter and summer can be reduced. This affects the system's cost structure but can also lead to lower $LCOE$ due to the reduction of HP electricity demand with higher universal network temperatures throughout the year.

7.2 System Autonomy

If the GCHP-system has integrated thermal and electrical energy production facilities for instance photovoltaic and/or solar thermal modules the external energy supply can be reduced, the system autonomy increases. Hybrid collectors that are PV-cells with attached solar thermal receiver could provide the system with thermal end electrical energy. Once this technology is better proved and settled on the market, it could be, together with electrical storage, a potential choice in achieving absolute system autonomy.

Bibliography

[1] M. Åberg et al. "Sensitivity of district heating system operation to heat demand reductions and electricity price variations: A Swedish example". In: *Energy* 41.1 (2012), pp. 525–540. ISSN: 03605442. DOI: 10.1016/j.energy.2012.02.034.

[2] Jonas Allegrini et al. "A review of modelling approaches and tools for the simulation of district-scale energy systems". In: *Renewable and Sustainable Energy Reviews* 52 (2015), pp. 1391–1404. ISSN: 13640321. DOI: 10.1016/j.rser.2015.07.123.

[3] Almbauer R. *Lastprofile nicht-leistungsgemessener Kunden (HE, HM, HG, PG, PK und PW) der Gasnetzbetreiber Österreichs: Überarbeitung 2008: im Auftrag des Fachverband Gas & Wärme*. Ed. by Institut für Verbrennungskraftmaschinen und Thermodynamik, Technische Universität Graz. 2008.

[4] *ASHRAE Fundamentals Handbook 2001 (SI Edition). Chapter 31: Energy estimating and modeling methods, American Society of Heating, Refrigerating, and Air-Conditioning Engineers*. Atlanta, GA, 2001.

[5] Austrian Energy Agency. *Heizkostenvergleich; thermisch unsaniertes Gebäude; thermisch saniertes Gebäude; Neubau: Vollkosten*. Wien, November 2017. URL: https://www.energyagency.at/fakten-service/heizkosten.html.

[6] Austrian Standards Institute. *ÖNORM B5019:2017-02-15 Hygienerelevante Planung, Ausführung, Betrieb, Überwachung und Sanierung*.

[7] Austrian Standards Institute. *ÖNORM EN12831:2003-12-01 Heizungsanlagen in Gebäuden: Verfahren zur Berechnung der Norm-Heizlast*.

[8] A. Ayad et al. "Developed hydraulic simulation model for water pipeline networks". In: *Alexandria Engineering Journal* 52.1 (2013), pp. 43–49. ISSN: 1110-0168. DOI: 10.1016/j.aej.2012.11.005.

[9] B. Geiger et al. *Entwicklung von Lastprofilen für die Gaswirtschaft: im Auftrag des Bundesverbandes der deutschen Gas- und Wasserwirtschaft und des Verbandes kommunaler Unternehmen*. Ed. by Lehrstuhl für Energietechnik und Anwendungstechnik im Institut für Energietechnik, TU München. 2002.

[10] D. Bauer. *Zur thermischen Modellierung von Erdwärmesonden und Erdsonden-Wärmespeichern: Doctor thesis.* Institut für Thermodynamik und Wärmetechnik, Universität Stuttgart, 2011.

[11] W. W. Baumann et al. *Finite-Volumen-Methode in der Numerischen Thermofluiddynamik: Manuskript zur Vorlesung im Fachgebiet Numerische Methoden der Thermofluiddynamik.* Technische Universität Berlin, Institut für Strömungsmechanik und technische Akustik, 2006.

[12] Bennet, J., Claesson, J., & Hellström, G. "Multipole method to compute the conductive heat flows to and between pipes in a composite cylinder". In: *Notes on Heat Transfer* 3 (1987).

[13] *BizEE Degree Days: Weather Data for Energy Professionals.* URL: `http://www.degreedays.net/#` (visited on 10/14/2017).

[14] D. Bothe. "Modellierung und Simulation von weit verzweigten, vermaschten Netzen für thermische Energie und Gas". Dissertation. Wien: TU Wien, 2016.

[15] Michele de Carli et al. "Energetic and economic aspects of a heating and cooling district in a mild climate based on closed loop ground source heat pump". In: *Applied Thermal Engineering* 71.2 (2014), pp. 895–904. ISSN: 13594311. DOI: `10.1016/j.applthermaleng.2014.01.064`.

[16] Horatio Scott Carslaw et al. *Conduction of Heat in Solids and Heat Conduction.* Vol. 1. Oxford, 1948. DOI: `10.1063/1.3066187`.

[17] Jung Chan Choi et al. "Numerical evaluation of the effects of groundwater flow on borehole heat exchanger arrays". In: *Renewable Energy* 52 (2013), pp. 230–240. ISSN: 09601481. DOI: `10.1016/j.renene.2012.10.028`.

[18] M. Christenson et al. "Climate warming impact on degree-days and building energy demand in Switzerland". In: *Energy Conversion and Management* 47.6 (2006), pp. 671–686. ISSN: 01968904. DOI: `10.1016/j.enconman.2005.06.009`.

[19] Raphaël Croteau et al. "Correlations for cost of ground-source heat pumps and for the effect of temperature on their performance". In: *International Journal of Energy Research* 39.3 (2015), pp. 433–438. ISSN: 0363907X. DOI: `10.1002/er.3243`.

[20] Ping Cui et al. "Simulation Modelling and Design Optimization of Vertical Ground Heat Exchanger-GEOSTAR Program". In: *Procedia Engineering* 121 (2015), pp. 906–914. ISSN: 18777058. DOI: `10.1016/j.proeng.2015.09.048`.

[21] A. Dalla Rosa et al. "Method for optimal design of pipes for low-energy district heating, with focus on heat losses". In: *Energy* 36.5 (2011), pp. 2407–2418. ISSN: 03605442. DOI: `10.1016/j.energy.2011.01.024`.

[22] Timothy A. Davis. *UMFPACK Version 5.4.0 User Guide.* 2009.

[23] Energie Tirol, ed. *Energieausweis: Energiebilanz ziehen! Wie viel Heizenergie verbraucht ein Gebäude?* URL: http://www.stanz.tirol.gv.at/gemeindeamt/download/219520226_1.pdf (visited on 10/14/2017).

[24] Gianpiero Evola et al. "Thermal inertia of heavyweight traditional buildings: Experimental measurements and simulated scenarios". In: *Energy Procedia* 133 (2017), pp. 42–52. ISSN: 18766102. DOI: 10.1016/j.egypro.2017.09.369.

[25] S. Falkner. "Modellierung und Simulation von thermischen Speichern". Diplomarbeit. Wien: TU Wien, 2014.

[26] Hao Fang et al. "Industrial waste heat utilization for low temperature district heating". In: *Energy Policy* 62 (2013), pp. 236–246. ISSN: 03014215. DOI: 10.1016/j.enpol.2013.06.104.

[27] Hao Fang et al. "Key issues and solutions in a district heating system using low-grade industrial waste heat". In: *Energy* 86 (2015), pp. 589–602. ISSN: 03605442. DOI: 10.1016/j.energy.2015.04.052.

[28] M. Farghadan et al. *Warmwasser: Technologieleitfaden.* Tech. rep. Wien: Magistrat der Stadt Wien, Magistratsabteilung 20 - Energieplanung, 2016.

[29] H. Farhangi. "The path of the smart grid". In: *IEEE Power and Energy Magazine* 8.1 (2010), pp. 18–28. ISSN: 1540-7977. DOI: 10.1109/MPE.2009.934876.

[30] Farzin M. Rad et al. "Combined solar thermal and ground source heat pump system". In: *Energy and Buildings* (2009), pp. 2297–2305. ISSN: 03787788.

[31] G. Franz et al. "Wärmeverluste von beheizten Rohreleitungen im Erdboden: Heat Losses of Buried Pipes". In: *Wärme- und Stoffübertragung* 1969.2 (1987), pp. 109–117.

[32] R. Gabbrielli et al. "Levelized Cost of Heat for Linear Fresnel Concentrated Solar Systems". In: *Energy Procedia* 49 (2014), pp. 1340–1349. ISSN: 18766102. DOI: 10.1016/j.egypro.2014.03.143.

[33] Rolf Dieter Grigorieff et al. "Modelling and Numerical Simulation of District Heating Networks with Time-Saving Solution Methods". In: *Mathematics — Key Technology for the Future: Joint Projects between Universities and Industry.* Ed. by Willi Jäger et al. Berlin, Heidelberg: Springer Berlin Heidelberg, 2003, pp. 252–262. ISBN: 978-3-642-55753-8. DOI: 10.1007/978-3-642-55753-8{\textunderscore}21. URL: https://doi.org/10.1007/978-3-642-55753-8_21.

[34] Grundfos Germany. *: NBE Geregelte Blockpumpen nach EN 733: Produktkatalog.* 2018. URL: https://product-selection.grundfos.com/catalogue.pump%20designs.einstufige%20blockpumpen.nb%20%3E%20blockpumpen%20nach%20en%20733.html (visited on 06/18/2018).

[35] O. Gudmundsson et al. "Cost analysis of district heating compared to its competing technologies". In: *ENERGY AND SUSTAINABILITY 2013*. Ed. by C. A. Brebbia et al. WIT Transactions on Ecology and The Environment. WIT PressSouthampton, UK, 2013, pp. 3–13. DOI: 10.2495/ESUS130091.

[36] Karl Martin Heissler et al. *Potenziale von Niedrigtemperaturnetzen zur Steigerung des Anteils erneuerbarer Energien in Quartieren*. Tech. rep. Bundesinstitut für Bau-, Stadt- und Raumforschung im Bundesamt für Bauwesen und Raumordnung, 2017.

[37] G. Hellström. *Ground heat storage: thermal analyses of duct storage systems: Doctor Thesis*. Sweden: Lund University, 1991.

[38] Samuel Henchoz et al. "Key energy and technological aspects of three innovative concepts of district energy networks". In: *Energy* 117 (2016), pp. 465–477. ISSN: 03605442. DOI: 10.1016/j.energy.2016.05.065.

[39] Arif Hepbasli. "Low exergy (LowEx) heating and cooling systems for sustainable buildings and societies". In: *Renewable and Sustainable Energy Reviews* 16.1 (2012), pp. 73–104. ISSN: 13640321. DOI: 10.1016/j.rser.2011.07.138.

[40] C. Hofstädter. "Wirtschaftlichkeitsrechnung eines Nahwärmebetreibers unter Berücksichtigung von Solarthermie". MA thesis. Technische Universität Wien, Institut für Energiesysteme und Elektrische Antriebe, 2015.

[41] M. Holzner. *Vorlesungsskript Numerical Hydraulics*. ETH Zürich, Dep. for Environmental Fluid Mechanics, 2017.

[42] K. Lucas et al. *Preisatlas: Ableitung von Kostenfunktionen für Komponenten der rationellen Energienutzung*. Ed. by Stiftung Industrieforschung. Duisburg-Rheinhausen, 2002.

[43] Asim Kaygusuz et al. "Renewable energy integration for smart sites". In: *Energy and Buildings* 64 (2013), pp. 456–462. ISSN: 03787788. DOI: 10.1016/j.enbuild.2013.05.031.

[44] Seama Koohi-Fayegh et al. "Examination of thermal interaction of multiple vertical ground heat exchangers". In: *Applied Energy* 97 (2012), pp. 962–969. ISSN: 03062619. DOI: 10.1016/j.apenergy.2012.02.018.

[45] Philipp Kräuchi et al. "Simulation thermischer Arealvernetzung mit IDA-ICE". In: *Proceedings in Fourth German-Austrian IBPSA Conference* (2012), pp. 205–211.

[46] K. Kulterer et al. *Leitfaden für Energieaudits für betriebliche Abwärmenutzung*. Tech. rep. Österreichische Energieagentur, 2015.

[47] Andrew Lake et al. "Review of district heating and cooling systems for a sustainable future". In: *Renewable and Sustainable Energy Reviews* 67 (2017), pp. 417–425. ISSN: 13640321. DOI: 10.1016/j.rser.2016.09.061.

[48] Louis Lamarche et al. "A new contribution to the finite line-source model for geothermal boreholes". In: *Energy and Buildings* 39.2 (2007), pp. 188–198. ISSN: 03787788. DOI: 10.1016/j.enbuild.2006.06.003.

[49] Hongwei Li et al. "Energy and exergy analysis of low temperature district heating network". In: *Energy* 45.1 (2012), pp. 237–246. ISSN: 03605442. DOI: 10.1016/j.energy.2012.03.056.

[50] Yu Li et al. "District heating and cooling optimization and enhancement – Towards integration of renewables, storage and smart grid". In: *Renewable and Sustainable Energy Reviews* 72 (2017), pp. 281–294. ISSN: 13640321. DOI: 10.1016/j.rser.2017.01.061.

[51] Xuezhi Liu et al. "Combined analysis of electricity and heat networks". In: *Applied Energy* 162 (2016), pp. 1238–1250. ISSN: 03062619. DOI: 10.1016/j.apenergy.2015.01.102.

[52] Lorenz GmbH & Co. Behälter und Apparatebau KG. *Groß-Pufferspeicher Typ PSG 2500-100000 l: Preisliste*. Landshut, 2014. (Visited on 10/01/2017).

[53] Henrik Lund et al. "4th Generation District Heating (4GDH)". In: *Energy* 68 (2014), pp. 1–11. ISSN: 03605442. DOI: 10.1016/j.energy.2014.02.089.

[54] Rasmus Lund et al. "Choice of insulation standard for pipe networks in 4 th generation district heating systems". In: *Applied Thermal Engineering* 98 (2016), pp. 256–264. ISSN: 13594311. DOI: 10.1016/j.applthermaleng.2015.12.015.

[55] M. Sulzer et al. *Kalte Fernwärme (Anergienetze): Grundlagen-/Thesenpapier*. Tech. rep. Hochschule Luzern, Technik & ArchitekturHochschule Luzern, Technik & Architektur, 2014.

[56] M. Sulzer et al. "Multi-Energy-Grid: Möglichkeiten der thermischen Vernetzung". In: *Aqua & Gas* 7/8 (2015), pp. 56–61.

[57] MA23, Wirtschaft, Arbeit, Statistik. *Wien in Zahlen 2017: Statistics about the City of Vienna*. 2017.

[58] F. Mauthner et al. *IEA SHC Task 52: Solar Heat and Energy Economics in Urban Environments: Technical Report Subtask C - Part C1*. 2016. (Visited on 10/01/2017).

[59] A. Molyneaux et al. "Environomic multi-objective optimisation of a district heating network considering centralized and decentralized heat pumps". In: *Energy* 35.2 (2010), pp. 751–758. ISSN: 03605442. DOI: 10.1016/j.energy.2009.09.028.

[60] M. Müller et al. *Wärmepumpen mit natürlichen Kältemitteln: Endbericht: im Auftrag des Umweltbundesamtes*. Dessau-Rosslau, 2013.

[61] F. Ochs et al. *Store4Grid: Optimierte Erdbecken-Wärmespeicher für Wärmenetze: Endbericht: im Auftrag des Klima- und Energiefonds des Bundes*. Wien, 2015.

[62] *Ökostromförderbeitragsverordnung 2018: BGBl. II381/*. 2017.

[63] Gbemi Oluleye et al. "Modelling and screening heat pump options for the exploitation of low grade waste heat in process sites". In: *Applied Energy* 169 (2016), pp. 267–286. ISSN: 03062619. DOI: 10.1016/j.apenergy.2016.02.015.

[64] Thomas Oppelt et al. "Dynamic thermo-hydraulic model of district cooling networks". In: *Applied Thermal Engineering* 102 (2016), pp. 336–345. ISSN: 13594311. DOI: 10.1016/j.applthermaleng.2016.03.168.

[65] Kristina Orehounig et al. "Integration of decentralized energy systems in neighbourhoods using the energy hub approach". In: *Applied Energy* 154 (2015), pp. 277–289. ISSN: 03062619. DOI: 10.1016/j.apenergy.2015.04.114.

[66] Österreichisches Institut für Bautechnik. *OIB-Richtlinie 6: Energieeinsparung und Wärmeschutz*. Wien, 3/2015.

[67] Österreichs Energie. *Strompreisanalyse 2017*. 2018. URL: https://oesterreichsenergie.at/files/Downloads%20Handel%20und%20Vertrieb/Infografiken%20Handel%20und%20Vertrieb/Strompreisanalyse_2017.pdf (visited on 06/20/2018).

[68] P. Eskilson. *Thermal Analysis of Heat Extraction Boreholes: Thesis*. Sweden: University of Lund, Dep. of Mathematical Pysics, 1987.

[69] D. Pahud et al. *The Ducht Ground Heat Storage Model (DST) for TRNSYS Used for the Simulation of Heat Exchanger Piles*. EPFL Lausanne, 1996.

[70] S. Patankar. *Numerical Heat Transfer and Fluid Flow*. Series in computational methods in mechanics and thermal sciences. Taylor & Francis, 1980. ISBN: 9780891165224. URL: https://books.google.it/books?id=5JMYZMX3OVcC.

[71] Ph. Kräuchi et al. "Modellbildung für thermische Arealvernetzung mit IDA-ICE". In: *Proceedings in Fifth German-Austrian IBPSA Conference, Aachen* (2014), pp. 160–165.

[72] D. Pietruschka et al. "Kalte Nahwärme: agrothermische Wärmeversorgung einer Plusenergiesiedlung". In: *bbr* 03 (2013), pp. 58–63.

[73] Ashreeta Prasanna et al. "Optimisation of a district energy system with a low temperature network". In: *Energy* 137 (2017), pp. 632–648. ISSN: 03605442. DOI: 10.1016/j.energy.2017.03.137.

[74] Zahra Rahimpour et al. "Using Thermal Inertia of Buildings with Phase Change Material for Demand Response". In: *Energy Procedia* 121 (2017), pp. 102–109. ISSN: 18766102. DOI: 10.1016/j.egypro.2017.07.483.

[75] Sayanthan Ramakrishnan et al. "Experimental and Numerical Study on Energy Performance of Buildings Integrated with Phase Change Materials". In: *Energy Procedia* 105 (2017), pp. 2214–2219. ISSN: 18766102. DOI: 10.1016/j.egypro.2017.03.627.

[76] Florian Ruesch et al. "Potential and limitations of using low-temperature district heating and cooling networks for direct cooling of buildings". In: *Energy Procedia* 122 (2017), pp. 1099–1104. ISSN: 18766102. DOI: 10.1016/j.egypro.2017.07.443.

[77] M. A. Sayegh et al. "Trends of European research and development in district heating technologies". In: *Renewable and Sustainable Energy Reviews* 68 (2017), pp. 1183–1192. ISSN: 13640321. DOI: 10.1016/j.rser.2016.02.023.

[78] Matthias Schlaisich. “Bestimmung der Heiz- und Kühlgradtage im Alpenraum”. MA thesis. Universität Wien, 2013.

[79] Dietrich Schmidt et al. “Low Temperature District Heating for Future Energy Systems”. In: *Energy Procedia* 116 (2017), pp. 26–38. ISSN: 18766102. DOI: 10.1016/j.egypro.2017.05.052.

[80] F. Schmitt et al. “Wärmetransport im Wettbewerb zu dislozierter Wärmeerzeugung und Maßnahmen zur Senkung der Baukosten von Transportleitungen”. In: *EnEff: Wärme - Kostengünstiger Fernwärmetransport für den Effektiven Ausbau der Kraft-Wärme-Kopplung*. Vol. 1. AGFW, 2014.

[81] Haiwen Shu et al. “Field measurement and energy efficiency enhancement potential of a seawater source heat pump district heating system”. In: *Energy and Buildings* 105 (2015), pp. 352–357. ISSN: 03787788. DOI: 10.1016/j.enbuild.2015.07.069.

[82] R. V. Southwell. *Relaxation Methods in Engineering Science - A Treatise on Approximate Computation*. Read Books Design, 2010. ISBN: 9781446513163. URL: https://books.google.it/books?id=mGeUX2ZBVtgC.

[83] Springer-VDI-Verlag GmbH & Co. “Gleichzeitigkeit - der unterschätzte Faktor: Effiziente Planung von Nahwärmenetzen”. In: *BWK das Energie-Fachmagazin* 12 (2012).

[84] J. Stene. *Design and Application of Ammonia Heat Pump Systems for Heating and Cooling of Non-Residential Buildings: 8th Gustav Lorentzen Conference on Natural Working Fluids*. Copenhagen, 2008.

[85] *Systemnutzungsentgelte-Verordnung 2018 SNE-V 2018: BGBl. II398/*. 2017.

[86] S. Thalmann et al. *Analyse und Optimierung von Fernwärmenetzen: Ist-Analyse von Fernwärmenetzen und Bewertungstool zur Netzoptimierung: Schlussbericht*. Ed. by Eidgenössisches Department für Umwelt, Verkehr, Energie und Kommunikation. Zürich, 2013.

[87] Herena Torío et al. “Development of system concepts for improving the performance of a waste heat district heating network with exergy analysis”. In: *Energy and Buildings* 42.10 (2010), pp. 1601–1609. ISSN: 03787788. DOI: 10.1016/j.enbuild.2010.04.002.

[88] Verein Deutscher Ingenieure e.V. *Wirtschaftlichkeit gebäudetechnischer Anlagen: Grundlagen und Kostenberechnung*. Düsseldorf, 2016. (Visited on 07/04/2018).

[89] N. Vetterli et al. “Dynamic analysis of the low-temperature district network "Suurstoffi" through monitoring”. In: *Proceedings of International Conference CISBAT 2015, LESO-PB, EPFL, Lausanne, Switzerland* (2015), pp. 517–522.

[90] Sven Werner. “International review of district heating and cooling”. In: *Energy* 137 (2017), pp. 617–631. ISSN: 03605442. DOI: 10.1016/j.energy.2017.04.045.

[91] S. Wolf et al. *Analyse des Potenzials von Industriewärmepumpen in Deutschland: Forschungsbericht: Im Auftrag des Bundesministeriums für Wirtschaft und Energie (BMWi) und der Energie Baden-Württemberg AG (EnBW)*. 2014.

[92] Don Wood et al. "Hydraulic Network Analysis Using Linear Theory". In: *Journal of the Hydraulics Division* 98 (1972), pp. 1157–1170.

[93] Tianhao Yuan et al. "Thermodynamic and economic analysis for ground-source heat pump system coupled with borehole free cooling". In: *Energy and Buildings* 155 (2017), pp. 185–197. ISSN: 03787788. DOI: 10.1016/j.enbuild.2017.09.018.

[94] P. Zangheri et al. *Heating and cooling energy demand and loads for building types in different countries of the EU, Entranze Project*. Tech. rep. Energy Economics Group, TU Wien, 2014.

[95] Changxing Zhang et al. "Optimal design of borehole heat exchangers based on hourly load simulation". In: *Energy* 116 (2016), pp. 1180–1190. ISSN: 03605442. DOI: 10.1016/j.energy.2016.10.045.

List of Figures

List of Tables

Appendix A

Network maps

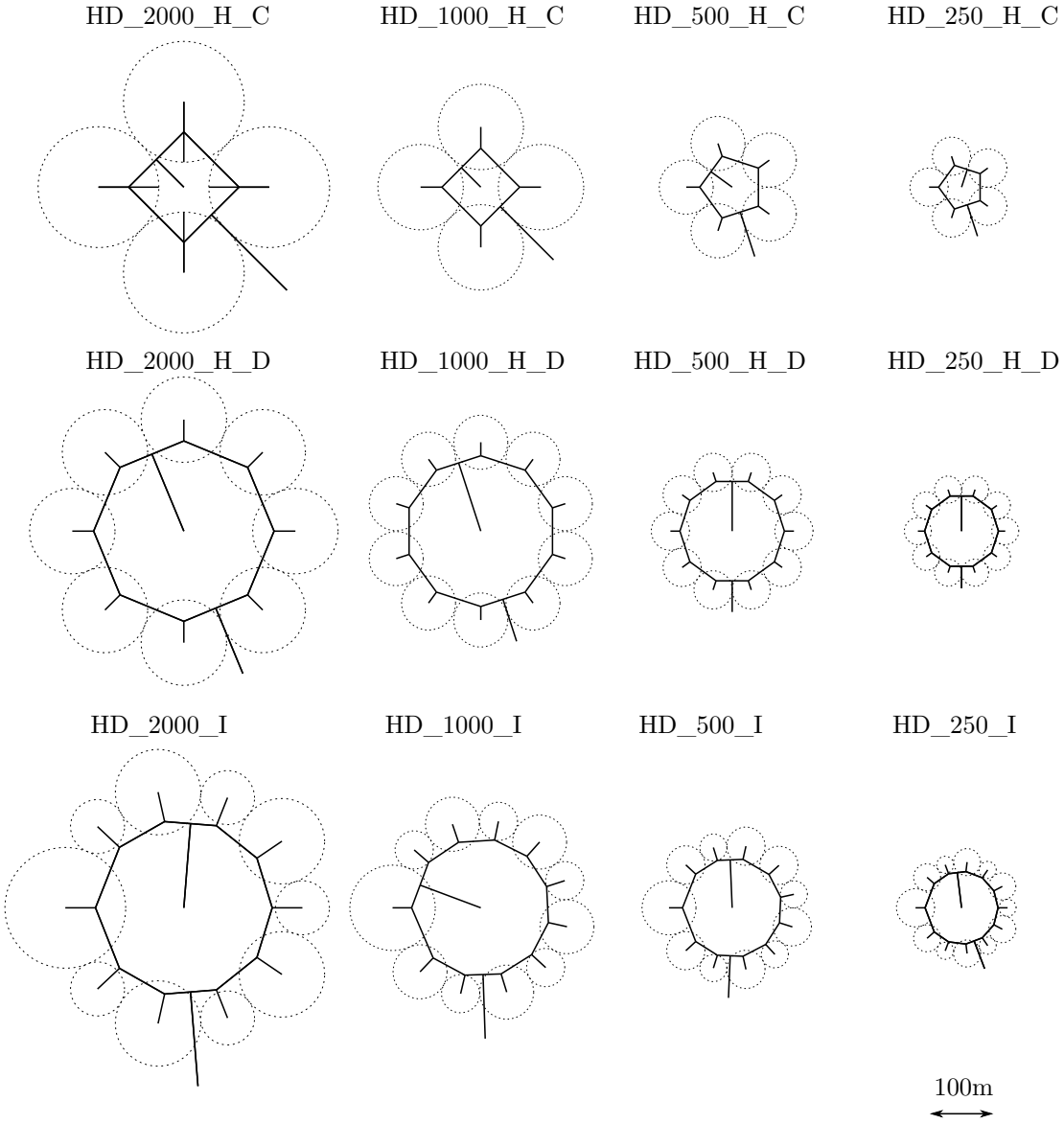

FIGURE A.1: Ring networks maps for high population density scenarios. The circles mark the building's space demand

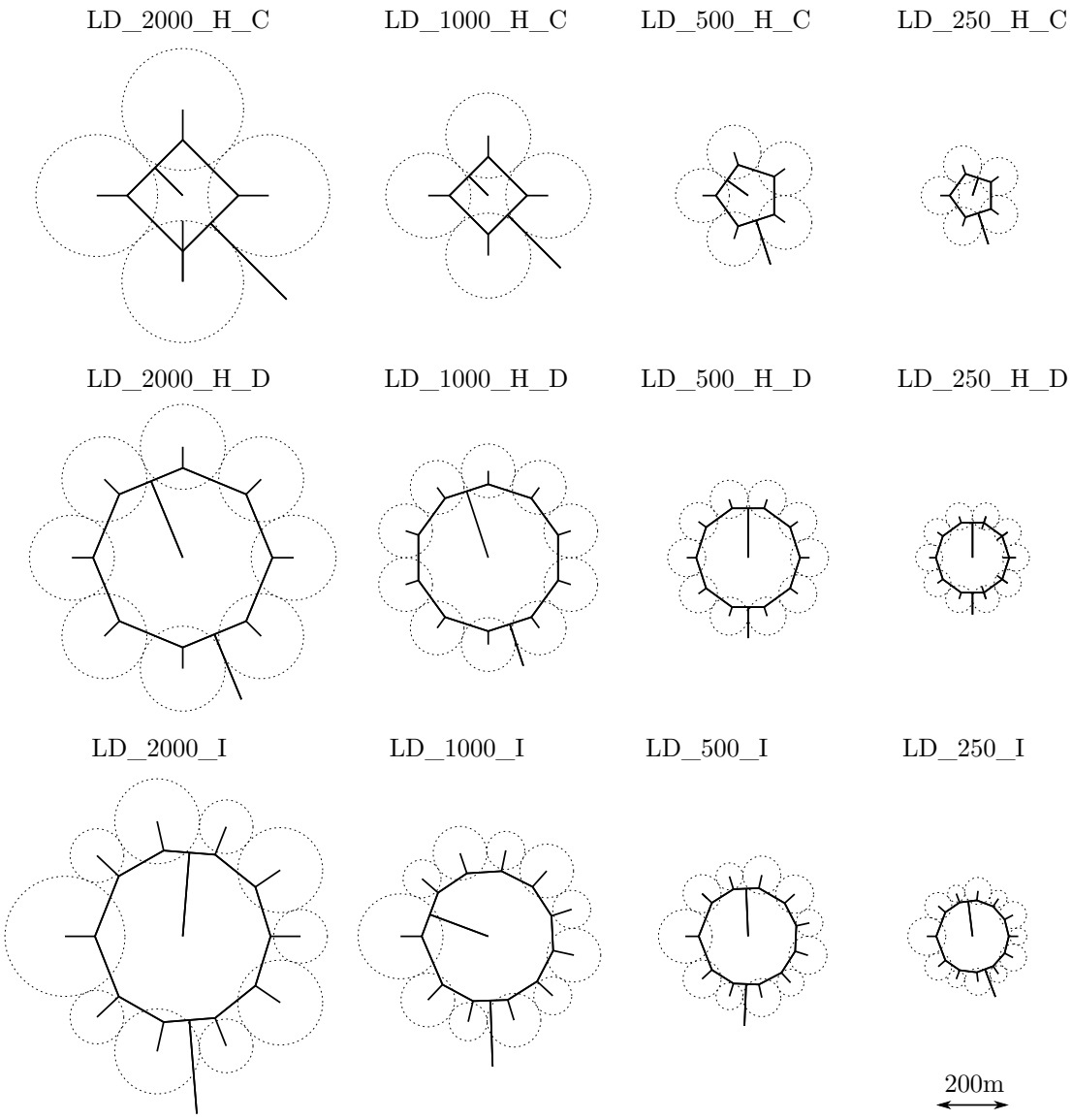

FIGURE A.2: Ring networks maps for low population density scenarios. The circles mark the building's space demand

Appendix B

Equation system factors

The factors for the equation system $EQS_{twinpipe,i}$ (eq. 3.58) from chapter 3.3.2 based on the resistance capacity model are stated here. For the factors R_i and C_i which satisfy $\dot{q} = \frac{\Delta T}{R_i}$ and $\dot{q} = C_i \frac{\partial T}{\partial t}$, please refer to [10].

$$\alpha_1^{(1)} = -\frac{\Delta t\, \lambda_f\, A_f}{C_f\, d_z^2} - \frac{\Delta t\, \dot{m}_f\, c_{p,f}}{C_f\, d_z} \quad \alpha_3^{(1)} = -\frac{\Delta t\, \lambda_f\, A_f}{C_f\, d_z^2}$$

$$\alpha_2^{(1)} = 1 - \alpha_1^{(1)} - \alpha_3^{(1)} - \alpha_4^{(1)}$$

$$\alpha_4^{(1)} = -\frac{\Delta t}{C_f\, R_{fg}} \quad \beta_1 = T_{1,i}^{(t)} \quad \beta_2 = T_{2,i}^{(t)}$$

$$\alpha_1^{(2)} = -\frac{\Delta t}{C_g\, R_{fg}}$$

$$\alpha_2^{(2)} = -\frac{\Delta t\, \lambda_g\, A_g}{C_g\, d_z^2} \quad \alpha_3^{(2)} = 1 - 2\,\alpha_2^{(2)} - \alpha_1^{(2)} - \alpha_4^{(2)} - \alpha_5^{(2)}$$

$$\alpha_4^{(2)} = -\frac{\Delta t}{C_g\, R_{gg}} \quad \alpha_5^{(2)} = -\frac{\Delta t}{C_g\, R_{gb}} \quad \beta_3 = T_{g1,i}^{(t)} \quad \beta_4 = T_{g2,i}^{(t)}$$

$$\alpha_1^{(3)} = -\frac{1}{R_{gb}} \quad \alpha_2^{(3)} = \frac{1}{R_{bs1}} + \frac{2}{R_{gb}} \quad \alpha_3^{(3)} = -\frac{1}{R_{bs1}}$$

$$\alpha_1^{(4)} = \frac{1}{R_{bc}} - \frac{1}{R_{s0}} \quad \alpha_2^{(4)} = \frac{1}{R_{s0}} \quad \beta_6 = \frac{T_{amb}}{R_{bc}}$$

The factors for the equation system $EQS_{btes,i}$ (eq. 4.20) from chapter 4.2.3 based on the resistance capacity model are stated here:

$$\alpha_1^{(1)} = -\frac{\Delta t\,\lambda_f\,A_f}{C_f\,d_z^2} - \frac{\Delta t\,\dot{m}_f\,c_{p,f}}{C_f\,d_z} \quad \alpha_3^{(1)} = -\frac{\Delta t\,\lambda_f\,A_f}{C_f\,d_z^2}$$
$$\alpha_2^{(1)} = 1 - \alpha_1^{(1)} - \alpha_3^{(1)} - \alpha_4^{(1)}$$
$$\alpha_4^{(1)} = -\frac{\Delta t}{C_f\,R_{fg}} \quad \beta_1 = T_{1,i}^{(t)} \quad \beta_2 = T_{2,i}^{(t)}$$

$$\alpha_1^{(2)} = -\frac{\Delta t}{C_g\,R_{fg}}$$
$$\alpha_2^{(2)} = -\frac{\Delta t\,\lambda_g\,A_g}{C_g\,d_z^2} \quad \alpha_3^{(2)} = 1 - 2\,\alpha_2^{(2)} - \alpha_1^{(2)} - \alpha_4^{(2)} - \alpha_5^{(2)}$$
$$\alpha_4^{(2)} = -\frac{\Delta t}{C_g\,R_{gg}} \quad \alpha_5^{(2)} = -\frac{\Delta t}{C_g\,R_{gb}} \quad \beta_3 = T_{g1,i}^{(t)} \quad \beta_4 = T_{g2,i}^{(t)}$$

$$\alpha_1^{(3)} = -\frac{1}{R_{gb}} \quad \alpha_2^{(3)} = \frac{1}{R_{bs1}} + \frac{2}{R_{gb}} \quad \alpha_3^{(3)} = -\frac{1}{R_{bs1}}$$

$$\alpha_1^{(4)} = -\frac{\Delta t}{C_{s1}\,R_{b,s1}} \quad \alpha_2^{(4)} = -\frac{\Delta t\,\lambda_s\,A_{s1}}{C_{s1}\,d_z^2} \quad \alpha_3^{(4)} = 1 - \alpha_1^{(4)} - \alpha_4^{(4)} - 2\,\alpha_2^{(4)}$$
$$\alpha_4^{(4)} = -\frac{\Delta t}{C_{s1}\,R_{s1,s2}}$$
$$\beta_6 = T_{s1,i}^{(t)}$$

$$\alpha_1^{(k)} = -\frac{\Delta t}{C_{sj}\,R_{s(j-1),sj}} \quad \alpha_2^{(k)} = -\frac{\Delta t\,\lambda_s\,A_{sj}}{C_{sj}\,d_z^2}$$
$$\alpha_3^{(k)} = 1 - \alpha_4^{(k)} - \alpha_1^{(k)} - 2\,\alpha_2^{(k)}$$
$$\alpha_4^{(k)} = -\frac{\Delta t}{C_{sj}\,R_{sj,s(j+1)}} \quad \beta_k = T_{sj,i}^{(t)}$$